Development of an interferon gamma biosensor towards the early detection of tuberculosis

by

Stephan Petri Schoeman

Thesis presented in partial fulfilment of the requirements for the degree of Master of Engineering in Electronic Engineering in the Faculty of Engineering at Stellenbosch University

Supervisor: Prof. W.J. Perold
Co-supervisor: Prof. R. Warren

April 2019

Acknowledgements

The financial assistance of the National Research Foundation (NRF) towards this research is hereby acknowledged. Opinions expressed and conclusions arrived at, are those of the author and are not necessarily to be attributed to the NRF.

Declaration

By submitting this thesis electronically, I declare that the entirety of the work contained therein is my own, original work, that I am the sole author thereof (save to the extent explicitly otherwise stated), that reproduction and publication thereof by Stellenbosch University will not infringe any third party rights and that I have not previously in its entirety or in part submitted it for obtaining any qualification.

Date: April 2019

Uittreksel

Tuberkulose is ‘n oordraagbare siekte wat een van die hoof oorsake vir sterftes in die wêreld is. Die huidige toetsmetodes wat gebruik word om tuberkulose te diagnoseer is nie sensitief genoeg nie en is duur om uit te voer. Die toetse is nie aanpasbaar vir individuele pasiënte nie, en dus is dit moeilik om kinders akkuraat te diagnoseer. Dit is uitsonderlik moeilik om tuberkulose in die vroeë stadium van infeksie te diagnoseer, aangesien die bakterieë nie volop in die pasiënt se sputummonsters voorkom nie. Daar is ‘n ernstige tekort aan toeste wat Tuberkulose spoedig en akkuraat kan diagnoseer.

Hierdie projek pak die bogenoemde probleem aan deur ‘n elektrochemiese biosensor te ontwikkel om die konsentrasie van interferon gamma in ‘n vloeistof te kwantifiseer. Interferon gamma is ‘n proteiën wat vrygestel word sodra ‘n individu in kontak kom met tuberkulose. Die projek se doelwitte was om die chemie vas te stel deur ‘n kommersiële elektrochemiese sensor te gebruik. Die toetse was suksesvol en ‘n soortgelyke sensor is ontwikkel deur gebruik te maak van produkte wat van die rak af gekoop kan word. Die sensor is getoets met interferon gamma, asook met ‘n etiket molekule, naamlik mieriks wortelperoksidase , te same met die proteiëne. Die eerste toets het ‘n lineêre stroomaanwins getoon vir konsentrasies vanaf 1ng/ml tot en met 1pg/ml. Die tweede toets het ‘n lineêre aanwins getoon vanaf 1ng/ml tot en met 100fg/ml. Hierdie resultate is in vergelyking gebring met bestaande navorsing. Die resultate was soortgelyk, of verbeter, in alle gevalle.

Die projek is saamgevat deur ‘n opsomming te maak van al die werk wat voltooi is en die moontlike toekomstige opsies is bespreek.

Abstract

Mycobacterium tuberculosis is one of the top ten causes of death in the world. Current diagnostic tests for tuberculosis are either limited in sensitivity, cost, or is not adaptable to different types of patients. The status of the infection is difficult to determine and the early detection, although very critical, is still an aspect that cannot fully be done with the speed and robustness required.

This project set out to develop an electrochemical sensor that would be able to determine the concentration of interferon gamma in a solution. Interferon gamma is a cytokine that is related to the infection of tuberculosis. The objectives of the project was to firstly develop a biochemical detection method for the interferon, and then develop a sensor with the knowledge gained from the first objective.

A commercial sensor was used to experimentally validate the biochemical interaction of the interferon gamma with the surface of the sensor. These tests were successful and the second objective was attempted. Using only off-the shelf products, an electrochemical sensor was developed and tested with the developed protocol. The home-built sensor was tested with two different modes, namely a label free protein and a horseradish peroxidase labelled protein. The linear operation range of the former was found to be 1 ng/ml to 1 pg/ml, and for the latter 1 ng/ml to 100 fg/ml. This was compared to literature that used a commercial sensor and it was found that the home-built sensor matched or improved on the findings.

The project was concluded with a summary and a critical review of the device. Future work would include testing with a more definite concentration range of the protein and the development of a potentiostatic circuit.

Contents

Acknowledgements i

Declaration ii

Uittreksel iii

Abstract iv

List of Tables viii

List of Figures ix

Nomenclature xii

1 Introduction 1
- 1.1 Background . . . 1
- 1.2 Motivation and approach . . . 2
- 1.3 Project scope . . . 2
- 1.4 Thesis outline . . . 3

2 Literature study 4
- 2.1 Introduction . . . 4
- 2.2 Current diagnostic methods . . . 4
  - 2.2.1 Target product profile . . . 8
  - 2.2.2 Conclusion . . . 9
- 2.3 Biosensors . . . 9
  - 2.3.1 Current biosensors . . . 10
  - 2.3.2 Electrochemical crosslinking . . . 16
  - 2.3.3 Biomarker . . . 19
  - 2.3.4 Summary . . . 19
- 2.4 Project objectives . . . 19
- 2.5 Proposed methodology . . . 20
  - 2.5.1 Methods . . . 20
  - 2.5.2 Materials and reagents . . . 21

3 Electrochemical study 22
- 3.1 Introduction . . . 22
- 3.2 Electrochemical methods . . . 22
  - 3.2.1 Cyclic voltammetry . . . 23
  - 3.2.2 Square wave voltammetry . . . 25

3.2.3 Implications . . . 26
3.3 Commercial potentiostats . . . 26
3.4 Research based potentiostatic devices . . . 28
3.4.1 CheapStat . . . 29
3.4.2 Point-of-need potentiostat . . . 29
3.4.3 Dual-microprocessor potentiostat . . . 30
3.4.4 DStat . . . 30
3.4.5 UWED . . . 31
3.4.6 Summary . . . 32
3.5 Conclusion . . . 32

4 Experimental methods 33
4.1 Introduction . . . 33
4.2 Biochemical detail design . . . 33
4.2.1 Chemical reactivity . . . 35
4.2.2 Crosslinking . . . 36
4.2.3 Linker activation . . . 38
4.2.4 Capture antibody linking . . . 39
4.2.5 Interferon-gamma capture . . . 40
4.2.6 Signal antibody linking . . . 41
4.2.7 Sensor development . . . 43
4.3 Measurement definitions . . . 43
4.4 Analysis techniques . . . 45
4.5 Design validity . . . 48
4.6 Methodological assumptions . . . 48

5 Hardware development 50
5.1 Development equipment . . . 50
5.2 DropSens clamp . . . 50
5.3 Fibre interface . . . 52
5.4 Sensor development . . . 54
5.4.1 Electrodes . . . 54
5.4.2 Sensor assembly manufacturing . . . 56

6 Commercial sensor findings 66
6.1 Brief overview . . . 66
6.2 DropSens experimental results . . . 66
6.2.1 Unmodified sensor response . . . 67
6.2.2 Electrografting . . . 68
6.2.3 Capture antibody . . . 71
6.2.4 Interferon gamma . . . 75
6.2.5 Horseradish peroxidase . . . 76
6.2.6 Horseradish peroxidase with H_2O_2 . . . 78
6.3 Descriptive analysis . . . 80
6.3.1 Effect of H_2O_2 . . . 80
6.3.2 SWV of different stages . . . 81
6.4 Conclusion . . . 82

7 Manufactured sensor findings 83

7.1 Brief overview . . . 83
7.2 Sensor selection . . . 83
7.3 Additional modifications . . . 84
7.4 Manufactured sensors experimental results . . . 85
7.4.1 Unmodified sensor response . . . 85
7.4.2 Electrografting . . . 88
7.4.3 Interferon gamma . . . 89
7.4.4 Horseradish peroxidase . . . 91
7.4.5 Negative control . . . 93
7.5 Conclusion . . . 95

8 Discussion **96**
8.1 Brief overview . . . 96
8.2 Experimental results . . . 96
8.2.1 Unmodified response . . . 96
8.2.2 Electrografting . . . 97
8.2.3 Unlabelled protein detection . . . 97
8.2.4 Labelled protein detection . . . 99
8.2.5 Literature review . . . 100
8.3 Algorithm review . . . 103
8.4 Project objectives . . . 103
8.5 Post-hoc analysis . . . 103

9 Conclusion **105**
9.1 Thesis summary . . . 105
9.2 Final conclusions . . . 106
9.3 Project implications . . . 106
9.4 Limitations of results . . . 106
9.5 Future research . . . 106

A Laser calibration **108**

B Gamry Interface 1000 specification sheet **111**

C Cost analysis **113**

Bibliography **114**

List of Tables

2.1 Key characteristics of a biomarker-based non-sputum-based test 9

3.1 Input potential characteristics of the commercial potentiostats 27
3.2 Measured current characteristics of the commercial potentiostats 27
3.3 Potentiostat weight comparison 28

6.1 Peak currents of the different electrografting experiments 71
6.2 Regression line error comparison for capture antibody concentration 74

8.1 Cyclic voltammetry peak comparison for the commercial and home-built sensor 96
8.2 Electrografting peak current decrease comparison 97

A.1 Technical specifications for the TS4040 laser cutting system 109

C.1 Projected cost of manufacturing a single sensor 113

List of Figures

2.1 Smear microscopy results for TB bacteria containing samples 5
2.2 Cepheid MTB/Rif assay 6
2.3 Automated molecular diagnostic system 7
2.4 Components of an affinity based biosensor 10
2.5 Testosterone assay using amperometry 11
2.6 Results of testosterone assay using amperometry 12
2.7 Fabrication steps of an ITO IFN-γ sensor 13
2.8 Fabrication steps of an ITO IFN-γ electrochemical sensor with amplification . 14
2.9 ESAT-6 electrochemical sensor 15
2.10 SMN electrochemical sensor 16
2.11 Antibody already attached to the diazonium salt before immobilisation 17
2.12 Diazonium salt reduction on surface followed by immobilisation 17
2.13 Successive cyclic voltammetry diazonium scans for different carbon electrodes 18

3.1 Typical experimental electrochemical setup 23
3.2 Four cyclic voltammetry potential sweeps 24
3.3 Square wave voltammetry potential sweep 25
3.4 Typical potentiostat control circuit 28
3.5 Dual processor potentiostat 30
3.6 Open circuit current standard deviations noise amplitudes 31
3.7 Universal Wireless Electrochemical Detection 32

4.1 Experimental design flow 34
4.2 DropSens screen printed electrode 35
4.3 4-Aminobenzoic acid 36
4.4 Diazonium salt degradation pathways 37
4.5 Electrochemical grafting on to carbon 37
4.6 Crosslinking base chemicals 38
4.7 Crosslinker activation and immobilisation protocol 38
4.8 Activation solution placed on working electrode 39
4.9 Monoclonal capture antibody linked to carbon 40
4.10 Interferon gamma captured by antibody 41
4.11 Secondary antibody on interferon gamma 42
4.12 Final sensor surface configuration 42
4.13 Sensor electron transfer 43
4.14 Different current response for SWV 44
4.15 Unfiltered measured current of SWV response example 45
4.16 Frame data used for analysis of SWV response example 46
4.17 Filtered SWV response example 46

4.18 Derivative of SWV response example . . . 47
4.19 Baseline and unfiltered SWV response example . . . 47
4.20 Normalised SWV response example . . . 48

5.1 Clamp model for DropSens sensors . . . 51
5.2 Biosensor clamp in use . . . 51
5.3 Photo of clamp being tested for experimental use . . . 52
5.4 Sensor interface connection procedure . . . 52
5.5 Sensor connection system in compression and uncompressed . . . 53
5.6 Sensor connection system . . . 53
5.7 Electrodes cut from the larger nanofibre sheet . . . 54
5.8 Scanning electron microscope images of the cuts of the carbon nanofibres . . . 55
5.9 Preprocessing of silver electrodes . . . 56
5.10 Metal rolling machine . . . 56
5.11 First sensor labelled view . . . 57
5.12 Components of first sensor . . . 57
5.13 First manufactured sensor . . . 58
5.14 Second sensor assembly view . . . 59
5.15 Second sensor layering procedure . . . 59
5.16 Sensor 2 assembly procedure . . . 60
5.17 NeverWet by Rust-Oleum. . . . 61
5.18 Hydrophobic coating of sensor . . . 61
5.19 Sensor 4 CAD design . . . 62
5.20 Sensor 4 components . . . 62
5.21 Hydrophobic coating of sensor . . . 63
5.22 Hydrophobic coating of sensor . . . 63

6.1 Unmodified DropSens sensor cyclic voltammogram . . . 67
6.2 Unmodified Dropsens square wave voltammetry . . . 68
6.3 Single cycle Dropsens cyclic voltammogram electrografting response . . . 68
6.4 Fifteen cycle Dropsens cyclic voltammogram electrografting response . . . 69
6.5 Current difference of the successive peaks of the electrografting . . . 70
6.6 DropSens electrografting peak comparison with square wave voltammetry . . . 70
6.7 DropSens 5 mM ferricyanide SWV capture antibody validation . . . 71
6.8 DropSens 5 mM ferricyanide SWV capture antibody validation for two concentrations . . . 72
6.9 Normalised SWV response for different concentrations of the capture antibody immobilised on the fibre surface . . . 73
6.10 SWV peak comparison for different concentrations of the capture antibody immobilised on the fibre surface . . . 73
6.11 Different regression lines representing the SWV peak currents . . . 74
6.12 DropSens protein SWV response . . . 75
6.13 DropSens protein SWV peaks . . . 75
6.14 DropSens protein calibration curve . . . 76
6.15 DropSens HRP labelled protein SWV response . . . 77
6.16 DropSens HRP labelled protein SWV peaks . . . 77
6.17 DropSens HRP labelled protein calibration curve . . . 78
6.18 DropSens HRP labelled protein with H_2O_2 SWV response . . . 79
6.19 DropSens HRP labelled protein with H_2O_2 SWV peak current . . . 79

6.20 DropSens HRP labelled protein with H_2O_2 SWV calibration curve 80
6.21 DropSens HRP labelled protein with H_2O_2 SWV peak current compared to the normal electrolytic liquid 81
6.22 Comparison of SVW peaks of sequential surface morphologies for a protein concentration on 1 ng/ml 81

7.1 Silver ions transferred to the different electrodes 84
7.2 A used and refurbished silver electrode coated in chloride 85
7.3 Unmodified sensor cyclic voltammetry response 85
7.4 Unmodified sensor square wave voltammetry response 86
7.5 Manufactured sensor SWV frequency increase response 86
7.6 Unmodified sensor SWV frequency change effect unfiltered 87
7.7 Unmodified sensor SWV frequency change effect normalised 87
7.8 Manufactured sensor SWV pulse increase response 88
7.9 Manufactured sensor four cycle electrografting 88
7.10 Manufactured sensor electrografting SWV peak comparison 89
7.11 Manufactured sensor captured protein unfiltered SWV current response 90
7.12 Manufactured sensor captured protein SWV current response 90
7.13 Manufactured sensor captured protein SWV peak currents 91
7.14 Manufactured sensor captured protein SWV peak calibration curve 91
7.15 Manufactured sensor captured labelled protein SWV response 92
7.16 Manufactured sensor captured labelled protein SWV peaks 92
7.17 Manufactured sensor captured labelled protein SWV peak calibration curve . . 93
7.18 Second capture antibody response curve 94
7.19 Negative control peak responses for 10 pg/ml proteins (IFN and CRP) 94
7.20 Lower peak response negative control 95

8.1 Sensor unlabelled SWV peak response comparison 98
8.2 Sensor labelled SWV peak response comparison 99
8.3 Electrografting of diazonium salt 100
8.4 Four cycle Dropsens cyclic voltammogram electrografting response 101
8.5 Unlabelled protein SWV peaks compared to literature 101
8.6 HRP-labelled protein DPV peaks 102

A.1 40W TS4040 CO_2 laser system 108
A.2 Top view of laser system 109
A.3 Alignment of laser mirror system 110

Nomenclature

Abbreviations

ADC	Analog to digital converter
CV	Cyclic Voltammetry
DPV	Differential Pulse Voltammetry
DAC	Digital to analog converter
ELISA	Enzyme-linked immunosorbent assay
FIND	Foundation for Innovative New Diagnostics
HRP	Horseradish peroxidase
IFN-γ	Interferon gamma
LV	Linear Voltemmetry
PBS	Phosphate buffered saline
SWV	Square Wave Voltammetry
TB	Tuberculosis
USB	Universal Serial Bus
WHO	World Health Organisation

Variables with units

E	Applied potential	$[\,\mathrm{V}\,]$
E^0	Former potential	$[\,\mathrm{V}\,]$
n	Electron amount	$[\,-\,]$
T	Temperature	$[\,\mathrm{K}\,]$
C_R	Reduced species concentration	$[\,\mathrm{mol\,L^{-1}}\,]$
C_O	Oxidised species concentration	$[\,\mathrm{mol\,L^{-1}}\,]$
i_p	Peak current	$[\,\mathrm{A}\,]$
A	Area	$[\,\mathrm{cm^2}\,]$
D_o	Oxidised diffussion coefficients	$[\,\mathrm{cm^2\,s^{-1}}\,]$
C^0	Bulk concentration	$[\,\mathrm{mol\,cm^{-3}}\,]$
v	Scan rate	$[\,\mathrm{Vs}{-}1\,]$
C_O^*	Apparent oxidised species bulk concentration	$[\,\mathrm{mol\,cm^{-3}}\,]$
$\Delta\psi_p$	Dimensionless peak current	$[\,-\,]$

Chapter 1

Introduction

"There are three phases to treatment: diagnosis, diagnosis and diagnosis."

$\sim$ *W.Osler*, 1892.

1.1 Background

In March 1882, a German physician and microbiologist called Dr Robert Koch announced to the world that he had discovered the bacteria called Mycobacterium tuberculosis [1]. The bacteria was the leading cause of death in certain European countries at that age.

Tuberculosis (TB) as a disease may be regarded in two different categories, pulmonary and extrapulmonary. Pulmonary TB is the most common manifestation of the disease [2], where the bacteria infects the lungs of the infected person. The infection spreads through droplets that are released into the air when the person coughs. These droplets are inhaled by a healthy person, which causes infection. In the case of TB, infection does not mean that the disease will develop. This is called latent TB, as opposed to active TB where the bacteria actively affects the host. People with a compromised immune system, such as HIV patients or infants, are more prone to develop TB as a disease [3].

In 2017, the WHO reported TB as one of the top ten causes of death in the world, causing sickness in approximately 10 million people yearly [4]. It has been the number one cause of death from an infectious agent, above HIV/AIDS. South Africa is part of the top 20 countries that make up 84% of the incidence rate of TB. 454 000 TB cases were reported in South Africa alone in 2015 [5].

Current diagnostic tests for tuberculosis are either limited in sensitivity or cost, or not adaptable for all types of patients, such as children. The latent and extrapulmonary cases are extremely difficult to detect and there is an urgent need to address these limitations by developing a new diagnostic test.

1.2 Motivation and approach

The World Health Organisation (WHO) established in their End TB Strategy a goal in conjunction with the United Nation's (UN) Sustainable Development Goals to end the global TB epidemic by 2035, starting in 2016 [6]. The first pillar of the WHO End TB Strategy is to develop methods for the early diagnosis of TB. This includes drug-susceptibility testing, and screening on a regular basis of people that live in areas where TB is prevalent. The aim is to increase discovery and development, and aid in the implementation and uptake of new systems and technologies. This aligns with sub-objective 2.2.1 of the South African National Strategic Plan (NSP) for 2017-2022. The objective details to diagnose 90% of the existing TB cases in South Africa and place them on appropriate treatment. The aim is to intensify the facility-level TB case-findings and to improve the diagnosis of drug sensitive and drug resistant tuberculosis in a laboratory environment. To realise this, the need for new diagnostic platforms were identified as one of the key aspects to be addressed [7].

The WHO had convened a meeting in April 2014 to establish target product profiles (TPP) for diagnostic devices. The aim of the TPPs are to ensure that the needs of the end-users are met by the specifications of the diagnostic products [8]. Four TPPs were highlighted:

1. A non-sputum based test that is capable of detecting all forms of TB by identifying biomarkers related to that form of TB.
2. A triage test. Built for simplicity, low cost, and can be used by first-contact personnel.
3. A sputum test that should replace smear microscopy to detect pulmonary TB.
4. A drug-susceptibility test that can be used to select the first-line regimen-based therapy.

The first three items should all be point-of-care devices, while the drug-susceptibility test will be used at microscopy-level centres. This project aims at developing a sensor that will be the first step towards fulfilling one of these TPPs.

1.3 Project scope

The scope of the project was to investigate bioaffinity based biosensors and attempt to develop such a sensor for the detection of a tuberculosis related biomarker. This was not limited to the detection method, but rather to the choice of biomarker. The biomarker had to be related to the diagnosis of tuberculosis and fit into a TPP set by the WHO.

1.4 Thesis outline

This report is composed of a literature study, followed by a review of the additional theory required to understand the detection method. It includes theory of the techniques used in the experimental methods. The review also compares the electronic devices developed by literature, listing the different characteristics of the devices and comparing it to commercially available equipment.

After covering the relevant background, the experimental methods are discussed in detail. This is followed by a chapter dedicated to the hardware development to improve the repeatability and accuracy of the experimental procedures.

The findings of the experiments are reported in two consecutive chapters, followed by a discussion and comparison of the different results. The thesis is then concluded with a chapter discussing the final thoughts on the project and future work.

Chapter 2

Literature study

This chapter reviews the relevant literature that was required to understand the mechanics of biosensing and the relation it has to tuberculosis. It covers the broad topics of current tuberculosis diagnostic methods, biosensors in general, and biomarkers related to tuberculosis. This knowledge is then applied to evaluate literature that covers the topic of biosensors and those aimed at diagnosing tuberculosis. The chapter concludes by evaluating the literature and the project scope, and sets up the proposed project methodology.

2.1 Introduction

The human immune system mobilises a whole body of natural and adaptive response molecules to defend itself against a countless amount of destructive foreign bodies. A key component of this complex system is the ability it has to differentiate between itself and an unknown substrate. Should the system fail to do so, called failure of self-tolerance, this becomes an autoimmune disease [9].

The natural immune system includes, but is not limited to, the epithelial barriers and the mucociliary blanket, the inhalation and ingestion of foreign particles, encoded by the germline genes. The adaptive immune system, which is of more interest towards this project, is expressed in targeted situations. Antigen-specific receptors are formed on the surfaces of T and B lymphocytes [10]. For example, in the case of tuberculosis, specific T-cells that represent pro- and anti-inflammatory features of the control of infection. Current TB diagnostic tests utilise occurrences like this in the peripheral blood to determine the status of infection [11].

2.2 Current diagnostic methods

The procedure used to diagnose TB is setting depended due to resource availability [12]. For active TB, the initial diagnosis is based on physical symptoms. This includes coughing, night sweating, loss of weight, fever, and hemoptysis [13]. This type of diagnosis is subject to incorrect assumptions and may fail to make the correct conclusion. Not all patients show these typical symptoms, especially in the early stages of infection, and it also fails to diagnose extrapulmonary TB. The patient that shows one or more of the symptoms should be sent for additional screening, and people in high risk areas should ideally have access to further testing before final diagnosis is made.

Traditional testing would include a chest X-ray or culture growth of the bacteria. These are both with numerous weaknesses. X-rays are subjected to the discretion of the doctor that has to make the diagnosis and it is limited to pulmonary TB [14]. Culture growth has the advantage of testing for drug susceptibility, but is expensive and takes up to six weeks before the status is known [3]. There are inherent problems that arise when using culture growth methods. The first is the requirement that the patient has to return when the results are known. This is not always possible in rural areas and reaching out to patients becomes virtually impossible. The second is the requirement to send the samples to a central laboratory, which increases the possibility of error. The third problem is the time required for diagnosis. In some areas the probability of contracting TB is considered to be high. A person that contracts a disease with similar symptoms as TB in such an area would be prone to be wrongly diagnosed since it seems unnecessary to wait for the diagnostic results.

Sputum smear microscopy is currently the primary microbiological method to test for TB in resource scarce countries [15]. The method involves collecting sputum from the respiratory tract of the person suspected to have been infected. The sputum is smeared on a glass slide and is treated with acid-containing liquids which stains the cell wall of the bacteria. The slides are then examined under a microscope to find traces of the bacteria. Two different methods are used, fluorescence (auramine staining) and Brightfield (carbol fuchsin staining). An example of both can be seen in Figure 2.1.

(a) Fluorescence microscopy (b) Brightfield microscopy

Figure 2.1: Smear microscopy results for TB bacteria containing samples [16]

The rate at which the slides are examined are dependent on the skill of the analyst. The tests require trivial laboratory equipment and has a 95 - 98% probability of diagnosing smear-positive cases [17]. It does lack the sensitivity required for full a diagnosis in specific patient groups. These groups include HIV/AIDS positive patients, children, and extrapulmonary TB cases [18]. Tools such as GeneXpert MTB/RIF and Line probe assay (LPA) were developed to overcome such limitations.

GeneXpert MTB/RIF [19] is a nucleic acid amplification technique that utilises fluorescence to determine the presence a specific gene sequence of the bacteria. A polymerase chain reaction (PCR) is used to amplify the gene. This is then introduced to a set of five probes that fluoresce at different frequencies. These probes are curved and approximates the fluorescent state, but cannot do so. When bound to the specific gene, they straighten out, and become fluorescent. This then is interpreted as an indication of the presence of the TB gene.

Figure 2.2 gives the sequence used by a Cepheid MTB/Rif (Cepheid, US) detection test to test for TB infection and rifampicin resistance mutations of TB. Rifampicin is an antibiotic used to treat several forms of mycobacterium [20]. The rifampicin resistant strain is not completely identical to the normal strain of TB. This feature is exploited by the choice of the probes. It fully reacts when the unmodified sequence of the DNA is present, but only partially with the mutated strain due to a sequence mismatch. The assay validates the experiment with an internal control of Bacillus globigii, which also reacts with the probes to provide a positive response.

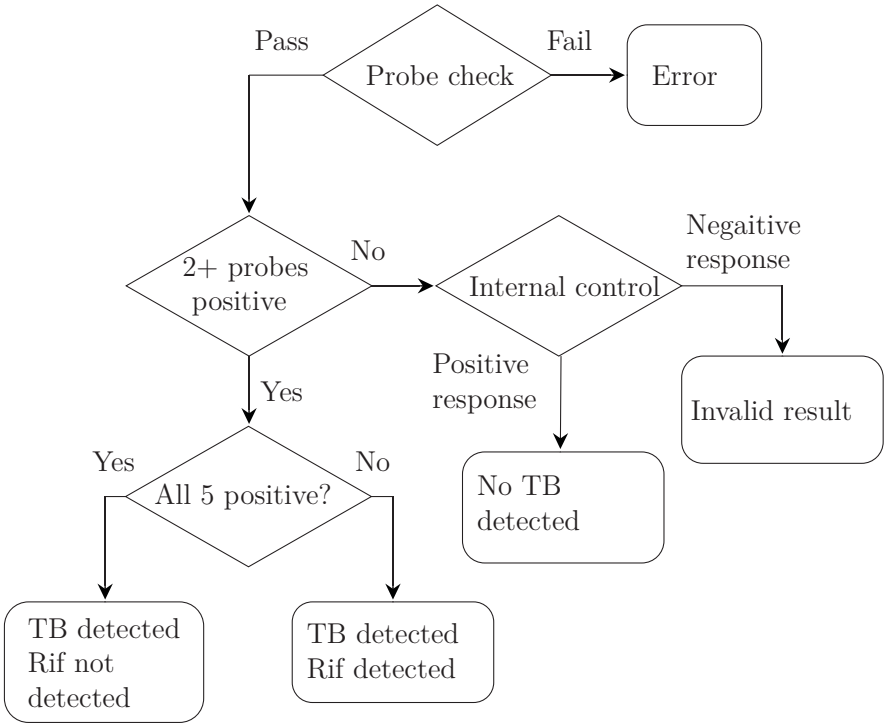

Figure 2.2: Cepheid MTB/Rif assay [21]

The experiments are conducted by adding the specific reagents to a sample suspected to contain the bacteria. This could be stool or sputum samples. The sample is then inserted in to a cartridge used specifically for GeneXpert tests. These cartridges are for single use only and disposable. The cartridge is placed in a molecular diagnostic system, as in Figure 2.3, where the rest of the process is automatically completed. The systems come in variant sizes with 1, 2, 4, 16, 48, or 80 modules [19]. Each test takes 2 hours to complete and can run independently. The cartridges have a lifetime of up to 2 weeks if stored properly.

Figure 2.3: Automated molecular diagnostic system [22].

The level of expertise required to conduct an Xpert test is low compared to these previously mentioned. The drug susceptibility testing is also more dynamic and negative testing is also automated. The disadvantages of GeneXpert are quickly realised when assessing that the method relies on the bacteria to be present in the sample. This means that it has the same preprocessing disadvantages as smear microscopy. The probability of detecting TB would be higher with the automated method, but it still relies on the successful collection of sputum containing the bacteria. It fails to diagnose latent TB, and cannot do early diagnostics. The device requires a stable power supply, and the cartridges have a limited lifetime.

There existed no specific diagnostic method for latent TB until approximately ten years ago [23]. Traditional testing involved a tuberculin skin test (TST). This involved the suspected patient to be injected with TB antigens below the skin. The reaction was monitored and the response of the surrounding skin indicated if the person was infected or not. This was prone to false positives due to the Bacille Calmette-Guérin vaccine, and required the patient to visit the medical care unit a second time. Interferon gamma release assays (IGRA) were developed to have a diagnostic procedure using blood. It is based on the principle that the blood contains antigen-specific T cells. This then becomes activated when exposed to TB and secretes interferon gamma. The plasma is separated from the blood and the interferon is then immobilised by a capture antibody. The interferon is labelled with a redox reactive label, which produces a colorimetric response. The disadvantages of IGRA is that the incubation of the protein has to happen overnight at very specific conditions. These tests are unable to determine the different stages of infection and is not sensitive enough to definitely rule out the infection

Another form of diagnosis is a lateral flow urine lipoarabinomannan assay (LF-LAM). The intended use is for the diagnosis and screening of HIV-infected patients that have active TB. This is a urine test that detects the presence of a LAM antigen. This is found in the cell wall and released from metabolically active or degenerating cells. It appears to be present only in TB infected hosts. The tests are inexpensive and has the advantage of not being a sputum-based test. According to the policy of the WHO, this test should only be used as a recommendation to aid in the diagnostics of TB because of possible false positive tests [24].

2.2.1 Target product profile

There exists multiple other diagnostic methods for TB, each with its own advantages and disadvantages. This was highlighted in the Global Tuberculosis Report of 2017, published by the World Health Organisation (WHO) [4]. Globally, even in the advancement of molecular tests such as GeneXpert, only 57% of the reported cased of pulmonary TB were bacteriologically confirmed. With Xpert tests at the front of the diagnostics recommended by the WHO, the need for better and point-of-care devices is acknowledged. Xpert test have a high sensitivity and specificity for pulmonary TB, but does not perform according to the need to diagnose smear-negative pulmonary and extrapulmonary cases. The classification of the activity of drug resistant TB is sometimes wrongly false-positive or false-negative when the bacteria is in low concentrations [25]. The need for a constant power supply at the diagnostic centres to run the GeneXpert assays disqualifies it as a point-of-care device [8].

The sputum based tests, as discussed previously, is hindered by the fact that sputum from the lungs has to be coughed up. The WHO published a report of high-priority target product profiles for new tuberculosis diagnostics [8]. In this list there exists calls for different types of diagnostic methods, namely:

1. A non-sputum based test that is capable of detecting all forms of TB by identifying biomarkers related to that form of TB.

2. A triage test. Built for simplicity, low cost, and can be used by first-contact personnel.

3. A sputum test that should replace smear microscopy to detect pulmonary TB.

4. A drug-susceptibility test that can be used to select the first-line regimen-based therapy.

Of these, Kik *et al.* [26] found that the most urgent was the development of a non-sputum biomarker-based diagnostic test that can be used as a point-of-care device. A summary of the technical specifications for this diagnostic method is given in Table 2.1.

The goal of such a test would be to expand the diagnostic horizon to detect childhood and extrapulmonary TB. The sample source should be from urine, blood, or breath condensate. The device itself should be more portable, simplistic, and durable, with little to no sample preparation. An additional factor that should be considered is the operation temperature range. This should be brought into consideration because of the diverse settings in which TB could be diagnosed and the difference in ambient temperature related to it.

Table 2.1: Key characteristics of a biomarker-based non-sputum-based test [8]

Characteristic	Optimal requirement	% of optimal	Minimal requirement	% of minimal
Diagnostic sensitivity for pulmonary TB in adults	$\geq$ 98% for smear positive culture positive, $\geq$ 68% for smear negative culture positive, $\geq$ 80% in adults with HIV infection	90%	Overall >60%, but >98% for smear positive culture positive	95%
Diagnostic sensitivity for extrapulmonary TB in adults	$\geq$ 85% in lymph node aspirates or tissue, $\geq$ 80% in cerebrospinal fluid	85%	No lower range was given	69%
Diagnostic sensitivity in children	$\geq$ 68% for childhood intrathoracic TB	85%	No lower range was given	72%
Diagnostic specificity	Distinguish between active and latent TB, at least as specific as Xpert MTB/RIF assays	92%	As optimal	87%
Time to assay result	Less than 20 minutes for complete assay	79%	Less than 1 hour for complete assay.	85%
Maintenance and calibration	Disposable, no maintenance	97%	Preventative maintenance after 1 year or 1000 samples, simple tools and knowledge, maintenance alert, remote calibration	90%
Price of individual test	<US$ 4.00	74%	<US$ 6.00	77%

The final remark regarding the development would be on one of the pillars of the End TB Strategy of the WHO [1]. The aim of the pillar is to intensify research and innovation. It reviewed the development of relevant assays and found that it has been stagnant in the past year (2017 - 2018). There is yet no point-of-care assay that can accurately determine if a patient has TB with speed and robustness required.

2.2.2 Conclusion

The diagnosis of TB has come a long way from sputum smear microscopy to methods such as GeneXpert. The current diagnostic tools leave a large gap of undiagnosed patients. This is due to method and tool limitations, and reachable range into resource-limited settings. A call was set out to address this with a non-sputum based biosensor. The following sections review biosensors and its relevancy towards the fulfilment of this project.

2.3 Biosensors

The definition of biosensors vary, but in this context it is composed of a biological recognition element bound to a transducer that either produces or influences a signal. This

signal is subject to the bound element reacting with an analyte and the concentration of this analyte. The biological recognition element could be an antibody, an anti-protein, or DNA [27]. Figure 2.4 shows the typical components found in an affinity based biosensor.

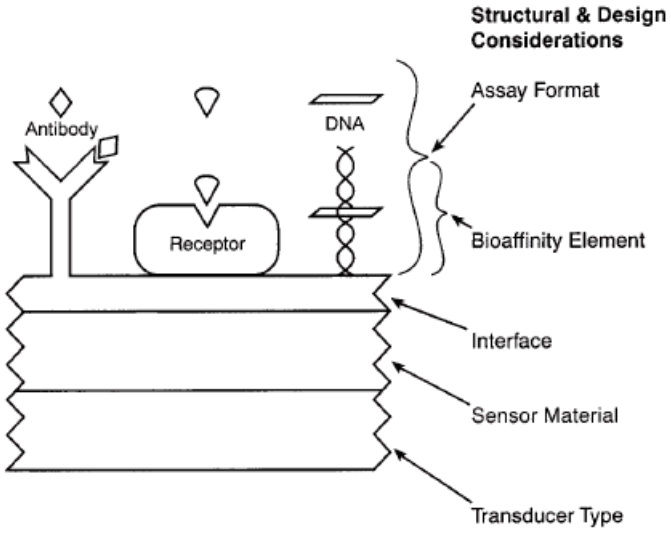

Figure 2.4: Components of an affinity based biosensor [27]

The transducer type is defined as the mechanism used to detect the concentration of the analyte. A selection of previously developed biosensors in literature will be discussed.

2.3.1 Current biosensors

There exists many types of biosensors with numerous sensing techniques. These include mass based, electrochemical, and optical biosensors [28]. These can then be further classified by the type of biorecognition element used for detection of the biomarker. Grieshaber *et al.* [29] did a review of the subject of electrochemical biosensors and concluded that these systems, such as the widely available glucose sensors, do not have the drawback of having a high setup cost or complexity. Electrochemical sensors have a high selectivity, robustness, sensitivity, and can be miniaturised to be used as a point-of-care device. There exists a need to develop these sensors with the goal of miniaturisation to aid in the signal to noise ratio, since the electrochemical effect is independent of the volume of the sample. This study aims to discuss different electrochemical methods used in literature.

Mahato *et al.* [30] discussed different electrochemical sensing techniques used to potentially diagnose cancer. Electrochemical techniques are classified as potentiometric, amperometric, impedimetric, and voltammetric. A biosensor used for electrochemical detection is commonly comprised of three electrodes. These are the working, secondary or counter, and reference electrodes [31].

The working electrode consist of a conductive material that is a chemically stable solid, for example carbon, platinum, or gold. The reference electrode usually is silver metal coated with a layer of silver chloride, and the counter electrode a wire made of platinum. The counter electrode serves as the connection to the solution so that a current could be

applied to the working electrode. The reference electrode is kept at a distance within the liquid to maintain a stable and known reference voltage [29]. The working electrode is functionalised and coupled with a physichemical transducer. This produces a signal by increasing the electron mobility [32]. An advantages of electrochemical detection techniques is that the measurements are not affected by the matrix effect, and since it is electronic there is no colour interference. This makes it possible to test liquids that may have hindered optical tests [33].

Potentiometric electrochemical techniques is to measure the potential at the working electrode when little to no current is flowing through the setup. These type of sensors are used to detect electroreactive agents, proteins, and metabolites [30]. A common example of this type of sensor is a glass electrode pH meter. By immobilising a biological agent to the surface of the electrode that forms and ion by catalysing a reaction, these sensors can measure the reaction by sensing these ions [34]. The indirect measurement of the biomatter linked to the surface was mentioned by Koncki [35], where it was suggested that this method be used to preferably study the nature of ions. The signal generated by potentiometric methods is influenced by non-specific adsorption which have a direct influence on the immobilised biomatter. When using a label based system to improve this, amperometric methods are preferred.

Inoue *et al.* [36] used amperometry to develop an electrochemical immunochromatographic assay to detect the concentration of testosterone. Using photolithography, they etched a three-electrode gold chip. The assay principle is shown in Figure 2.5.

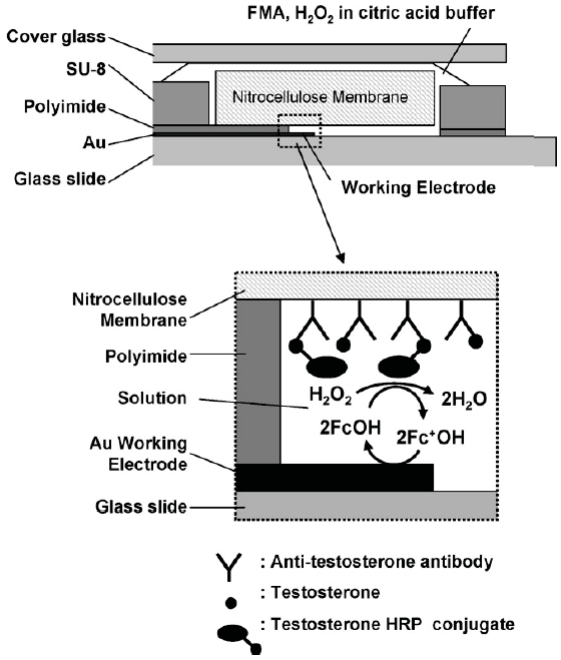

Figure 2.5: Testosterone assay using amperometry [36]

The assay used a competitive immunoassay method where a controlled horseradish-peroxidase (HRP) labelled testosterone competed against plain testosterone for binding sites on a nitrocellulose membrane near the transducer. After the HRP-testosterone and

testosterone mixture flowed through the nitrocellulose strip, a square was cut from the nitrocellulose test line, placed on the working electrode, and pressed down with a glass slide as in Figure 2.5. A citric acid buffer containing FcOH and hydrochloric acid (H_2O_2) was dropped on the sensing area with a laboratory pipette. The following reaction took place in the buffer, induced by the HRP with

$$2\,\mathrm{FcOH} + \mathrm{H_2O_2} + 2\,\mathrm{H^+} \longrightarrow 2\,\mathrm{Fc^+OH} + 2\,\mathrm{F_2O}, \tag{2.1}$$

and then

$$\mathrm{Fc^+OH} + \mathrm{e^-} \longrightarrow \mathrm{FcOH}, \tag{2.2}$$

at the working electrode. The working electrode potential versus the reference electrode's was kept at -0.3 V. The current produced by the reaction served as the indicator of the quantity of HRP that was captured by the antibodies, which in turn indicated the concentration of the testosterone. Figure 2.6 shows the current measurement at the working electrode for different concentrations of testosterone.

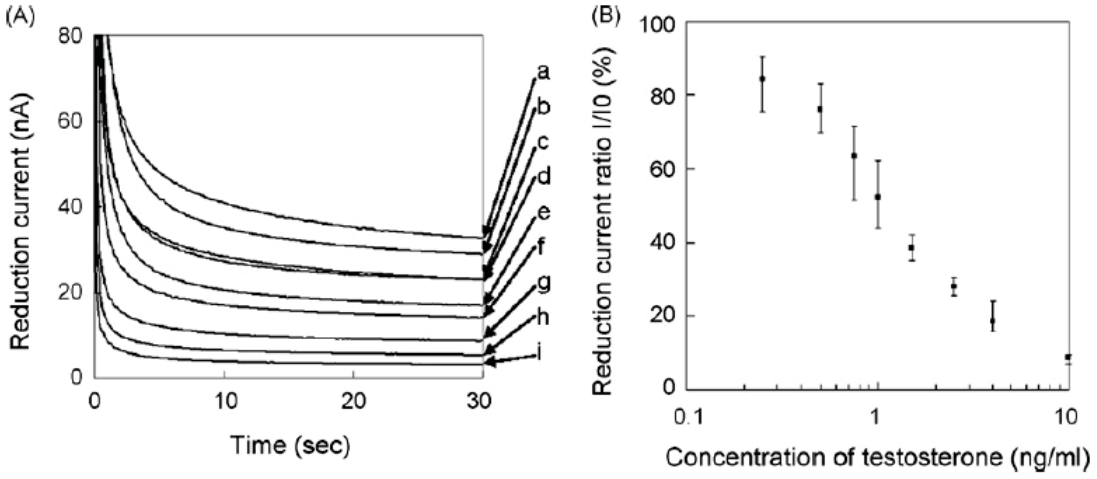

Figure 2.6: Results of testosterone assay using amperometry [36]

The different lines in Figure 2.6(a) each indicate the reduction current at different concentrations of testosterone. The buffer had a pH of 4.5. This could be a limiting fact when working with proteins. The pH to prevent protein denaturation is typically around 7 [37].

Assessing the results of Figure 2.6, the difference in the magnitude of the current ranges in the nano range. This is due to the nature of the test, where the current is generated by spontaneous reaction due to the applied potential. This level of current measurements is prone to noise disturbances if the grade of the measurement device is not sufficient. Another disadvantage of amperometry is the presence of the catalyst. If the target molecule is not electrochemically active, the use of a label is required to work as a catalyst for the buffer reactions to occur.

In their review, Ronkainen *et al.* [34] stated that amperiometric based biosensors have increased selectivity because the fixed reference to working potential is unique for each analyte type. This is supported by the work done by Inoue *et al.* [36], setting the voltage relationship to -0.3 V. The sensor was characterised by using cyclic volammetry. They

first proved that the electrodes were stable in the buffer solution in the absence of the HRP-labelled testosterone. by the repeatability of the cyclic voltammetry curves. The next step was to add HRP-labelled testosterone and monitored the change in the voltammograms. Based on the changes, the parameters of the amperometry were derived. The derivation process would be unique for all voltammetry-to-amperomety sensors, but provides initiative to pursue the possibility of both measurement techniques. Ronkainen *et al.* [34] recommended using interdigitated electrodes to enable the cycling of the redox process of the enzyme. This would enable the enzymes to contribute to the current more than once, enabling lower limits of detection.

Voltammetry electochemical techniques include cyclic (CV), linear sweep (LSV), square wave (SWV), stripping (SV), and differential pulse voltammetry (DPV). It is the dynamic measurement of current flowing versus the controlled voltage change [31]. Cyclic voltammetry is a linear potential sweep between an upper and lower potential, swept multiple times upwards and downwards. Square wave voltammetry is a pulsed square wave with a set frequency, superimposed on a step function. This is typically swept from a higher potential to a lower potential and the current sampling is done at the end of each pulse. Stripping voltammetry involves a linear potential sweep with a preapplied potential step to clean and electroplate the electrodes. Differential pulse voltammetry is the same as SWV, but with the current sampling at the beginning of each pulse.

Zhang *et al.* [38] built an interferon-gamma-based indium tin oxide (ITO) detector for latent tuberculosis. The detection method deployed in this case was differential pulse voltammetry. The fabrication steps of the ITO sensor are shown in Figure 2.7.

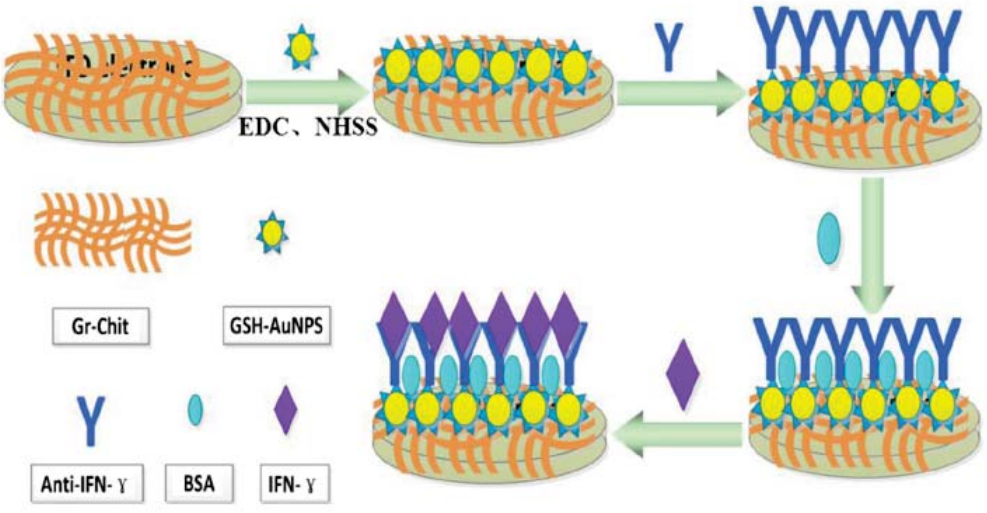

Figure 2.7: Fabrication steps of an ITO sensor [38]

The interferon gamma (IFN-γ) acted as a resistive element, decreasing the peak currents relative to the concentration of the IFN-γ present.

An interesting, and relevant topic presented by this paper is that the performance of an electrochemical sensor could and will be affected by external factors. They took into account the pH of the solution, surrounding temperature, and incubation time of the

IFN-γ . Their analysis looked at the different DPV current peaks at these varying conditions. They found that for their sensor a pH of 7.0 was ideal, and a corresponding PBS buffer was used. The ideal operating temperature was found to be 35°C for the lowest DPV current peaks. The incubation time was set to two hours, because the sensor became saturated after this time and it made little difference waiting longer than this.

In a later study done by Zhang *et al.* [39], the conditions were found to be quite similar. A pH of 7.0 and an incubation time of 35 minutes were found to be optimal. The other conditions were not considered in the publication. They did take into account the concentrations of the elements that participated in the oxidation and reduction reactions. The DPV measurements were made in a 0.1 M PBS buffer with different concentrations of Hydroquinone (HQ) and H_2O_2. The sensor developed is given in Figure 2.8.

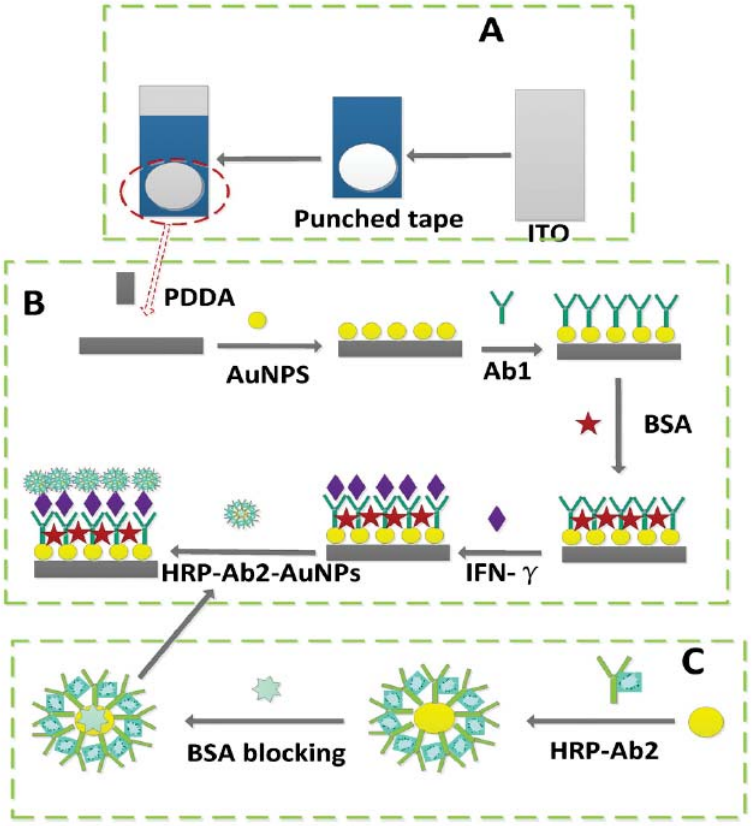

Figure 2.8: Fabrication steps of an ITO IFN-γ electrochemical sensor [39]

The working principle of the assays developed effectively is the same as that developed by Inoue *et al.* [36], with the difference that this reaction was potential driven and not spontaneous. The chemical equations were given as

$$H_2O_2 + HRP_{RED} \longrightarrow H_2O + HRP_{OX}, \tag{2.3}$$

$$HRP_{OX} + HQ_{RED} \longrightarrow HRP_{RED} + HQ_{OX}, \tag{2.4}$$

$$HQ_{OX} + 2\,H^+ + 2\,e^- \longrightarrow HQ_{RED}, \tag{2.5}$$

with a net reaction of

$$H_2O_2 + 2\,e^- + 2\,H^+ \longrightarrow 2\,H_2O. \tag{2.6}$$

The linear detection range for the sensors was reported to be 0.1 pg/ml to 10 ng/ml. Again, it can be seen that the label played an important role as it was oxidised by the hydrogen peroxide. Fethi *et al.* [40] developed a label free electrochemical biosensor to aid in the diagnosis of TB by detecting different concentrations of ESAT-6.

The anti-ESAT-6 antibodies were immobilised on a gold screen printed electrode of a commercial sensor, using a self-assembled thiol layer. The sensors used were DropSens screen printed electrode disposable electrochemical sensors (DropSens, Spain). After the capture of the ESAT-6 antigen, the electrodes were analysed with square wave voltammetry and the results are given in Figure 2.9. The study evaluated the different surface changes between different experiments with SWV to indicate if the effects were successful by comparing the change in peaks between the stages.

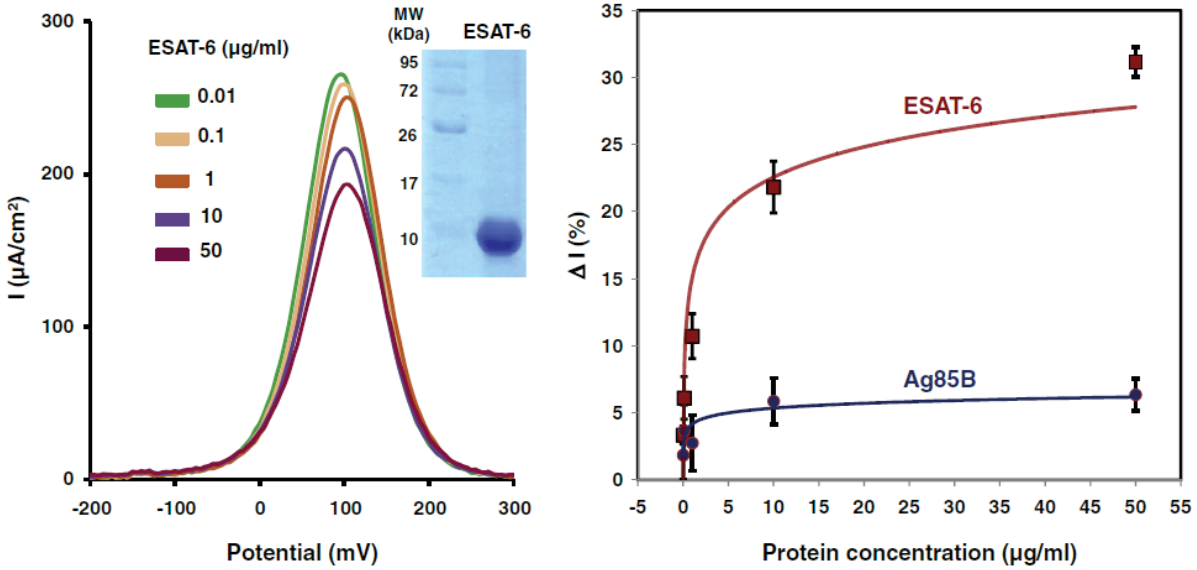

Figure 2.9: ESAT-6 electrochemical sensor analysed with square wave voltammetry [40]

The reported detection limit was 7 ng/ml. An interesting comment to be made about the SWV results in Figure 2.9 is that the current was given as a function of the electrode area. This is the current density of the measurements, and not the actual current measured. The diameter of the working electrode was reported to be 4 mm, thus at a peak current density of approximately 267 µA/cm^2 would mean that the measured peak current was 33.6 µA. The peak currents recorded with the antigen present was only graphically reported. The current density range seems to be approximately 190 µA/cm^2 to 270 µA/cm^2, meaning that the measured currents ranged between 23.9 and 33.9 µA. When comparing this to the results of another study done by Eissa *et al.* [41], the results seem to be comparable. Eissa *et al.* used the same type of electrochemical setup to detect an unlabelled survival motor neuron (SMN) protein, but with carbon nanofibres as the electrode material. The results are given in Figure 2.10.

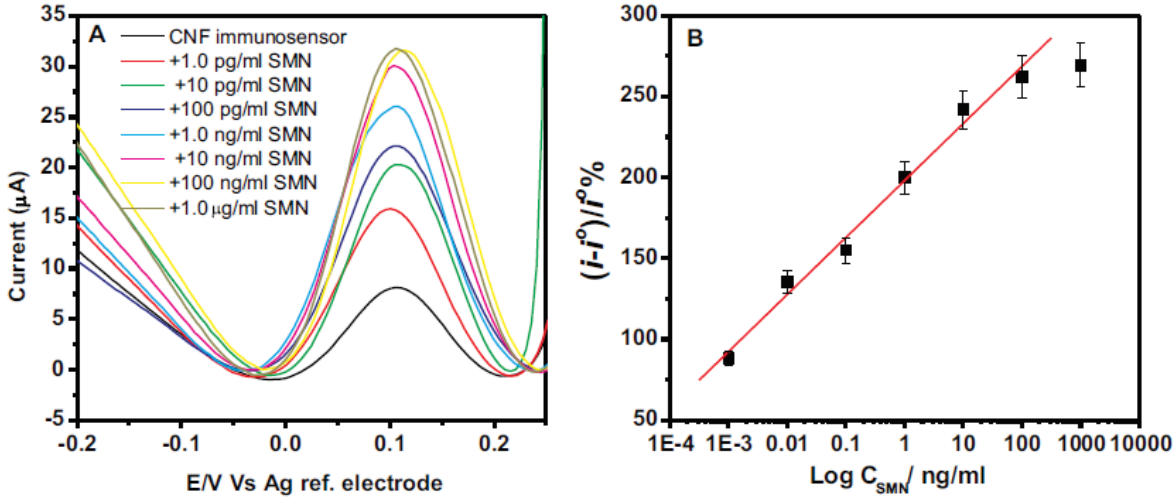

Figure 2.10: SMN electrochemical sensor analysed with square wave voltammetry [41]

The current range for these tests ranged from approximately 6 µA to 33 µA. The detection limit for this study was 0.75 pg/ml.

2.3.2 Electrochemical crosslinking

For affinity biosensing applications, a critical component is the linking of the antibody to the transducer. There are multiple immobilisation techniques. These include adsorption, covalent bonding, entrapment, crosslinking, encapsulation, and whole cell immobilisation. Covalent bonding is the most common for bioreceptor molecules because of the strong linkages and the wide applicability [42].

Covalent methods include diazonium ion reduction, thermal and photochemical modifications, amine and carboxylate oxidation, and "click" chemistry [43]. The most developed and tested method appears to be the diazonium ion reduction technique. Aryl diazonium salt has been used in many studies to modify the surface of the transducer of biosensors to covalently bond the sensing element. Polsky *et al.* [44] reported electrochemically immobilising enzyme-liked horseradish peroxidase to an electrode. The advantages of using such a technique is the preparation is easy, the covalent bonding to the surface is stable, and the potential of binding the protein spatially onto miniature electrodes-arrays. The setup enables direct electron transfer between the enzyme and the electrode, which simplifies the analysis procedure. Bourdillon *et al.* [45] immobilised glucose oxidase on glassy carbon disks by covalently binding it to I-phenylacetic acid diazonium fluoroborate 1 using a home-built potentiostat.

The electrochemical method in which a diazonium salt is bound on to the surface of the substrate is called electrogafting [46]. The substrate (silicon, carbon, or a metal) is set up as the cathode by using a potentiostat. The method involves dissolving a diazonium salt in an aprotic medium containing a supporting electrolyte or an acidic aqueous medium. The diazonium salt is then reduced and the surface of the working electrode is used as a cathode. The voltage of the cathode is set to the potential of the diazonium salt's voltammetric peak, or to a more cathodic potential for a certain amount of time. Washing steps may follow to remove the excess salt and the weaker bonds [43], [47].

A subject of more interest would be the immobilisation of antibodies, since this aligns with the biomarker based assays given by the WHO Global TB . This is not limited to antibodies since DNA, peptides, and whole cells can be immobilised onto electrodes using the electrografting technique [48]. One approach used by Corgier *et al.* [49] was to firstly conjugate 4-carboxymethylaniline to immunoglobulin G (IgG) antibodies, followed by the diazotization of the conjugate to the surface of their graphite electrodes. The sequence is given in Figure 2.11.

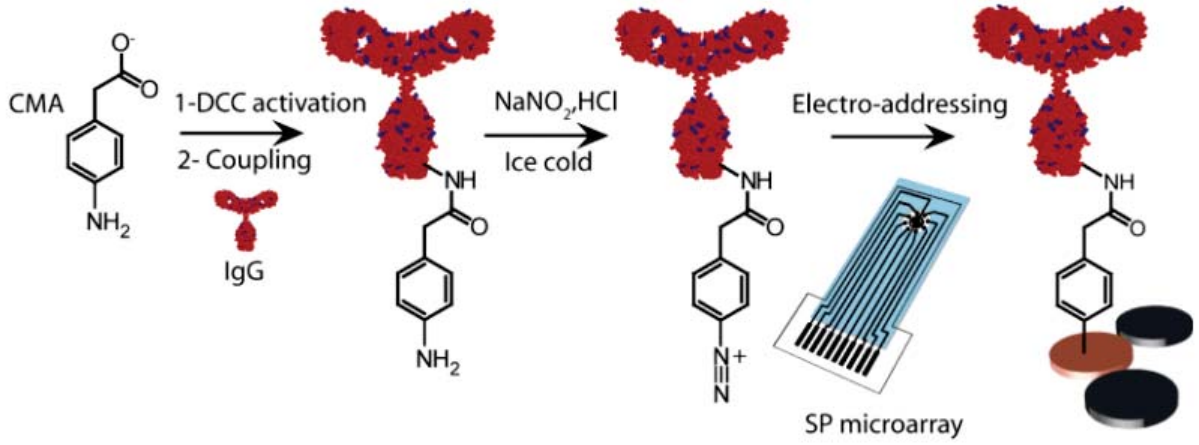

Figure 2.11: Antibody already attached to the diazonium salt before immobilisation [49]

Eissa *et al.* [41] developed a sensor for the detection of survival motor neuron (SMN) protein using screen printed electrodes. The difference between the work done by Eissa *et al.* and Corgier *et al.* is that the former firstly modified the surface of the working electrode, followed by the immobilisation of the SMN protein. This was done by activating the carboxylic groups with a 1-ethyl-3-(3-dimethylaminopropyl) carbodiimide hydrochloride (EDC) and N-hydroxysuccinimidyl-4-azidosalicylic acid (NHS) buffer. This is shown in Figure 2.12, and can be compared to the method followed by Corgier *et al.*, Figure 2.11.

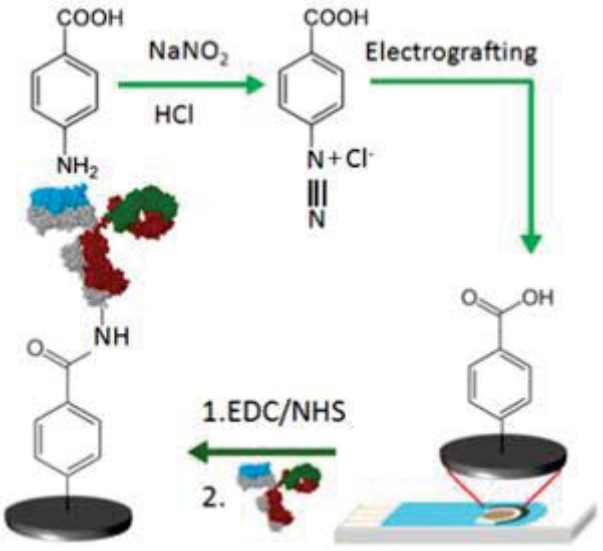

Figure 2.12: Diazonium salt reduction on surface followed by immobilisation [41]

Eissa *et al.* [41] used a standard three-electrode configuration to measure the potential change in their working substrate. The electrodes were in all cases a form of carbon. These were carbon screen printed, single walled carbon nanaotubes, multi walled carbon nanaotubes, graphene, graphene oxide, and carbon nanofibres. The counter electrode was composed of a similar carbon structure, and the reference electrode silver. A reference electrode has to have a stable reference potential with time and temperature, and not affected by small system disturbances [50].

Eissa *et al.* [41] functionalised the working electrodes by the electroreduction of 4-carboxylpenyl diazonium salt using scanning CV. The voltage was varied in a range of -0.6 V to 0.2 V with a rate of 100 mV/s^{-1}. They used a potentiostat to record the cyclic voltammetry and square wave voltammetry electrochemical measurements.

An interesting observation made by Eissa *et al.* was the amount of cycles it took do fully modify the different surfaces. The cycles are shown in Figure 2.13

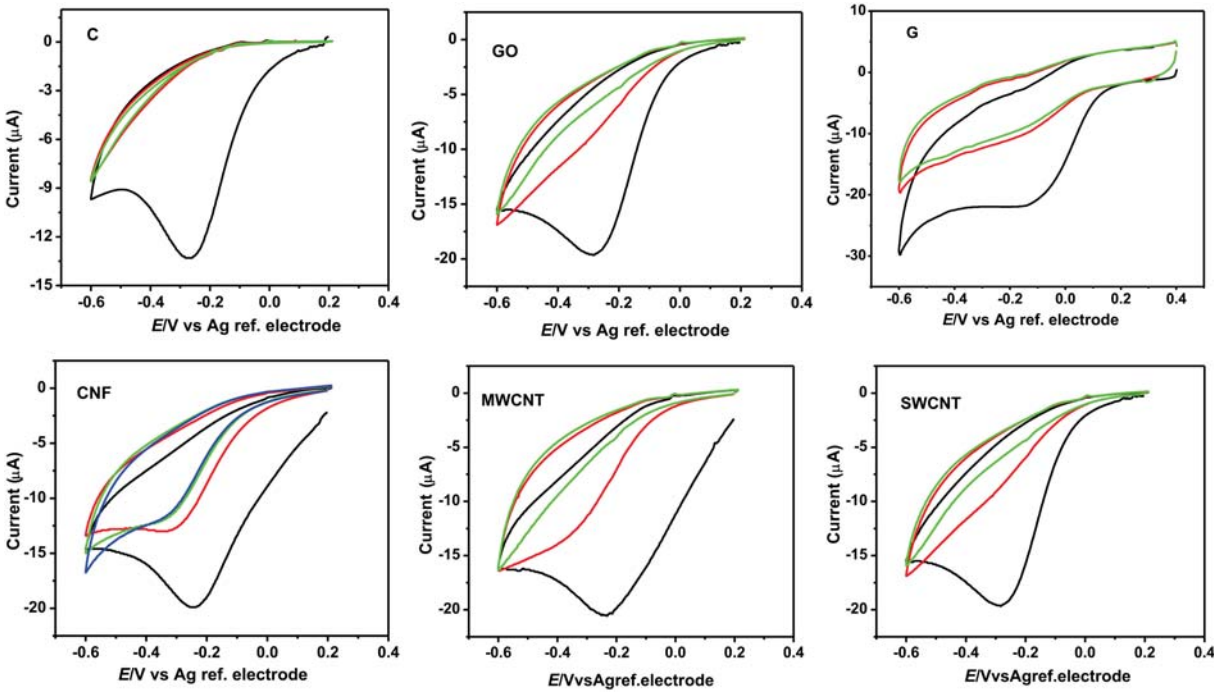

Figure 2.13: Successive cyclic voltammetry diazonium scans for different carbon electrodes [41]

It was noted that the electrodes with a larger surface area required more cycles to reach saturation. The successive cycles also progressively diminished the the cathodic peaks (seen at approximately -0.3 to -0.2 V in all cases). This is due to the coverage of the surface with a film of the salt, saturating the usable binding areas with each cycle. The same results have been reported by Bélanger and Pinson, and Corgier *et al.*

Some drawbacks of using aryldiazonium ion reduction techniques to form an organic layer is that there may be a multilayer formation which yields a varying thickness adhered to the electrode [51]. The formation of the layers on pyrolyzed photoresist (PPF) were characterised by an atomic force microscope (AFM) by both Brooksby and Downard [51]

and Anariba *et al.* [52], and the monolayer was reported to be an irreversible binding of radicals, but subject to multilayer formation.

2.3.3 Biomarker

This section gives a short discussion regarding the biomarker chosen for this project. It was decided that interferon gamma would be used as the protein to be quantified by the biosensor. Interferon gamma is released from CD4+ and CD8+ antigen-specific T cells upon exposure to tuberculosis. This property is also used in standard IGRAs where blood is stimulated with TB antigens overnight to produce the protein.

Interferon gamma is not the ultimate solution to TB diagnostics. Many different studies have been done to find the appropriate combination of biosignatures that will properly indicate the infection of in the host body specifically for tuberculosis. The complexity of the diagnosis is also increased when considering that TB has not only one state of infection: pulmonary, extrapulmonary, which in turn could be active or latent, the difference in children and adult responses, and the different strains of tuberculosis [53]. To illustrate the complexity of TB diagnostics with biomarkers, Wergeland *et al.* [54] examined 27 different markers detected in QFT supernatants to differentiate between the stages of the infection of TB and concluded that the results were too inconsistent between patients. Chegou *et al.* [55] did an extensive review of individual biomarkers that might be useful for the detection of Mycobacterium tuberculosis and stated that the interaction between TB and the infected host is not yet completely understood. The same study concluded that markers such as induced protein 10, interleukin 2, monocyte chemoattractant protein 1, monocyte chemoattractant protein 2, interleukin 1 receptor antagonist and macrophages inflammatory protein-1beta might be promising for future work, as they are induced in high levels which makes them easier to utilise for diagnostics.

This study is specifically focused on the development of a biosensor and its functionality can theoretically be expanded to different biorecognition elements. This makes it a versatile tool to be adapted to detect different types of protein. The justification for this biomarker is because of its use in commercial devices to detect tuberculosis.

2.3.4 Summary

This section discussed various types of electrochemical detection methods used in literature. This includes potentiometric, amperometric, and volammetric detection modes. The differences were highlighted and its implementation was critically discussed. The subject of electrochemical experiments was expanded to include the topic of crosslinking. Some of the mechanics of crosslinking were discussed and different methods were compared. The choice of biomarker is discussed and it was concluded that it is a practical choice for the purpose of the project.

2.4 Project objectives

The primary objective of the project is to investigate the possibility of detection of interferon gamma with a biosensor and develop a protocol for this method. It was decided that the focus to achieve this objective would be on electrochemical sensing techniques,

based on the literature previously discussed. A review of the techniques is done in the following chapter.

The secondary objective is to develop a biosensor based on the findings if interferon gamma can successfully be detected. The goal is expanded to:

1. match or improve on the findings of the commercial sensor
2. be developed in house with the available resources and equipment
3. be fabricated from materials that do not require special treatment
4. be simple and straightforward in design

2.5 Proposed methodology

The proposed methodology to meet the objectives of the project is to firstly develop the biochemical detection of interferon gamma with a commercial sensor. With the success of this, a similar sensor can be developed with the secondary objectives in mind. A short summary of the proposed methods are given here, followed by a list of the main materials and reagents. An expanded and detailed description of the methods are given in Chapter 4.

2.5.1 Methods

The methods to be used by this study was derived from a number of different sources. Taking into consideration the different aspects of a biosensor, the following can be said:

Transducer: The proposed transducer is a carbon nanofibre mat, as used in Eissa *et al.* The study came to the conclusion that the nanofibres outperformed other electrochemical sensors due to the high surface area the fibres provide.

Crosslinking: The crosslinking follows the promising work of diazonium salt electrografting to the sensor surface. The carboxyl group activation would then be done with a standard EDC/NHS protocol.

Biomarker: Interferon gamma is to be used as the biomarker because of its commercial use to diagnose tuberculosis.

Detection: The proposed detection method is to be determined by analysing the effect of thee different cases, namely unlabelled protein detection, labelled protein detection, H_2O_2 addition to the electrolytic buffer to induce the spontaneous reaction, given by 2.3. The chosen electrochemical detection method is square wave voltammetry, due to its sensitivity to surface chemistry.

2.5.2 Materials and reagents

The carbon nanofibres used in this experiment was the remainder of a previous project. It was puchased at Pyrograf Products Inc. The product name is Pyrograf III Carbon Nanomat PR-19-XT-HHT.

The ELISA (enzyme-linked immunosorbent assay) kit was provided by Division of Molecular Biology and Human Genetics located at the Tygerberg campus of the University of Stellenbosch. Two kits were supplied, equine and human interferon gamma. The supplying company was Mabtech, Sweden.

The commercial electrochemical biosensor was purchased at DropSens, Spain. The product was 50 sensor with screen printed carbon electrodes modified with carbon nanofibres.

Chapter 3

Electrochemical study

This chapter briefly reviews the theory of electrochemistry and the potentiostats used for electrochemical measurements. This is followed by a comparison of literature regarding commercial and research based potentiostats.

3.1 Introduction

The chapter discusses the theory of electrochemical measurements, and was adapted from the fundamentals and applications textbook, Electrochemical Methods, written by A. Bard and L. Faulkner [56]. It is described in context of the intended biosensing system. The goal is to present the necessary information to someone with an electrical engineering background to understand the intended chemistry of the detection method.

3.2 Electrochemical methods

Electrochemistry is a broad field that studies the interaction of chemical reactions and the electrical properties of these reactions. This includes the charge of electrical fields and the current passage due to these reactions.

In this project, the interest is the study of the interaction of an electrolyte and electrodes. A typical electrochemical cell would have two or three electrodes immersed in the electrolyte. The electrodes are named the working and counter, and the additional third the reference electrode. The electrolytic liquid is an ionic conductor that has certain electrical characteristics.

The working principle of the electrochemical cell is that the potential of the system results in a current that is related to the conditions of the materials and composition of the electrodes and electrolyte. The potential can be varied with time in different methods to produce a characteristic changing current. This changing current can be analysed to provide useful information regarding the chemistry in the electrolyte and the electrodes.

In a three electrode cell the current is passed between the counter and working electrodes. The counter electrode composition is usually chosen so that it does not produce ions that may interact with the working electrode. Instead, the working electrode is used as a completion of the cell circuit for the passage of electrons. The reference electrode is used to monitor the potential of the working electrode by placing it in close proximity. It is

chosen to have a high-input impedance so that the current flow from it might be negligible to the system. For the purpose of surface chemistry, the three electrode system is preferred because of the independence of the potential monitoring via the reference electrode.

The basic experimental setup is given in Figure 3.1. The experiment is controlled with a potentiostat. These devices are developed to deliver the required potential sweep and measure the current based on the timings used by the sweep, unique to different analysis techniques.

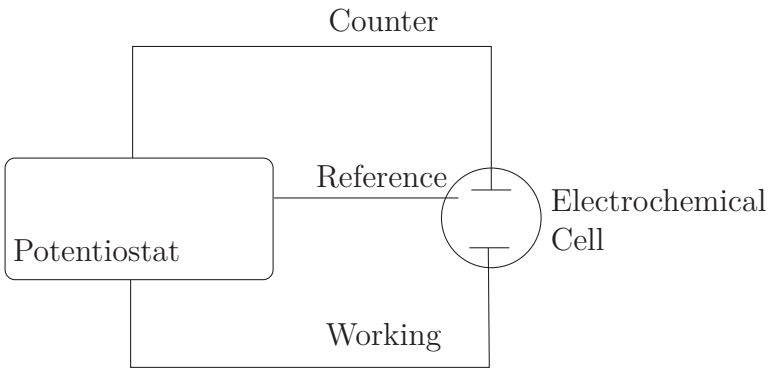

Figure 3.1: Typical experimental electrochemical setup

There exists two main type of processes at the electrodes. The first is the electron transfer due to the faradaic processes. This is illustrated by a simple redox couple in the reaction given by 3.1, and is governed by Faraday's law. This is the response that is of interest when conducting experiments. It is also the only process that contributes to the current flowing between the electrolyte and the electrodes, where the electrons can move between the solution and the electrodes.

$$\mathrm{Ox} + \mathrm{e} \rightleftharpoons \mathrm{Red} \tag{3.1}$$

The second type of process is all the nonfaradaic elements that exist at the interface of the solution and the electrodes. These effects do not contribute to the electron transfer across the interface, but instead can act as a capacitor, resulting in a charging current that reduces over time. Another effect is the electric double layer. This is described by considering the electrolyte as layers surrounding the electrodes, with the innermost adsorbed to it. The outer layers of the electrolyte can only interact with the electrodes with weak electrostatic forces, which makes these interactions independent of their chemical characteristics.

There exists many types of techniques used to analyse the current produced by the chemical reactions of the electrolyte. Two of these will be discussed, cyclic voltammetry and square wave voltammetry.

3.2.1 Cyclic voltammetry

Cyclic voltammetry is a linear potential sweep that is swept successively in both directions. The variables of such a sweep is the upper and lower switching potentials, the starting potential, and the scan rate. A sample of a four-cycle sweep is given in Figure 3.2, with the switching potentials at $\pm$ 600 mV, the scan rate 200 mV/s, and starting at 600 mV.

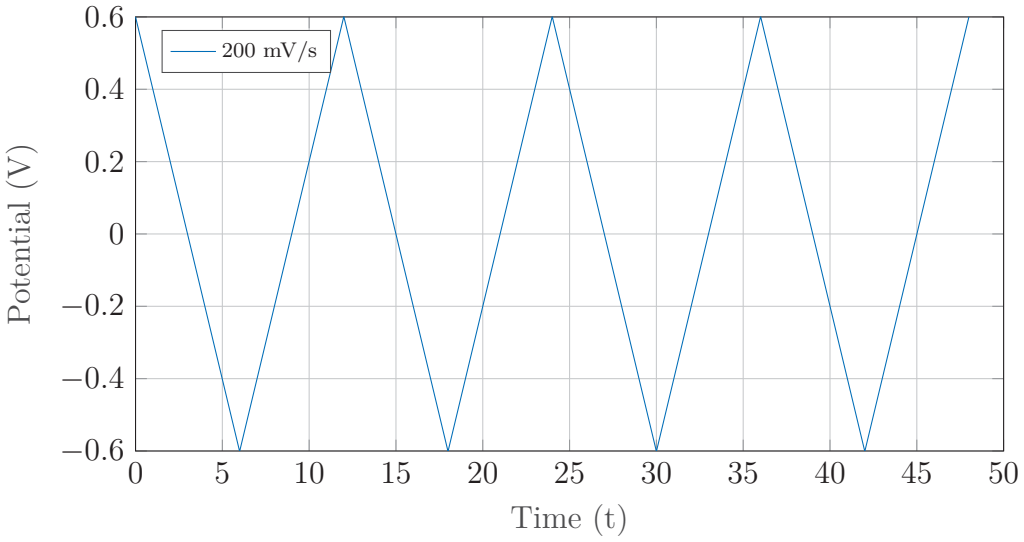

Figure 3.2: Four cyclic voltammetry potential sweeps

The effect of the potential sweep can be described by the Nernst equation [57] as

$$E = E^0 - \frac{RT}{nF} \ln\left(\frac{C_R}{C_O}\right), \tag{3.2}$$

where E (V) is the applied potential, n the amount of electrons transferred by the redox reaction, F (C mol^{-1}) the Faraday constant, T (K) the temperature, E^0 (V) is the former potential of the electrolyte relative to a hydrogen reference electrode, and R the universal gas constant. C_R and C_O (mol L^{-1}) are the concentrations of the reduced and oxidised species near the electrode surface, respectively. As the potential of the cell is changed, the only factor that can keep 3.2 balanced a the change in concentration of the two species present.

The measurements of interest with cyclic voltammetry is the ratio of the peak current of the forward and backward sweeps. For a nerstian response with a stable product, the anodic and cathodic peak current ratio should be 1. This is independent of the scan rate and the coefficients of diffusion of the electrolytic liquid. The only requirement for this is given by the switching potential as

$$E_\lambda > \frac{35}{n} \text{ mV}, \tag{3.3}$$

and the expected peak current can be described by the Randles-Sevcik equation as

$$i_p = 0.4463nFAC^0\left(\frac{nFvD_o}{RT}\right)^{\frac{1}{2}}, \tag{3.4}$$

where i_p (A) is the peak current, A (cm^2) the electrode surface area, D_o (cm^2 s^{-1}) the diffusion coefficient of the oxidised element, C^0 (mol cm^{-3}) the bulk concentration, v (V s^{-1}) the potential scan rate [57]. The interest of this equation is the indication that the surface area of the electrodes have a linear influence on the peak current of the redox reaction. The reason this is highlighted is because of the proposed design of the electrodes, using nanofibres. This has a high surface area, thus the peak current can be expected to

be proportionally higher. The other variable of interest is the square root of the scan rate, which has the same effect on the peak current as the electrode area. This is due to the decrease of the diffusion layer size because of less time for the ions to be transported away from the electrodes before undergoing the reverse reaction due to a reversed potential sweep. The measured current is not independent of the nonfaradaic currents in cyclic voltammetry due to the linearly applied voltage.

3.2.2 Square wave voltammetry

The second electrochemical method is square wave voltammetry. Square wave voltammetry is a pulsed voltammetry technique superimposed on a staircase voltammetry sweep.

The current is sampled at the end of each pulse and the difference of the upper and lower pulse sample is plotted relative to the staircase voltage at that point. An example of the potential function is given in Figure 3.3. The sampling technique allows for the influence of the capacitive current of the solution to be minimal, taking the sample when the current reached equilibrium. The forward and reverse pulsed currents, if plotted together, resembles a cyclic voltammogram. The variables of a SWV sweep are: ΔE_p (V) the pulse height, ΔE_s (V) the step size, f (Hz) the frequency of the steps, and t_p (s) the time per pulse. The time per pulse is often written as $f_s = 1/2t_p$ (Hz).

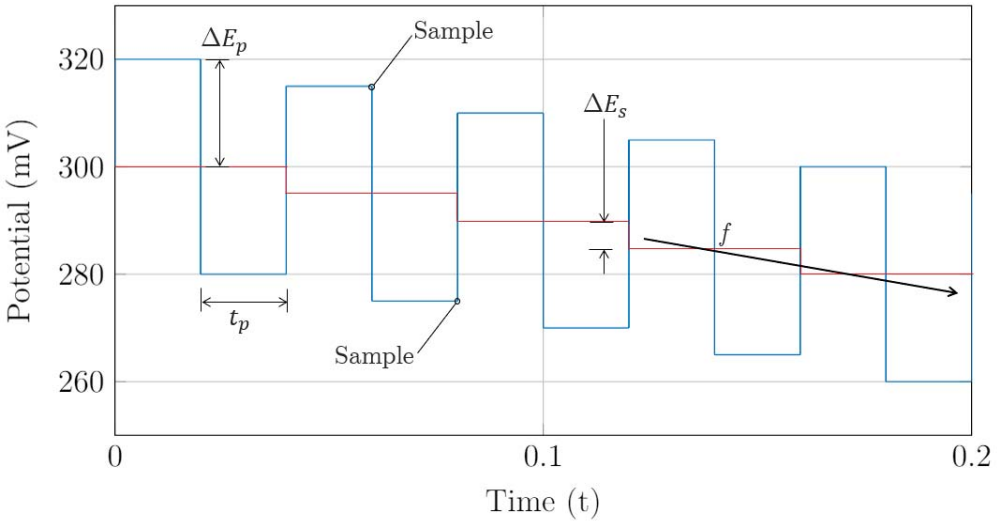

Figure 3.3: Square wave voltammetry potential sweep

The current response of the setup theoretically would be similar in different experiments if the following is kept constant: the potentiostat settings, the electrode material and surface area, and the concentration of the electrolytic liquid at the electrode surfaces. The peak current in the voltammogram will be reached at the half wave potential. This is described by the Nernst equation, under assumption that the reaction is fully reversible as

$$E_{1/2} = E^0 + \frac{RT}{nF} \ln \left(\frac{D_R}{D_O} \right)^{1/2}, \tag{3.5}$$

with D_R and D_O the diffusion coefficients of the two species. It can be seen that this potential is also a function of temperature and the standard potential of the electrolytic

liquid. Both these variables can be used to explain differences in the reduction potential of similar experiments, because of constant diffusion coefficients. The peak current at the half wave potential is described by

$$\Delta i_p = \frac{nFAD_O^{1/2}C_O^*}{\pi^{1/2}t_p^{1/2}}\Delta\psi_p, \tag{3.6}$$

where C_O^* is the apparent oxidised species bulk concentration. $\Delta\psi_p$ is a dimensionless peak current that depends on the amount of electrons transferred per event, the pulse height, and the step size. The equation demonstrates the influence the different parameters have on the experimental results. Since the peak current of SWV is a linear function of area and the concentration of the oxidised species, and counters the effect of the nonfaradaic currents extensively, it is a preferable choice for biosensing practices. This is because the interface of the electrolyte and the electrodes can be changed by immobilising biological matter to the electrodes.

3.2.3 Implications

The different techniques that will be employed in this project was discussed in full. While cyclic voltammetry is a simple linear sweep, compared to square wave voltammetry, it is not the preferred choice to employ for biosensing. This is due to the advantage of reducing the effect of nonfaradaic currents with SWV. Shown by 3.6, SWV is sensitive to perturbations to the electrolyte electrode interface. This project will utilise this characteristic to attempt to detect the concentration of the protein once immobilised on the surface of the working electrode.

3.3 Commercial potentiostats

An aspect of the system shown in Figure 3.1 that requires attention is the potentiostat. This section evaluates five commercial potentiostats. The different potentiostats are the entry level product for the range of devices they are a part of. These were selected because the following section reviews research based potentiostats, where cost was considered as the main driving factor for their development. The potentiostats reviewed are the Interface 1010T [58] (Gamry, USA), PalmSens4 [59] (PalmSens, Netherlands), PGSTAT101 [60] (Metrohm Autolab, Netherlands), DropStat [61] and µStat 200 [62] (DropSens, Spain).

A summary of the input potential characteristics for these devices are given in Table 3.1 and the output current characteristics is given in Table 3.2.

Device	Applied potential		
	Range	**Accuracy**	**Resolution**
Interface 1010T	±0.4 V, ±1.6 V, ±6.4 V	±1 mV ±0.2 % of setting	12,5µV, 50 µV, 200 µV
PalmSens4	±5 V, ±10 V	0.1 % ±1 mV offset	75 µV
PGSTAT101	±10 V	±0.2 %	3 µV
DropStat	±2 V	not available	1 mV
µStat 200	±2 V	0.1 %	1 mV

Table 3.1: Input potential characteristics of the commercial potentiostats

The PGSTAT101 device has the smallest potential resolution of the different devices, the largest potentail range (shared with the PalmSens4), and the best accuracy. An interesting feature of the Interface 1010T is the ability to set up multiple devices of the Interface to interact as a multichannel device. This enables seamless data acquisition. This device, the PalmSens4, and the PGSTAT101, are well documented, compared to that of DropSens. The DropSens devices have a potential resolution five times larger than the closest competitor, thus making it a decisive factor against it. The PalmSens4 and the PGSTAT101 have the largest range of potentials.

Device	Measured current		
	Range	**Accuracy**	**Resolution**
Interface 1010T	±100 mA (6 ranges)	±5 pA ±0.3 % of setting	±5 pA ±0.3 % of setting
PalmSens4	100 pA to 10 mA (9 ranges)	0.1 % at full scale	0.0006 % 5 fA on 100 pA
PGSTAT101	10 nA to 10 mA	±0.2 %	0.0003 % of current range
DropStat	±200 µA	not available	0.1 %
µStat 200	1 nA to 100 µA (6 ranges)	not available	0.1 %

Table 3.2: Measured current characteristics of the commercial potentiostats

The µStat claims to have the ability to do the lowest measurable current. The PGSTAT101 has the best resolution, but the PalmSens a higher accuracy. An interesting component of the characterisation of the devices is the accuracy and resolution of the measured currents are a function of the measurement setting selected by the device. This is due to the fact that current cannot be directly measured and has to be converted to a potential. The ranges of the current, such as the 9 ranges of the PalmSens4, means that for a select current range a specific resistor is used as the amplification factor to convert the current to a potential within the range of the analog to digital converter.

An additional factor that is worth mentioning is the size and weight of the potentiostats. All of the potentiostats are benchtop devices, with the exception of the DropStat. This

device is handheld and is powered by an internal battery. This explains the low input range. The weight comparison is given in Table 3.3. The DropSens potentiostats are the most portable potentiostats.

Device	Interface 1010T	PalmSens4	PGSTAT101	DropStat	µStat 200
Weight (kg)	2	0.5	2.1	0.071	0.09

Table 3.3: Potentiostat weight comparison

This comparison was done to get an understanding of the characteristics of commercial potentiostats. When selecting a device, it is important to understand the dynamics of the experiments that will be performed and the requirements of the measurements.

3.4 Research based potentiostatic devices

This section reviews different potentiostats developed in literature. The basic design of a potentiostatic system is given by Figure 3.4. The key components of the device are the control amplifier, the generated signal, the cell potential regulation, the current to voltage conversion, and finally the current voltage measurement.

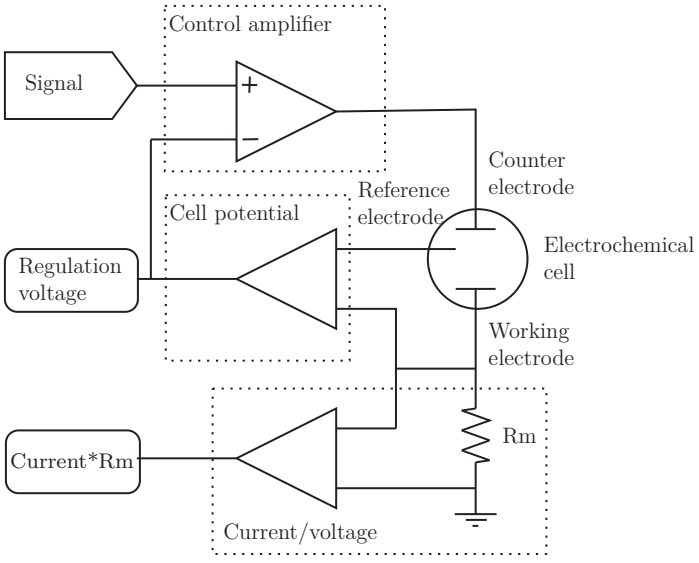

Figure 3.4: Typical potentiostat control circuit [63].

The design in Figure 3.4 is only a representation of the functions of the different components. A realistic model would use more complicated components and circuitry. This is due to the nature of the electrochemical cell and the function of potentiostat to control the potential of the cell regardless of its impedance. As seen in Section 3.3, the measurements are a function of the stability and reliability of not only the current measurements, but also the input potential.

These potentiostats can be controlled by either a microcontroller that communicates with a computer, or purely by a microcontroller on its own. The grade of amplifiers used in the design in conjunction with the digital to analog converter (DAC) would mainly determine the resolution of the system. Classic trade-offs such as speed versus resolution, cost versus

accuracy, and many more are a design factors in cheap devices. Five devices were selected from literature and reviewed in the following sections.

3.4.1 CheapStat

A device was developed by Rowe *et al.* [64], named the CheapStat potentiostat. The motivation for the development was to provide the means for poor settings to have access to a cheap potentiostat. This includes teaching environments and food monitoring.

The device could generate waveforms for anodic stripping, square wave, cyclic, and linear voltammetry. The hardware and software design were released under an open licence. The operation of the device was tested with different techniques. This included a method to electrochemically detect the concentration of a specific DNA sequence with square wave voltammetry, and by recording the response of ferricyanide to cyclic voltammetry. The microcontroller that controls the system is an Atmel XMEGA with inbuilt analog to digital converter (ADC) and DAC capabilities. Texas Instuments TLC2262CP operational amplifiers were used because of their low input bias current. The device has an applied voltage range of ±990 mV and a wave form generator of 1 to 1000 Hz. The measured current ranges from 100 nA to 50 µA. This is measured over a constant resistance, thus the range can be changed by manually changing this resistance accordingly. The device weighs a total of 115 g and is powered and controlled by a computer via a Universal Serial Bus (USB) connection.

There was no reported accuracy, resolution, or a comparison to a commercial device. The device was tested under various conditions and reported to function as expected. The goal of the project was achieved, where a product was developed that was able to provide an easily fabricated, usable, and modifiable potentiostat.

3.4.2 Point-of-need potentiostat

Bezuidenhout *et al.* [65] developed a potentiostat based on an LMP91000 sensor [66] (Texas Instruments, USA). An interesting aspect of the device is that it was developed in South Africa, by a research group at the University of Pretoria. The device utilises the internal voltage regulator of the microcontroller, Arduino UNO, to create the upper and lower voltage range of the applied potential. This is done by setting the reference voltage to a certain value of the internal 5 V supply. This creates a maximum dynamic range of 5 V either upwards or downwards, but at the cost of the other. The device was compared to a commercial potentiostat using cyclic voltammetry with 0.1 M KCl in a solution of 5 mM ferricyanide as the electrolyte and Dropsens electrodes. The results were compared on the base of the peaks of the average of three potential cycles. The standard deviation for these cycles were compared, finding that the developed device similarly produced repeatable results.

The key component of the device is the LMP91000. This component is a programmable analogue front-end that is used as the potentiostatic device. The current ranges from 5 µA to 750 µA, with an unknown accuracy and resolution. The applied potential has a resolution of ±2% generally. It has 7 programmable gain resistors and 3 reference voltage modes.

3.4.3 Dual-microprocessor potentiostat

Huang [67] addressed the signal processing capabilities of a potentiostat but utilising two microprocessors for a single electrochemical setup. The first microprocessor was used to generate the required waveform. The second was used to measure and process the measurements. This processor was also used in conjunction with a programmable resistor to select the range of the measured potential relative to the current flowing through the working electrode. The schematic of this device is given in Figure 3.5.

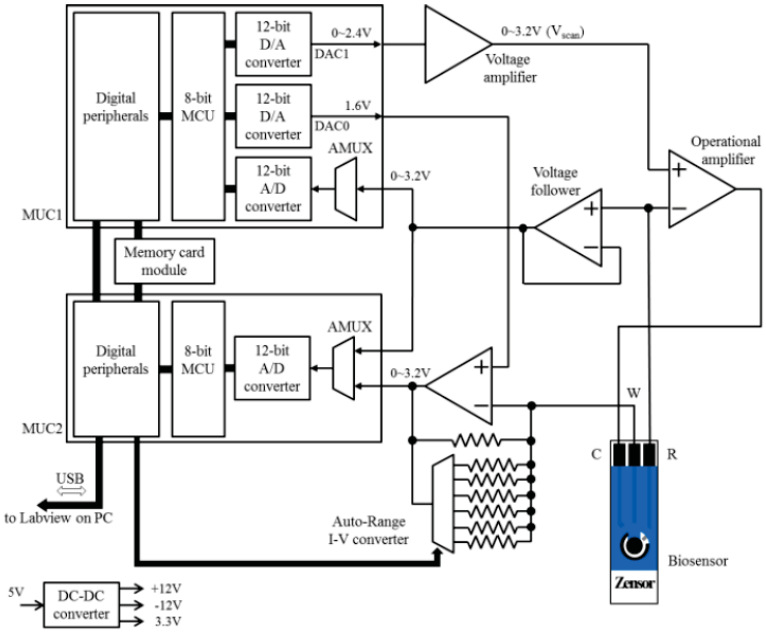

Figure 3.5: Dual processor potentiostat [67].

The specifications of the device was given as: potential range ±1.6 V, 1 mV resolution, scan rate of a minimum 5 mV/s, and a current range of 160 mA to 16 mA, at a resolution of 8 µA and 80 pA, respectively. The device uses C8051F005 microcontrollers with 12 bit ADCs and 12 bit DACs. The device was compared to a commercial potentiostat, and found to have comparable results. The exact comparison was only presented graphically, and the amount of experiments unknown.

3.4.4 DStat

A potentiostat called DStat was developed by Dryden and Wheeler [22]. The motivation for this was to add to the knowledge gap of the operation of potentiostats. This device was compared in literature to that of the CheapStat device discussed in Section 3.4.1.

The device used a 16-bit DAC to achieve a resolution of 46 µV on the input potential. An observation made by Dryden and Wheeler was that the resolution of the ADC was limited by the step size, not the noise of the analogue system. This was validated by simulating the open circuit noise levels and experimental tests. The current-to-voltage gain was increased and the resulting standard deviation of the noise amplitudes were calculated. This can be seen in Figure 3.6. It can be seen that their use of a 16-bit ADC was justified.

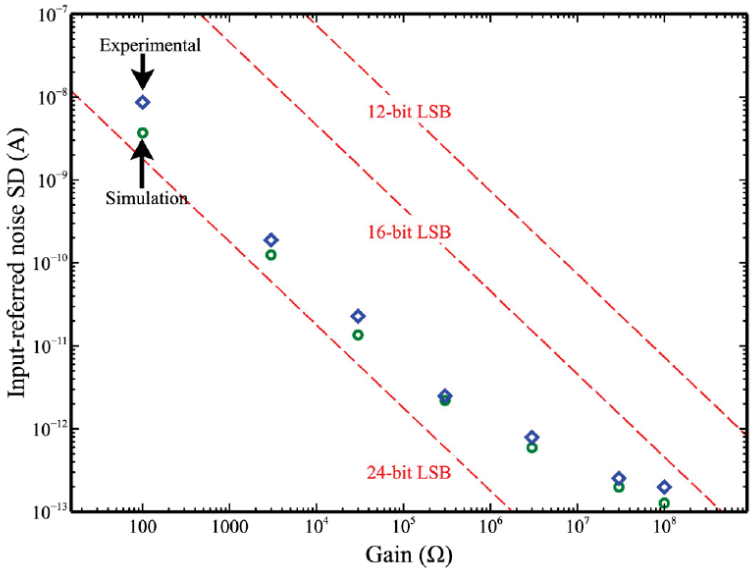

Figure 3.6: Open circuit current standard deviations noise amplitudes [22].

The microcontroller used was a ATxmega256A3U to transmit the measured data to a computer for analysis. An upper frequency limit of 30 kHz for the input signal was reported. The circuit was simulated to get the absolute errors of the input potential and measured current. These were found to be 1 nV and 50 fA, respectively. The control amplifiers used (listed in the supporting material) are LMP7702 and LMP7721 operational amplifiers. The LMP7702 was used for the potential control and the feedback buffer. This amplifier was chosen because of its large bandwidth, low input bias current, a large open loop gain, and small voltage noise densities. The LMP7721 was used as a transimpedance amplifier because of its extremely low input bias current of ±20 fA.

3.4.5 UWED

The final research-based potentiostat that was reviewed was developed by Ainla *et al.* [68]. The device was called a Universal Wireless Electrochemical Detector (UWED). The motivation to develop the device was to enable resource-limited areas to do electrochemical testing on an inexpensive, hand held, battery powered device, with only a smartphone at hand. It communicates with the smartphone via BLE (Bluetooth Low Energy). The smartphone app then uploads the data to a cloud server where it can be analysed further. The UWED requires a certain protocol to be uploaded to the device, limiting its capabilities until a new protocol can be flashed. The device is shown in Figure 3.7 in comparison with a smartphone for size.

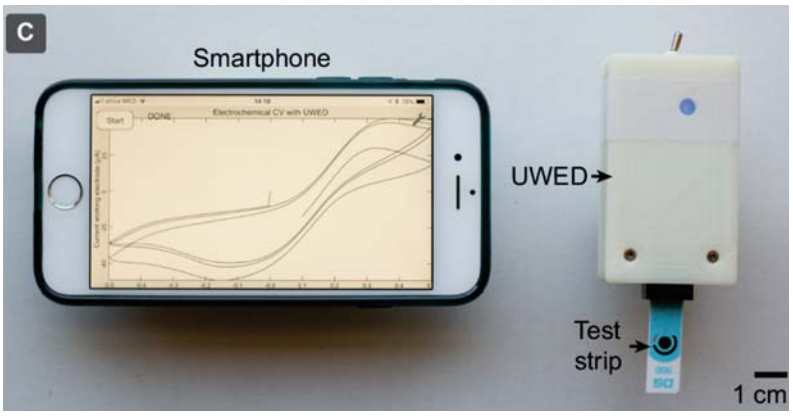

Figure 3.7: Universal Wireless Electrochemical Detection [22].

The device was reported to have a potential range of ±1.5 V and a current measurement range of ±180 µA. An RFduino microcontroller was used to control the device, and a 10-bit ADC. The noise level ranged from 27 µV to 47 µV. The software and hardware was released as open-source. An interesting aspect of the design was that the DAC signal was post-filtered for noise suppression before being applied to the counter electrode.

3.4.6 Summary

The most important aspect addressed by literature on potentiostatic devices was the cost. This was the main driving force for the development of these projects. These devices do not perform as well as the commercial devices, which would be expected of a project where cost and performance have to be weighed against each other. It was found that the literature potentiostats were not as well characterised as commercial devices. Commercial devices are easily classified according to their range, accuracy, and resolution from the data sheets provided.

Home-built potentiostats lack a specific reliability test. An example would be where a calibration cell could be used to used to test the response of the potentiostats. The current measurement and applied potential systems have to be tested and validated separately before integration. All this said, the literature does help bridge the gap towards understanding the dynamics and requirements of a potentiostatic system.

3.5 Conclusion

This chapter discussed the fundamentals of electrochemistry required to understand the development and goal of the project. The operation of potentiostatic devices was reviewed and the available potentiostats were briefly discussed. The potentiostat is a critical component for the experiments that were conducted for the fulfilment of this project.

Chapter 4

Experimental methods

This chapter discusses the experimental procedures followed. The validation of the different aspects of the sensor was discussed.

4.1 Introduction

The procedure followed to prove the assay validity was divided into two objectives. The first objective was to test the biosignature binding and electrical signal with an existing biosensor, and the second the development and testing of a manufactured biosensor. All electrochemical testing conducted in this chapter were done with a Gamry Interface 1000. The specification sheet can be found in Appendix B.

4.2 Biochemical detail design

The methodology that was developed to test the validity of the biochemical aspect is given in Figure 4.1. It was developed from literature and the ELISA protocol of the protein. The goal was to determine the validity of the sensing mechanics by using a similar sensor used in literature, but with the chosen protein. An important design choice is the type of electrolytic liquid used for the electrochemical tests. It was decided that potassium ferricyanide dissolved in phosphate buffed saline (PBS) would be used, since it is the standard used in many other studies.

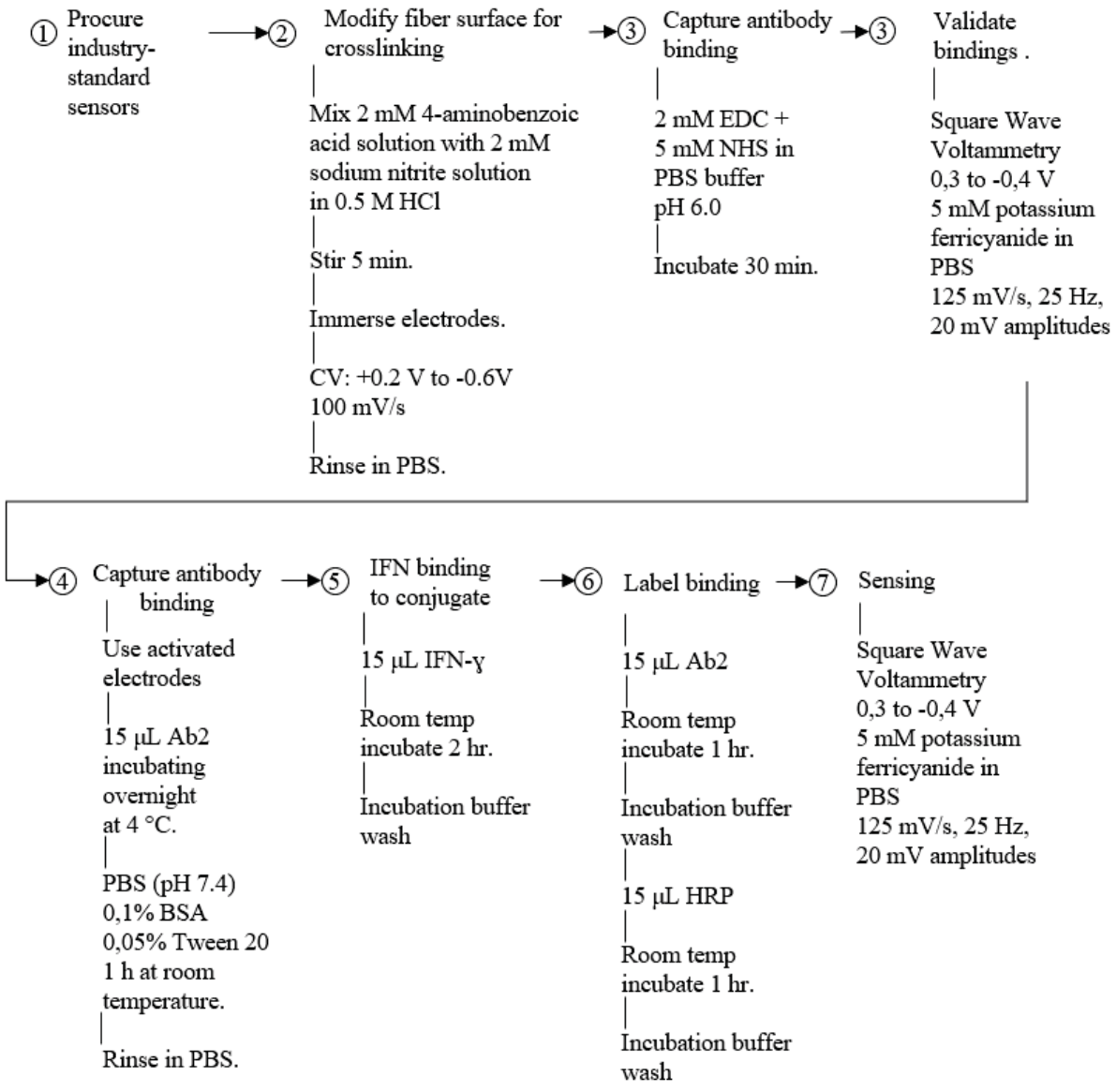

Figure 4.1: Experimental design flow

The sensors procured to validate the assay principle is a DropSens 110D carbon screen printed electrode (SPE) with a modified carbon fibre surface. An example of a sensor is given in Figure 4.2.

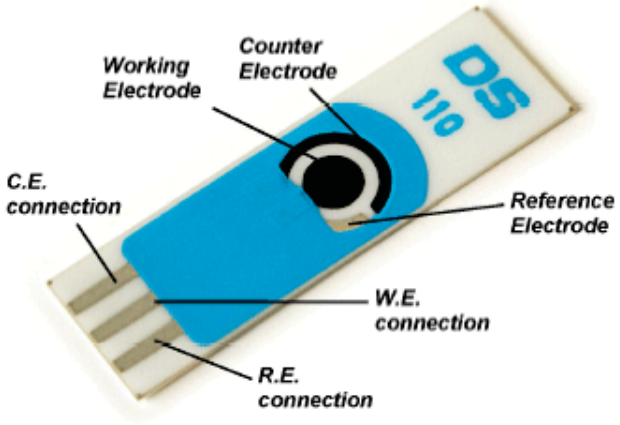

Figure 4.2: DropSens screen printed electrode [69]

4.2.1 Chemical reactivity

The goal of the first tests were to validate the electroreactivity of the sensor. The DropSens sensors were purchased and the sensors were tested before any surface modification was done. The first experiments were simple cyclic voltammetry sweeps to determine the sensor stability and to test for any defects. The cycles were conducted in 5 mM potassium ferricyanide dissolved in PBS. The PBS was a good choice for a buffer because it has an anodic peak at 1.16 V and cathodic at 0.69 V [70]. This is well above the redox potential of ferricyanide of 0.3704 V [71]. The electrolytic liquid reaction is given by

$$\mathrm{Fe(CN)_6}^{3-} + \mathrm{e}^- \rightleftharpoons \mathrm{Fe(CN)_6}^{4-} \qquad [0.3704V]. \tag{4.1}$$

In order to compare the sensors with literature, the CV parameters were set to be as follows: 4 cycles at 100 mV per second, 2 mV steps, and swept between a potential of +0.6V to -0.6V.

The second unmodified test conducted was square wave voltammetry. The experiments were conducted by adding the electrolytic liquid on to the sensor and applying a potential sweep to the electrodes. The current was recorded and analysed to confirm its electrolytic activity. Again, the concentration of potassium ferricyanide used was 5 mM, dissolved in the PBS. The specific concentration was chosen from literature to enable comparison. The current at which protein denaturation would happen was unknown, thus it was decided that the chosen concentration was sufficient because it has been used in similar experiments before. The concentration of the electrolytic analyte at the reference electrode proportionally affects the peak current of the measurement [36], thus an increased concentration would also lead to increased peak current measurements, which is also verified with 3.6. The SWV settings were as follows: sweep from +0.3V to -0.4V in steps of 5mV, 20 mV amplitude, 125 mV per second, and 25 Hz.

A sweep of the unmodified fibres can be used as a reference graph to indicate any changes that happened on the surface of the electrodes between experiments. For example, if a molecule is attached to the surface of the carbon, the interaction of that general area between the electrode and electrolytic liquid might be obstructed due to the charge of the attached molecule. This would proportionately affect the measured peak current flowing

between the electrodes because of the lower concentration of the electroactive species at the immediate surface of the electrodes. The difference in the current peaks between unmodified fibres and functionalised fibres would theoretically indicate this change. That said, the current might not diminish as the result of the additional molecule on the surface. A positively charged molecule could attract the negatively charged electrolytic fluid and under ideal conditions not interact with it. This would probably be the case if the reduction potential of the charged molecule is far away from the potential of the electrochemical cell at that stage. If the potential sweep passes the redox peak of the electrolytic liquid, the negative mass would be in large quantities at the surface of the carbon, resulting in a higher peak current than expected. This peak current might not be higher than that of the unmodified fibres, but relatively higher than an electrode with a different concentration of the same molecule on its surface.

4.2.2 Crosslinking

The diazonium salt was prepared in situ, followed by electrografting it to the sensors. The base molecule used for crosslinking was 4-aminobenzoic acid ($C_7H_7NO_2$), given in Figure 4.3.

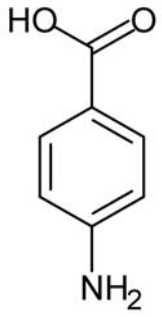

Figure 4.3: 4-Aminobenzoic acid

Firstly, hydrochloric acid (HCl) was diluted to 0.5 M in deionised water. This was done by adding 28.48 ml HCl (32% weight) slowly to 125 ml deionised water. The remaining amount of water was used to fill up the beaker to 500 mL to achieve the desired concentration. The salt was prepared by adding 2mM 4-aminobenzoic acid to the HCl solution. 2mM sodium nitrite ($NaNO_2$) was added to the mixture and the solution was stirred for five minutes before use. This was done at room temperature and the pH of the final solution was 3.5. 50 ml of the diazonium salt was freshly prepared before a set of tests to ensure that the repeatable results were obtained. The salt degrades in one of two ways, heterolytic or homolytic [72], shown in Figure 4.4. The heterolytic degradation, or dediazoniation, forms a stable N_2 and a metastable intermediate that finally forms phenols. This degradation is spontaneous and happens over time. The homolytic dediazoniation requires an external source for an electron transfer. This can come from an additional solvent, photochemistry, or by undergoing reduction at an electrode of an electrochemical cell.

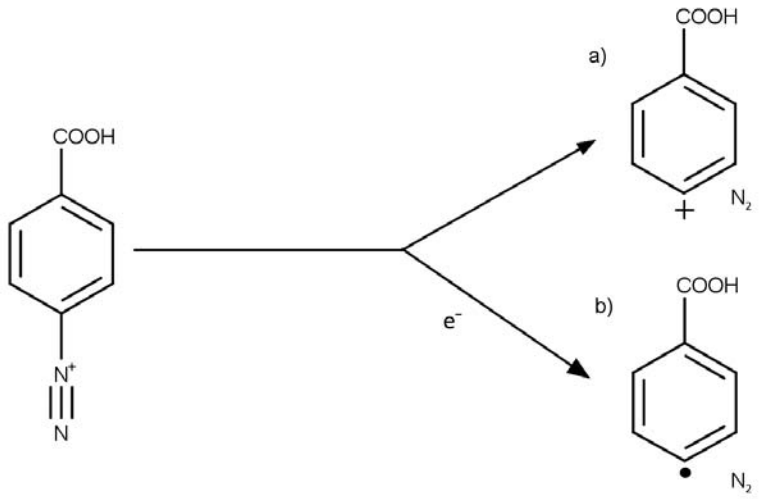

Figure 4.4: Diazonium salt degradation pathways: (a) heterolytic and (b) homolytic

The aryl radical produced by the homolytic reaction covalently bonds with the carbon electrode after the reduction of the diazonium salt. This is due to adsorption of the salt to the electrode surface before reduction, and the radical reduction potential is much more positive from that of the diazonium salt [73]. The electrografting was conducted by applying the salt to the sensor electrodes. In suspension, the sensor was connected to the potentiostat and subjected to a number of potential sweeps. The potential was swept at 100 mV per second between +0.2 V and -0.6 V, starting and finishing at +0.2 V. The potential was chosen from literature [41] where the same solution was used in an electrochemical setup with similar electrodes. The amount of sweeps were varied between 1 and 15 to test for the ideal amount of cycles for sufficient surface coverage. The chemical process induced by this electrochemical reduction is given in Figure 4.5.

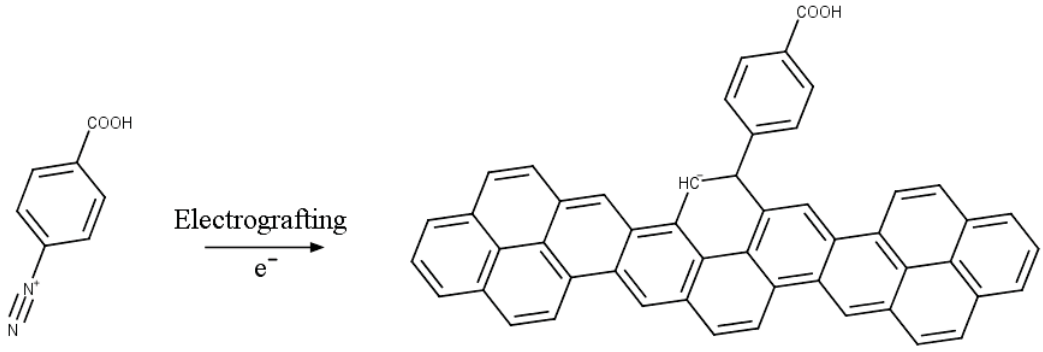

Figure 4.5: Electrochemical grafting on to carbon

The grafting was validated by using SWV and analysing the relative peak change to the clean carbon SWV graphs. The paramaters and electrolytic liquid used was the same as that described in Section 4.2.1. The immobilised substrate provided carboxyl groups that could be activated for crosslinking. The use of this method provided stable covalent crosslinking sites to the carbon nanofibres with high surface coverage.

4.2.3 Linker activation

After electrografting the nanofibres, the available carboxyl groups were activated by using EDC (1-ethyl-3-[3-dimethylaminopropyl]carbodiimide hydrochloride) and NHS (N-hydroxysuccinimide), both given in Figure 4.6. EDC is a carboxyl and amine-reactive zero-length crosslinker. The EDC is used to react with the carboxyl groups, which then forms an isourea by-product. After the initial reaction, the EDC forms an amine-reactive O-acylisourea. This in turn froms an amide bond after reacting with an amino group. The solution formed is unstable, and thus the procedure relies on NHS for stabilisation.

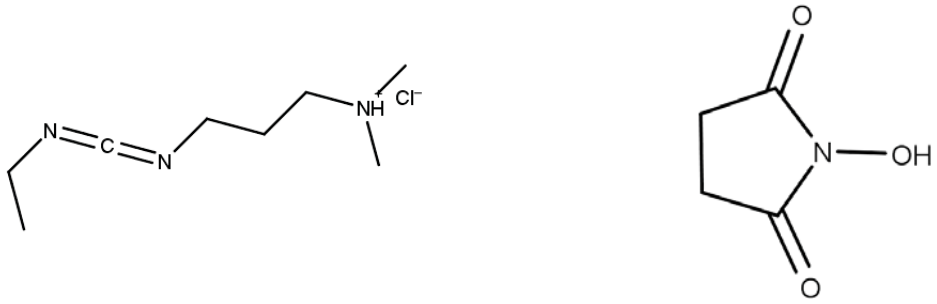

(a) The skeletal formula for EDC (b) The skeletal formula for NHS

Figure 4.6: Crosslinking base chemicals

The protocol started by creating the acidic condition for the carbodiimide reaction. A MES (4-morpholinoethanesulfonic acid) buffer was created by dissolving 0.1 M MES in 40 ml deionized water. 0.5 M NaCl was added to the solution. The pH of the buffer was increased to 6 by slowly adding $NaNO_3$ and periodic stirring of the solution in the beaker. 2mM EDC was added to the solution, followed by 5 mM NHS. The procedure is shown in Figure 4.7.

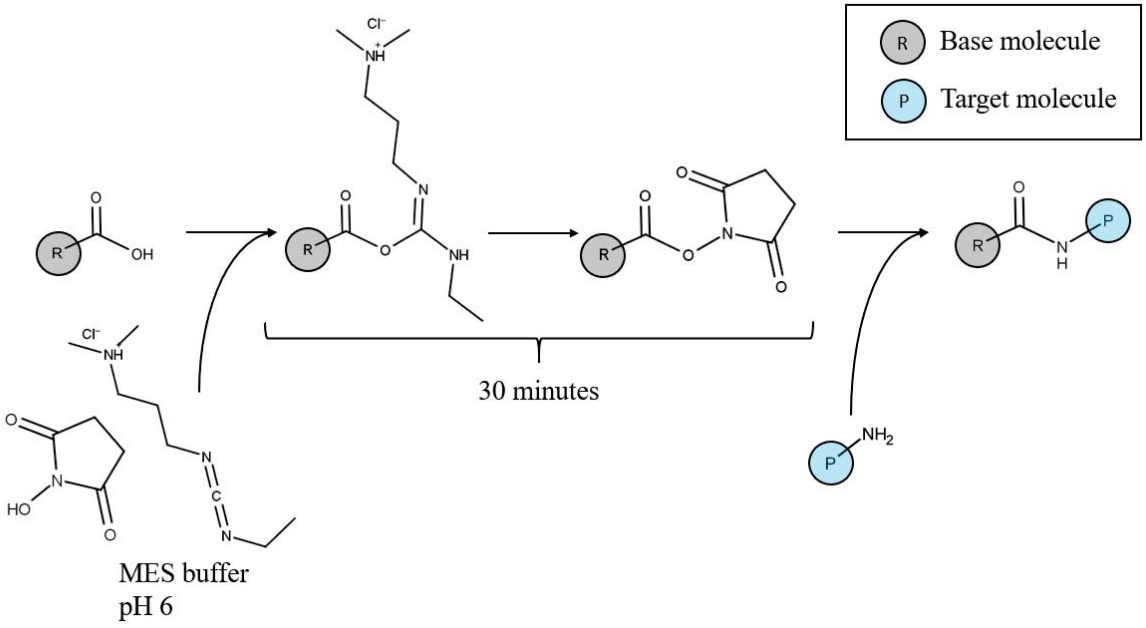

Figure 4.7: Crosslinker activation and immobilisation protocol

The activation solution was then placed on the electrografted sensors by adding 15 µl on the working electrode of each sensor. This is shown in Figure 4.8.

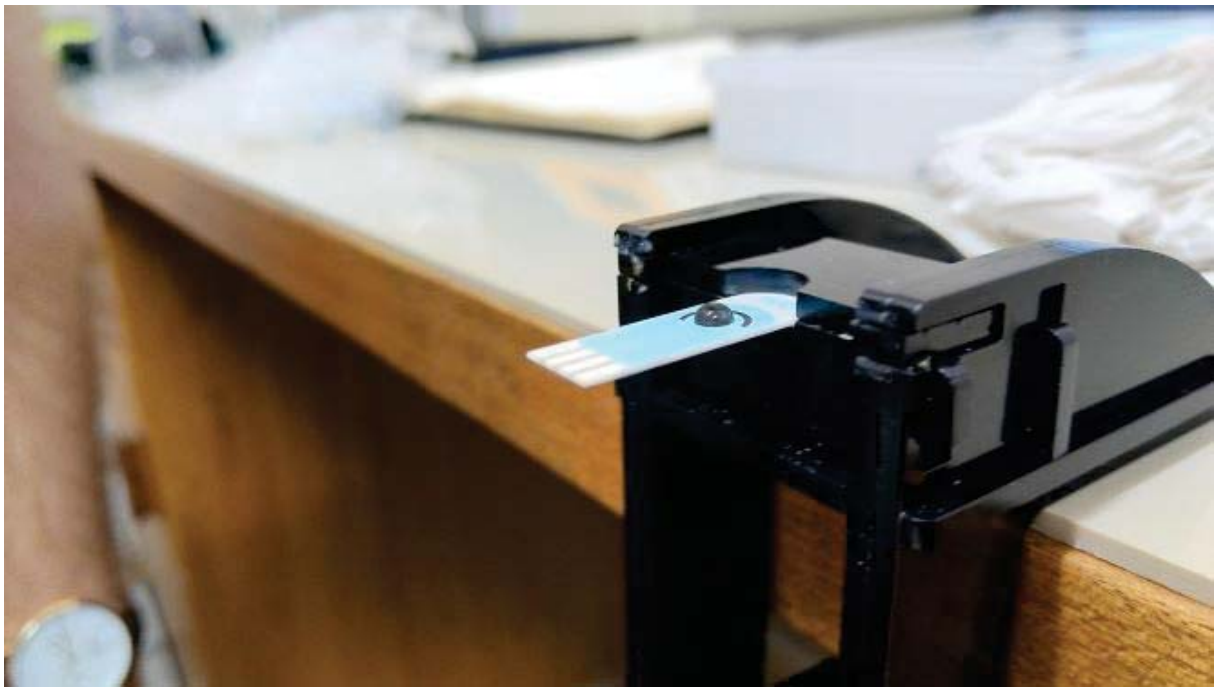

Figure 4.8: Activation solution placed on working electrode

The requirement for the target molecule shown in Figure 4.7 is that it should have amino groups available for the reaction. An antibody is a good example, because it has readily available amino groups for immobilisation. The immoblilisation happens because of the amide bond that form, as previously described.

4.2.4 Capture antibody linking

Following activation of the carboxyl groups, the target molecule was placed on the working electrode of the sensors for immobilisation. The protocol for this was developed from the ELISA protocols suggested by the supplying company (Mabtech). When not in use, the antibody was stored in the original container at 4°C.

The firstly the antibody saturation concentration was to be determined. The available antibody was equine anti-IFN-γ , a monoclonal capture antibody (MT 166). The antibody came in a 300 µl vial at a concentration of 0.5 mg/ml in sterile-filtered PBS with sodium azide (0.02%). The ELISA protocol requires the antibody to be diluted to 2 µg/ml in PBS which has a pH of 7.4, and then adding 100 µl of the solution per well. Since it was not possible to accurately determine the surface coverage of the linker, the ideal concentration of the antibody had to be determined.

The antibodies were diluted from 0.5 mg/ml to a set of five different concentrations. These concentrations were 100, 10, 1, 0.1, and 0.01 µg/ml. The highest concentration was achieved by pipetting 4 µl of the original sample in to 16 µl of PBS, pH 7.4. This was mixed by repeatably aspirating the sample with a pipette. The next concentration was made by removing 2 µl of the higher concentration to a new container containing 18 µl

PBS, thus diluting it with a factor of 10. The process was repeated until all of the desired concentrations were made.

The working electrodes of five DropSens sensors that had activated carboxyl groups were covered with 15µl of the different concentrations of the antibody solutions. This is the same as was illustrated in Figure 4.8. The sensors were then placed in an unused petri dish. An additional 1 ml of deionised water was placed in the petri dish separately. The water prevented the 15µl droplets to evaporate. It created a water saturated environment in the petri dish by dominating the initial evaporation until the environment reached equilibrium. Deionised water was chosen as a suitable liquid since the main ingredient of PBS is water. The petri dish was then placed in 4°C and left to incubate overnight.

Once the incubation was completed, the water was drained from the petri dish and the sensors carefully removed. Each sensor was washed with PBS two times to remove any unbound antibodies that might interfere with the sequential processes. The washed sensors were incubated for one hour at room temperature in PBS containing 0.05% Tween 20 and 0.1% bovine serum albumin (BSA), from now on referred to as the incubation buffer. The Tween 20 is a frequently used nonionic detergent that prevents nonspecific binding. The BSA is a stable globular protein that, in this case, blocks any open binding sites that might have not reacted with the antibodies. An illustration of the linked antibody is given in Figure 4.9.

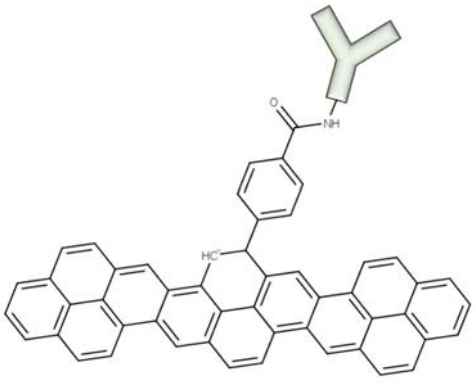

Figure 4.9: Monoclonal capture antibody linked to carbon

The sensors were washed finally with PBS containing 0.05% Tween 20 five times to remove all remaining unwanted molecules, henceforth called the wash buffer. Finally, the antibody linking was validated by SWV as in Section 4.2.1.

4.2.5 Interferon-gamma capture

The results of Section 4.2.4 provided by the SWV tests were used to decide on a suitable concentration of capture antibodies to use for the detection of IFN-γ . The process described by Section 4.2.2 and 4.2.4 was repeated, but with a single concentration of the capture antibody.

The next step was to bind the IFN-γ protein to the capture antibody. The same process was followed to dilute the protein as was when diluting the capture antibody. The protein

was supplied by the medical campus of Stellenbosch University, Tygerberg. The protein was recombinant equine standard at a concentration of 0.5 µg/ml and it was stored at -20°C when not used.

The protein was diluted to 100, 10, 1, 0.1, and 0.01 ng/ml. The first dilution was done by adding 8 µl of the original concentration to 32 µl of the incubation buffer. This was aspirated multiple times to mix the solution. The following dilutions were done by placing 4 µl of the higher concentration solution in 36 µl of the incubation buffer, until the final concentration was obtained. The solutions were placed in 15µl quantities on the sensors and incubated at room temperature for 2 hours. After incubation the sensors were washed five times the wash buffer. The sensor state at this stage is given in Figure 4.10.

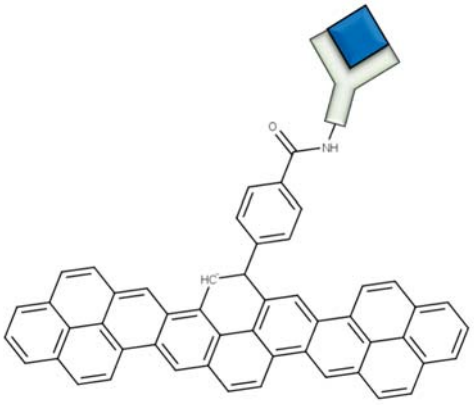

Figure 4.10: Interferon gamma captured by antibody

4.2.6 Signal antibody linking

The label molecule chosen was horseradish peroxidase (HRP), because this is the standard molecule used for a visual quantification in an ELISA test. The secondary antibody had to be linked to the interferon gamma to provide a base for the HRP to bind to.

The biotinylated antibody was diluted from 0.5 mg/ml to 1µg/ml in the incubation buffer as in an ELISA test. This was done by placing 1 µl of the antibody in 499 µl of the buffer. The diluted secondary antibody solution was placed on the sensors in 15 µl aliquots and incubated at room temperature for one hour. The sensors were then washed five times with the wash buffer. The capture second antibody is shown in Figure 4.11.

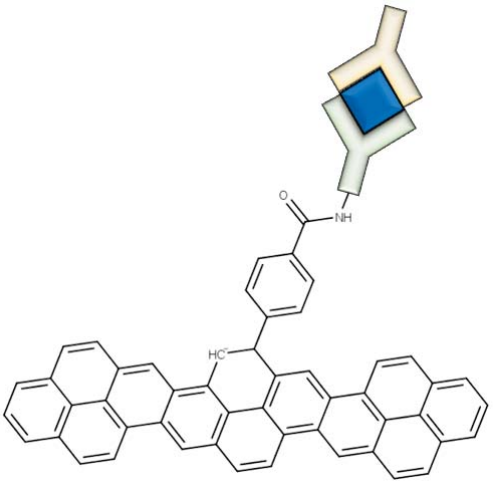

Figure 4.11: Secondary antibody on interferon gamma

The Streptavadin-HRP was diluted 1:1000 in the incubation buffer. This was placed on the sensors in 15 µl aliquots and incubated at room temperature for one hour. The sensors were washed five times with the wash buffer. The final configuration is shown in Figure 4.12.

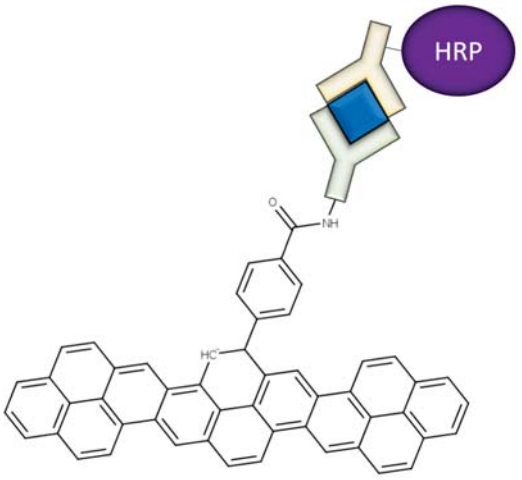

Figure 4.12: Final sensor surface configuration

The sensors were then tested with SWV as in Section 4.2.1, but with 5 mM hydrogen peroxide added to the ferricyanide electrolytic solution. The cycle of the theoretical electron transfer given in Figure 4.13. The purpose of the HRP labelling was to act as an amplifier for the standard electrolytic electron transfer.

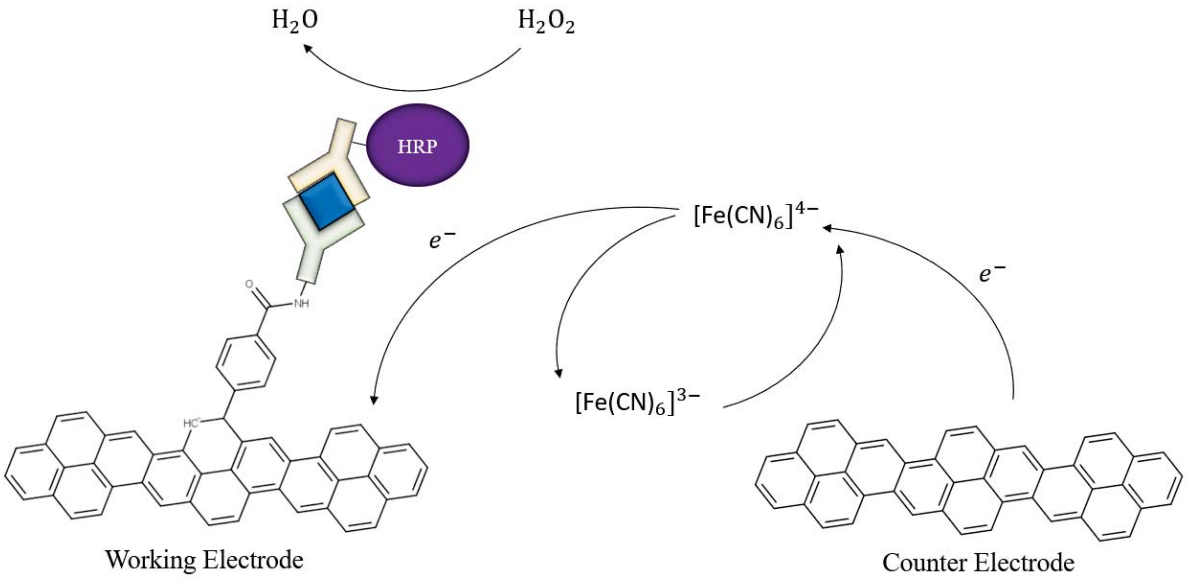

Figure 4.13: Sensor electron transfer

The usual reaction that took place is the same as in 4.1 with the addition of HRP to produce the well known oxidation of ferrocyanide by HRP [74]. This reaction starts with

$$\mathrm{HRP} + \mathrm{H_2O_2} \longrightarrow \mathrm{HRP{-}I}, \tag{4.2}$$

where the HRP is reduced to a first reduction state. It is further reduced by

$$\mathrm{HRP{-}I} + \mathrm{Fe(CN)_6}^{4-} \longrightarrow \mathrm{HRP{-}II} + \mathrm{Fe(CN)_6}^{3-}, \tag{4.3}$$

and then after the second reduction it is oxidised again

$$\mathrm{HRP{-}II} + \mathrm{Fe(CN)_6}^{4-} \longrightarrow \mathrm{HRP} + \mathrm{Fe(CN)_6}^{3-}. \tag{4.4}$$

4.2.7 Sensor development

The goal of the second phase of the project was to develop a biosensor in-house with the available equipment and materials as far as possible. The DropSens geometries were used as a design to base the sensors on because of its proven stability and to enable comparison of the signals of the different sensors. The geometry of the electrodes has no influence on the peak current of a reversible SWV system [75], but for thoroughness it was not changed. In total, seven different configurations were tested and tried to achieve a functioning sensor, four of which were worth mentioning. The development of these sensors are discussed in the next Chapter. The experimental procedures followed for the validation of these sensors were the same as the experiments completed by the DropSens sensors, starting at Section 4.2.1 and ending at Section 4.2.6. If a procedure was changed, this was noted in the experimental discussion.

4.3 Measurement definitions

The typical measurements that were taken during a SWV sweep are given in Figure 4.14. The forward current is the current sampled at the end of the upwards pulses of a

voltammetry sweep, and the reverse current that of the downwards pulses. The difference of these currents are then presented as the SWV voltammogram.

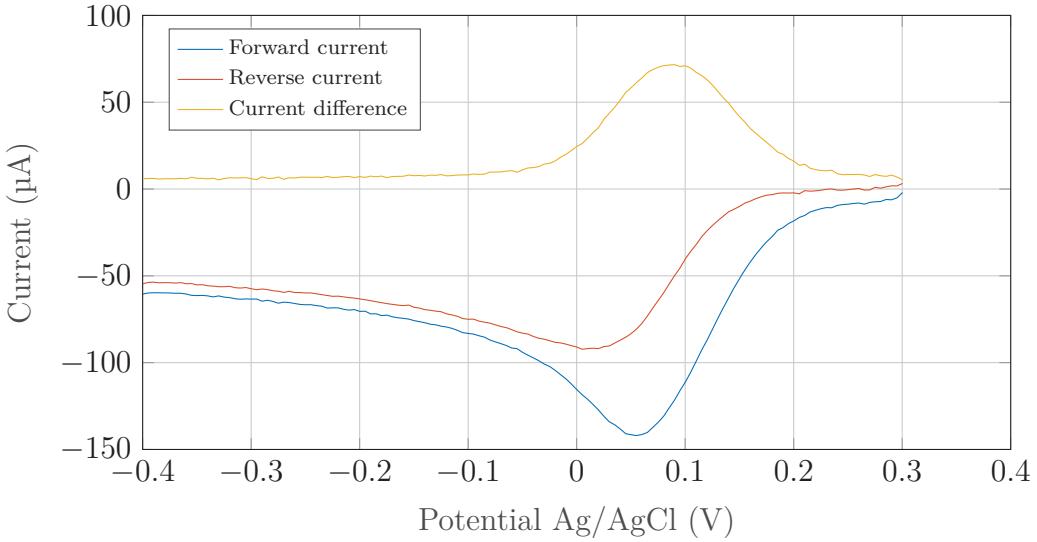

Figure 4.14: Different current response for SWV

Both the forward and reverse current curves carry information of the electrolytic system, but for this project only the current difference was considered in the data analysis to determine concentrations. The peak of the current difference curve relative to zero was used to compare the results of the different SWV experiments, after baseline corrections.

4.4 Analysis techniques

The key to square wave voltammery concentration analysis the comparison of the peak current of the different experiments. There exists elements embedded in the data that makes it not possible to compare unfiltered results.

The first of these is system noise picked up during data sampling. Depending on the signal-to-noise ratio, this can be improved by using a simple software filter. The second elements that could have an impact is the startup current of the electrochemical reaction. Acting as a charging capacitor, the current increases until it reaches an equilibrium value. The equilibrium value can be determined and then subtracted to aid in the analysis. The final major element is a general trend throughout the experiment. This could be due to an additional reaction because of contamination or a defect in the sensor, such as additional metal ion transfers between the electrodes. A normalising algorithm was developed to minimise the effect of these elements, and this was applied to each individual data set gathered from the experiments.

The main purpose of the normalisation algorithm was to identify the inflection points of the redox peak in the data set, add a baseline to these points, and compare the peaks relative to their baselines. This method was developed from analysing experimental results presented in literature and the data gathered during the experiments conducted for this project.

An example of the experimental results is given in Figure 4.15. Here the startup current can clearly be observed. This has no effect on the redox peak of the voltammogram, but from a data analysis perspective it would hinder sensitive minimum and maximum value finding methods. The data itself also seems noisy. The noise to signal ratio does not seem to be closely related. The peak itself is well defined beyond the noise and the steady state currents.

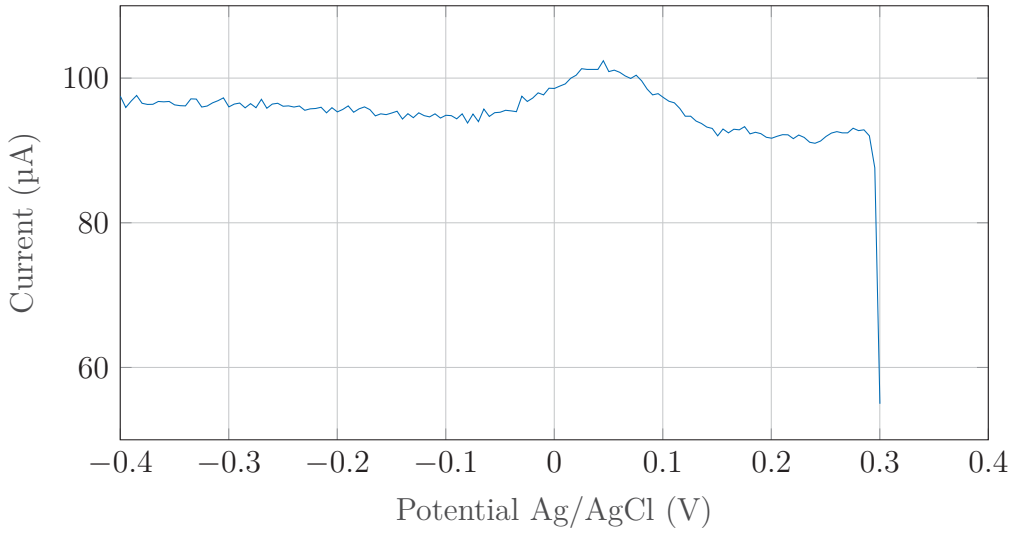

Figure 4.15: Unfiltered measured current of SWV response example

For analysis purposes, the startup current was removed from the data. Figure 4.16 shows the framed data used further by the algorithm to analyse the data to determine a baseline.

The data was also moved so that the final value was centred on zero. This helped keep track of accedental data skewing by visually comparing the final peaks with the centred data.

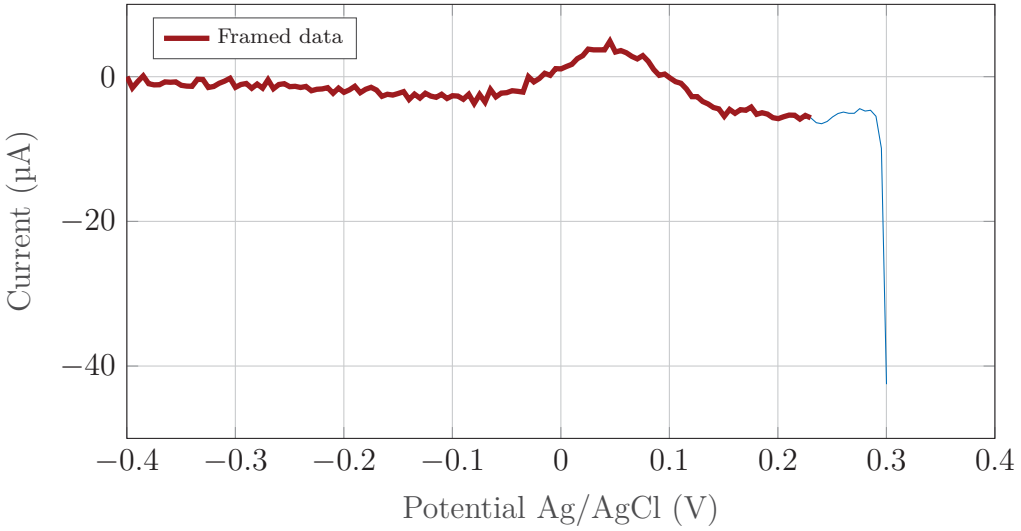

Figure 4.16: Frame data used for analysis of SWV response example

The next step was to filter the data with a low-pass filter. The chosen filter was a Savitzky-Golay smoothing filter. The filter employs convolution to preserve the original form of the data and reject noise. The filtered frame of data can be seen in Figure 4.17. In contrast to a moving average filtering technique, for a select frame of the data the Savitzky-Golay filter approximates the underlying function with polonomial function instead of an average constant. The frame of data, here a frame within the selected frame of data, is fitted with a polonomial of a certain degree by using a least squares fit. The process is repeated by moving the frame of data to include the next point in the data set after a successful polonomial fit to the previous frame. The accuracy of representing the original set of data is increased by increasing the order of the polonomial, and the smoothing increased with a decrease in polonomial order.

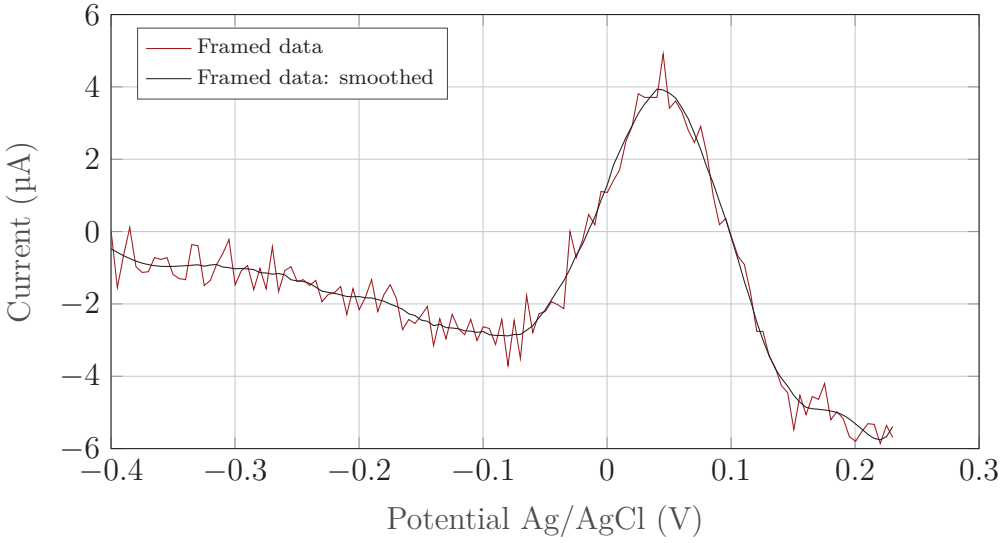

Figure 4.17: Filtered SWV response example

The derivative of the filtered data was used to determine the inflection points of the peak to the steady state current. This was done by finding the maximum and minimum values of the derivative near the expected redox reaction potential. The values indicated approximately the midpoint towards the sought inflection points. The iterations that followed searched for a minimum or maximum, or a zero to the left and right of the minimum and maximum values, respectively. These all indicated a change in the original data, which were the inflection points. A visual representation of the iterations can be seen in Figure 4.18.

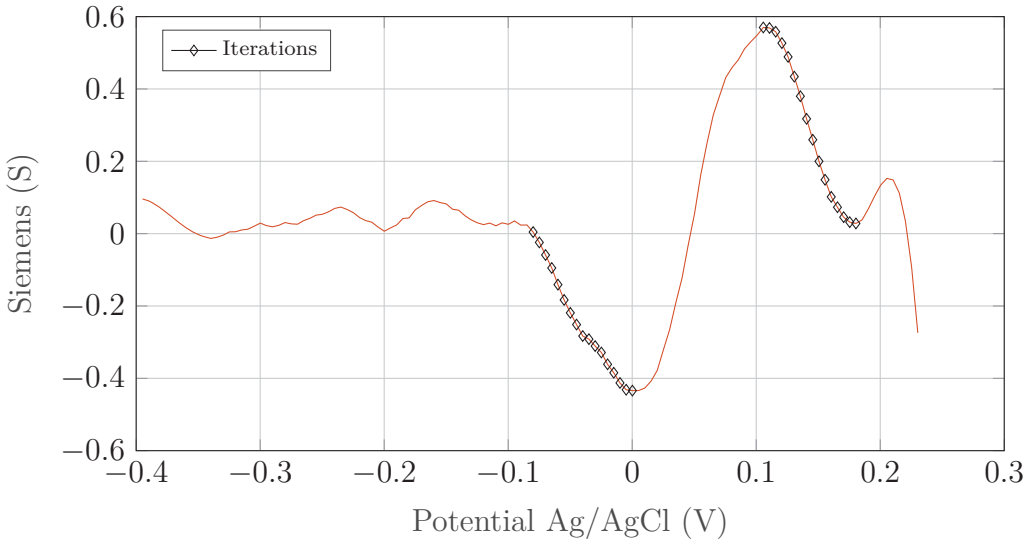

Figure 4.18: Derivative of SWV response example

The potential of the inflection points found with the derivative was then used to construct a baseline on the original set of data. The baseline constructed with the original unfiltered and uncropped data can be seen in Figure 4.19.

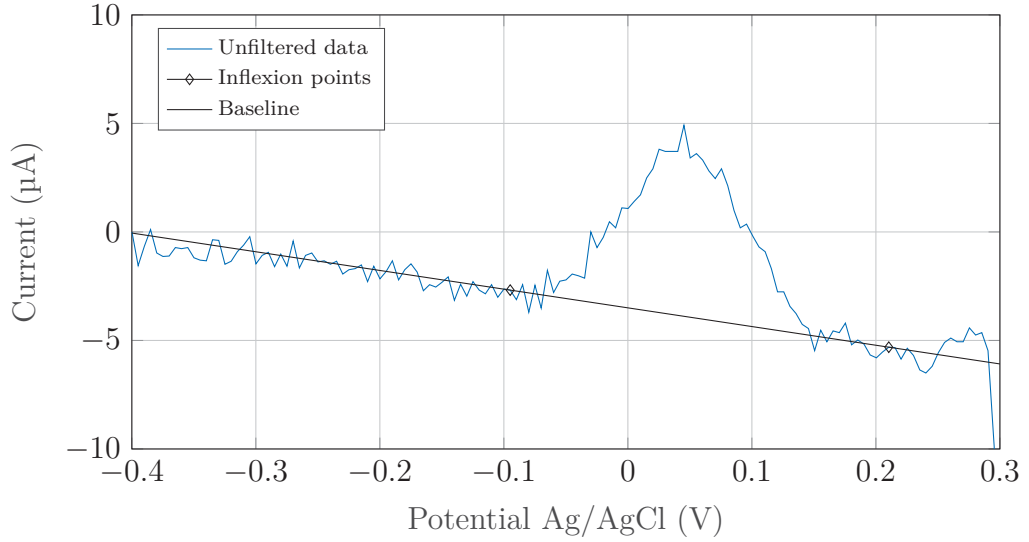

Figure 4.19: Baseline and unfiltered SWV response example

The baseline was subtracted from the data to have it centred around zero. This was used to calculate the different peak currents to compare the different SWV sets. The centring also allowed for visual interpretation of the peak currents. The final data was smoothed with the same Savitzky-Golay filter. The centred data of the example experiment is given in Figure 4.20. Note the peak generated by the smoothing and baseline subtraction. This element was kept in the example, but was post-processed if the final result required it.

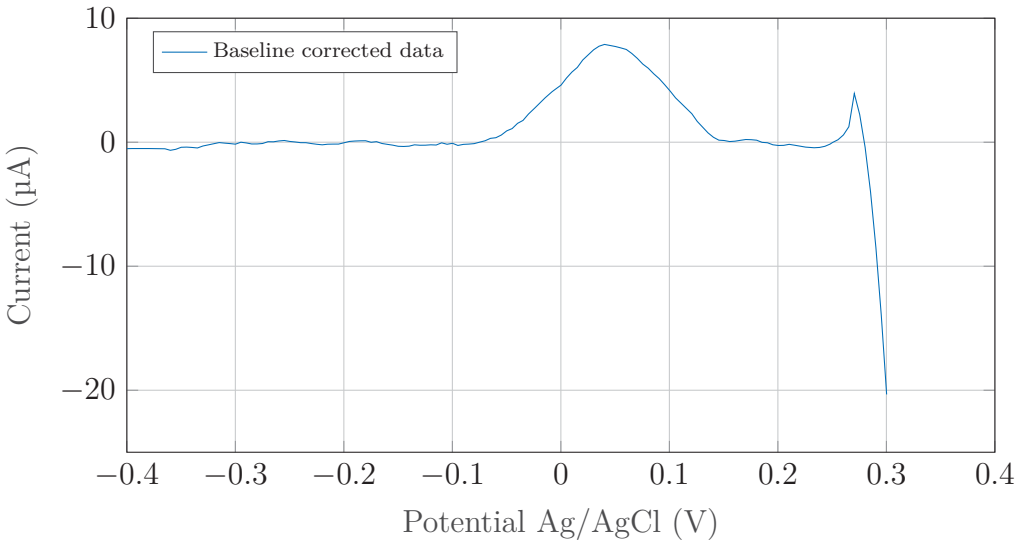

Figure 4.20: Normalised SWV response example

4.5 Design validity

As mentioned previously, the project was composed of two different phases. The first phase was to develop the biochemical aspect of the project, and the second to develop a sensor with the already working biochemical system.

In order to develop the biochemical system, the sensor had to be a proven product with supporting literature and a close enough approximation of the sensor that was intended to be developed. This was to simulate the environment in which the final sensors would operate and test the electrochemical sensing mechanism with the intended biological matter. The results of these would then compare with literature to some extent for validation, enabling further development where literature would add less value to the interpretation of the sensor system dynamics. The DropSens electrodes provided the basis required to do just this. The SPE modified with nanofibres was a close approximation of the sensors that were to be developed, and the supporting literature for these sensors were adequate to validate experimental results contextually.

4.6 Methodological assumptions

The designed method works under the assumption that pure interferon gamma is placed on the sensor. The interferon was placed in a buffer to prevent nonspecific bindings. In a realistic assay, as given by the WHO specifications in Table 2.1, would be developed for a point-of-care device where such resources and training would not be readily available.

It was assumed that no critical components of the data was affected with the baseline correction algorithm that was developed and employed. It was developed as critically as possible, with no transformation directly done on the original data except at the very end of the algorithm, namely the smoothing and baseline subtraction, and possible startup current removal. Each data set was individually examined and the algorithm success was validated in the same fashion as explained in Section 4.4. The device also functions under the assumption that the data could be interpreted relative to reasonable calibrated measurements. Methods such as baseline correction prove to be ineffective if the conditions differ from the laboratory setup such as where the experiments of the project was conducted. In these cases baseline correction should be calibrated for the matching conditions and developed to be more robust.

Chapter 5

Hardware development

This chapter reviews the hardware development related to the experimental methods of Chapter 4.

5.1 Development equipment

During the development of all of the supporting hardware it was decided to keep the designs simple and easy to replicate. One key piece of equipment used to develop the hardware is a TS4040 CO_2 laser cutting system. The system was added to the laboratory equipment at the start of the project and thereafter used in every single manufacturing process of this project. All designs were therefore based on the advantages and limitations imposed by the laser cutting method. The calibration of the system is discussed in Appendix A.

5.2 DropSens clamp

In order to facilitate a repeatable experimental setup, a clamp was designed and fabricated to hold the DropSens sensor while doing measurements. Figure 5.1 gives a Computer Aided Design (CAD) model of the design.

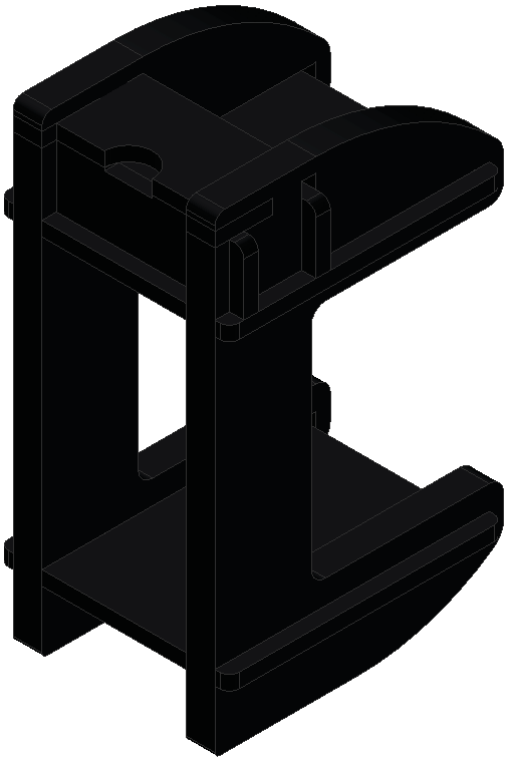

Figure 5.1: Clamp model for DropSens sensors

Figure 5.2a gives an exploded view of the different components that makes up the device (excluding the tightening bolt), and Figure 5.2b depicts the intended use of the device.

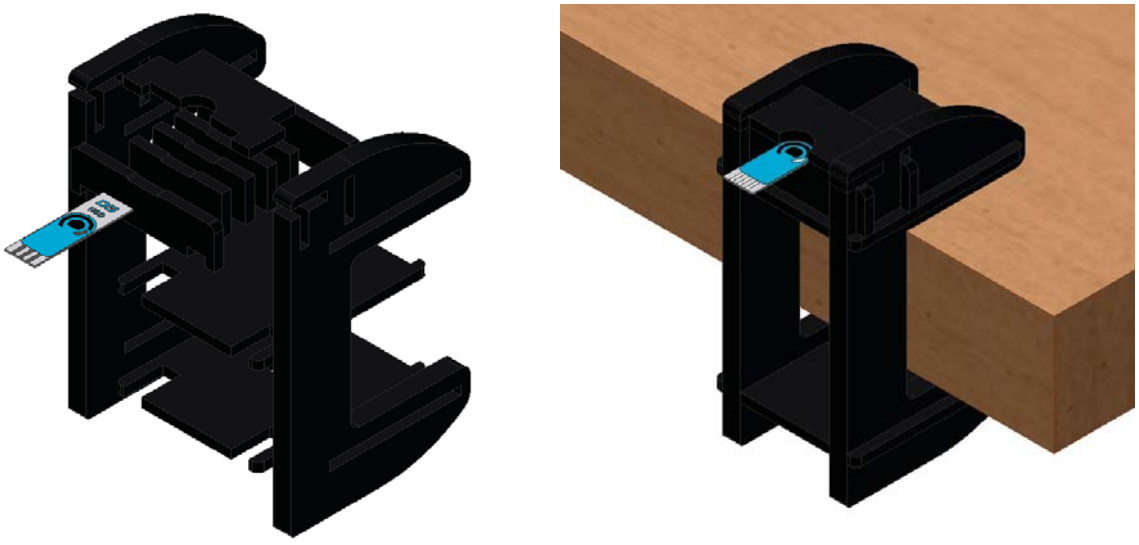

(a) Exploded view of model

(b) Clamp model intended use

Figure 5.2: Biosensor clamp in use

The goal of the device was to enable a stable sensor throughout the experiment with easy access to the electrodes where the cable connected to it. The photo given by Figure 5.3 shows the device being used and the cable attached to the biosensor.

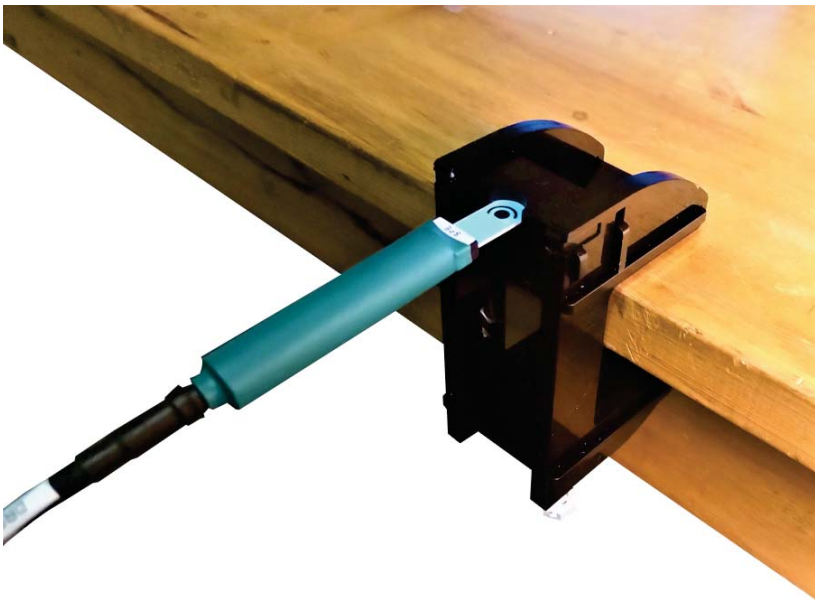

Figure 5.3: Photo of clamp being tested for experimental use

5.3 Fibre interface

A common problem faced with building a repeatable sensor configuration is the interface between the electronics and the sensor transducer. A tool was designed to ensure a repeatable, stable connection to the sensor with the advantage of being modular at the same time. This interface enabled a seamless transition between the different sensors and types of sensors. A CAD version of the connection procedure is given in Figure 5.4.

The mechanism is locked in to place by a movable key. This key is shown in orange in Figure 5.4. The first step is press down on the key handle, shown between Figure 5.4a and Figure 5.4b. The movement is then secured by sliding the key backwards into a groove.

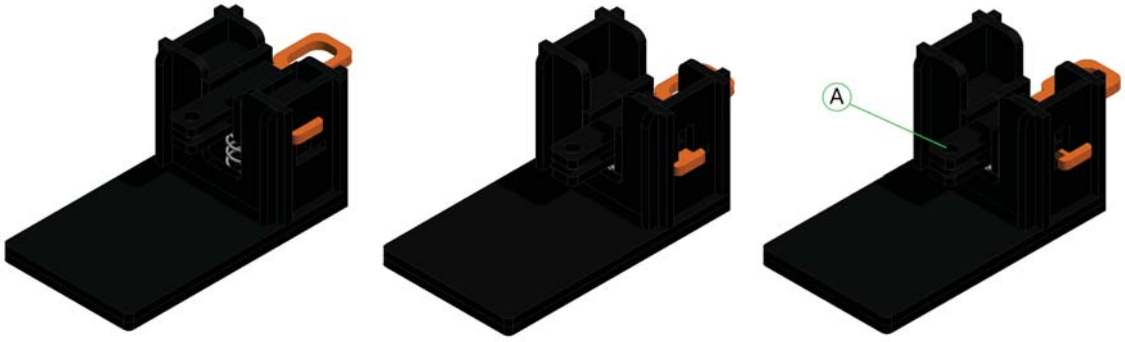

(a) Step 1 of connection (b) Step 2 of connection (c) Step 3 of connection

Figure 5.4: Sensor interface connection procedure

The mechanism was also designed to hold different types of tools, shown by A in Figure 5.4c. This was to ensure that different types of sensors could be connected without redesigning and manufacturing a whole new mechanism, but instead just design and

manufacture a replacement tool. The system is forced upwards by a spring on release. The mechanism is shown in its compressed and uncompressed state in Figure 5.5.

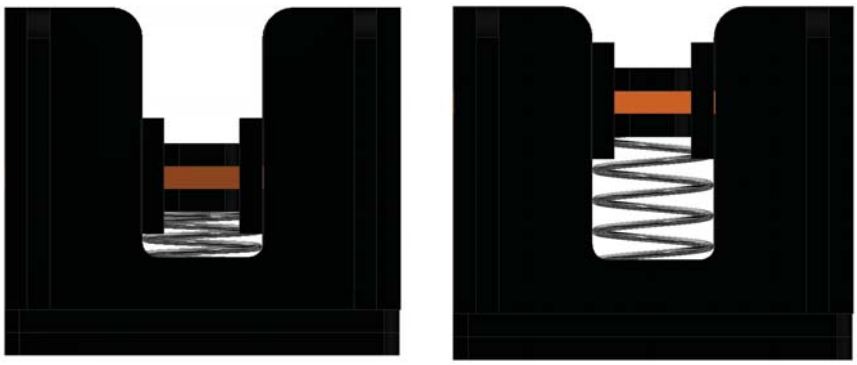

(a) Compressed system (b) Uncompressed system

Figure 5.5: Sensor connection system in compression and uncompressed

The final mechanism is shown in Figure 5.6 in its uncompressed and compressed states. The tool inserted is three connector spring-loaded spring probes with additional movement. This movement enabled the connection of sensors with varying heights and helped to relieve the pressure applied by the spring probes on the fibres. The spring probes were nickel and gold plated probes P1113CV3 from Harwin, England.

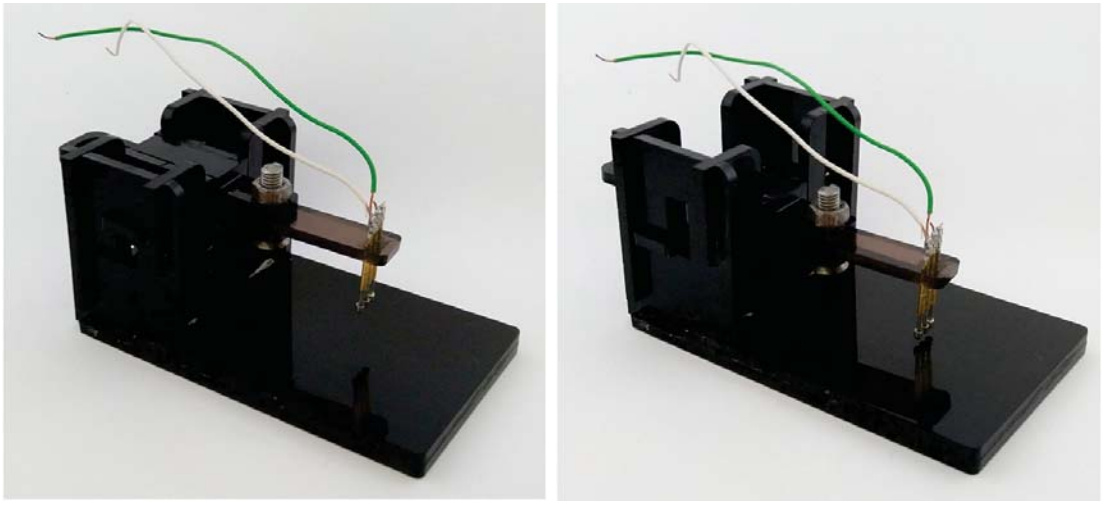

(a) Uncompressed system (b) Compressed system

Figure 5.6: Sensor connection system

5.4 Sensor development

The DropSens sensors were analysed while being used in the first phase, and certain observations were made:

1. The electrodes are covered with a hydrophobic material, except for the areas of interest
2. The connection to the sensor tracks are far away from the sensor itself
3. The connection itself is easy to repeat
4. The ceramic backing provides essential support for the sensor and is nonreactive to the electrolytic liquid

5.4.1 Electrodes

The first challenge was the fabrication of the working and counter electrodes. The DropSens electrodes are screen printed electrodes with carbon nanofibres on top of the layer of printed carbon. The research group had experience with carbon nanofibres from previous projects, but very little regarding specific shape cutting of the fibres. A sheet of carbon nanofibre that was used in the previous projects was used to fabricate the electrodes for this project. The sheet was a PR-19-XT-LHT highly conductive carbon nanofibre mat produced by Pyrograf ®.

The first cutting of the nanofibres resulted in charring, but with sufficient practice the fibres could be cut with a single pass of the laser. The importance of proper calibration of the laser focus was realised in this process. Figure 5.7 shows the size of some fibres that were cut. All fibres were cut on a glass backing that absorbed the laser beam once it passed through the fibres. The fibres were always handled with gloves and clean tweezers, and excessive touching was avoided.

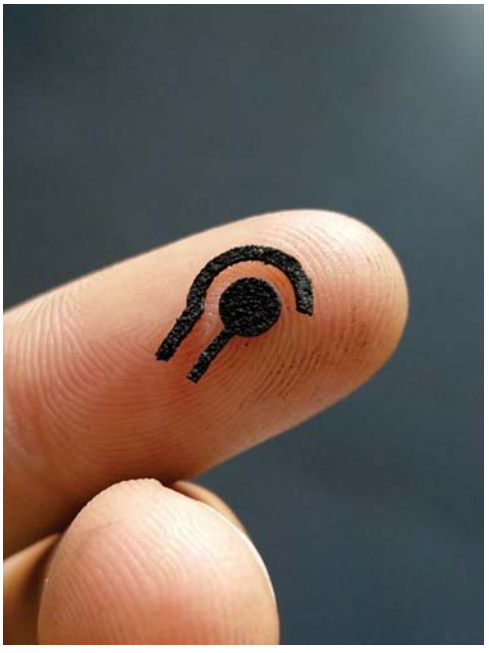

Figure 5.7: Electrodes cut from the larger nanofibre sheet

Successful cuts are shown in Figure 5.8a and 5.8b. It was found that the power setting had the greatest influence on the fibre cutting, relative to the speed at which the cut was conducted. At a too low power setting the nanofibres were successfully cut, but the microfibres stayed in tact, rendering the cut useless. This is shown in Figure 5.8c. At a too high power setting the surrounding fibres were charred and the nanofibres were burnt far away from the cut by backburn as in Figure 5.8d.

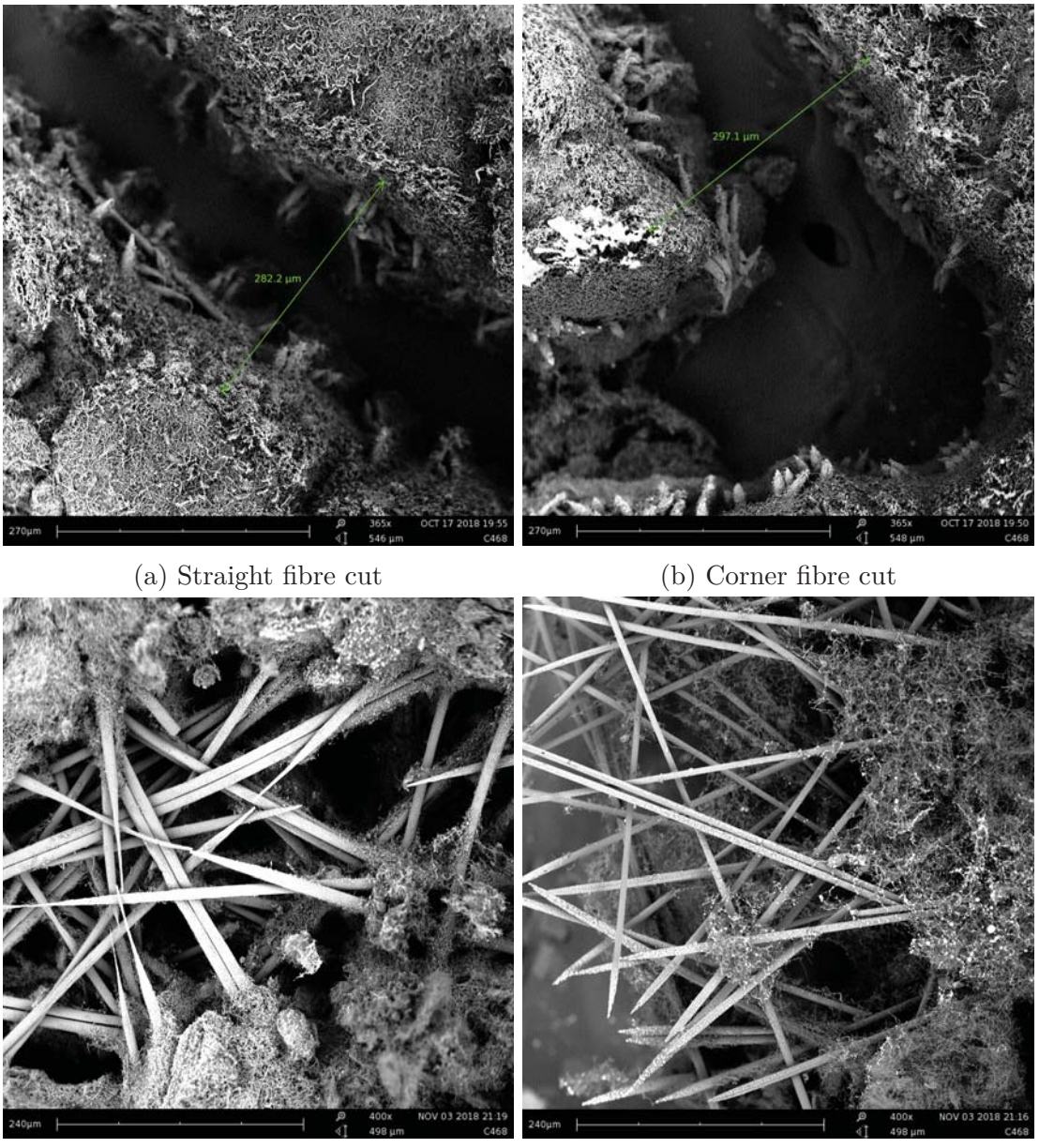

(a) Straight fibre cut

(b) Corner fibre cut

(c) Low power cut

(d) High power cut

Figure 5.8: Scanning electron microscope images of the cuts of the carbon nanofibres

The silver electrode was made from 99.9% pure fine silver. This was supplied by the Jewellery Department of the Visual Arts Faculty of the University of Stellenbosch. The silver nugget is shown in Figure 5.9a. The silver was rolled until the minimum thickness was achieved by the rolling machine. This was approximately 20 µm. The rolling machine is shown in Figure 5.10. The rolled out silver is shown in Figure 5.9b.

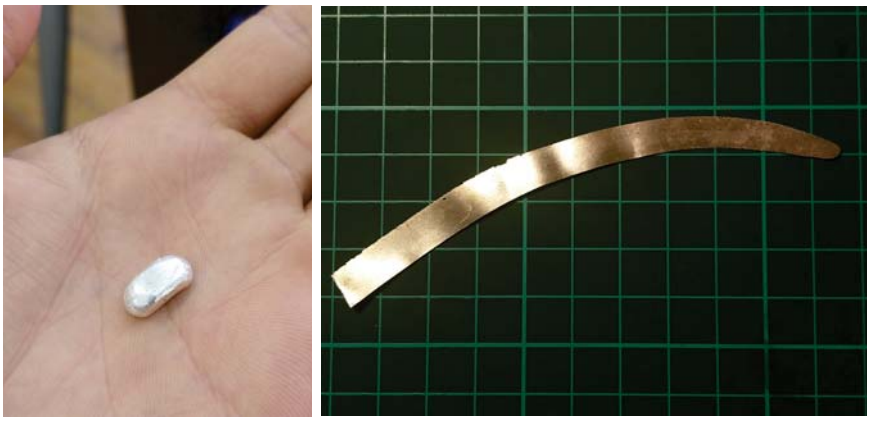

(a) Silver nugget (b) Flat rolled silver

Figure 5.9: Preprocessing of silver electrodes

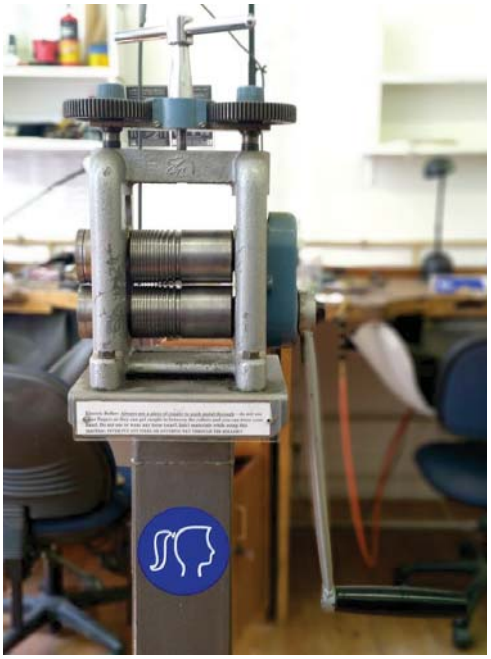

Figure 5.10: Metal rolling machine

The silver was annealed with a blowtorch to improve the surface finishing. It was cleaned by wiping it with acetone and rinsed in deionised water. It was stored in a petri dish until further use. The desired shapes were cut with a fine tin scissor. The electrodes were always cleaned in the same procedure before use.

5.4.2 Sensor assembly manufacturing

With the DropSens characteristic parameters in mind, four different sensors were designed with the same geometries but different casing assemblies. This Section discusses the sensors in detail and concludes with a summary of all of the sensors.

The spring probe material proved to be an interesting element of the design. Under ideal conditions the probes would not react in any way with the chosen electrolytic liquid.

This should be so because the redox reaction would then be purely recorded for the interaction between the liquid and the carbon nanofibres. The fibres were hydrophilic, thus without proper precaution the electrolytic liquid seeped to the contact between the fibres and the spring probes. Initially it was thought that the spring probes might be coated with silver to avoid electrochemical interactions, but this was not enough to prevent additional peak formations in the voltammetric experiments. The final strategy employed was to seal the sensor target area from the spring probe contact points.

Sensor 1

A labelled view of the components of the first sensor is given in Figure 5.11.

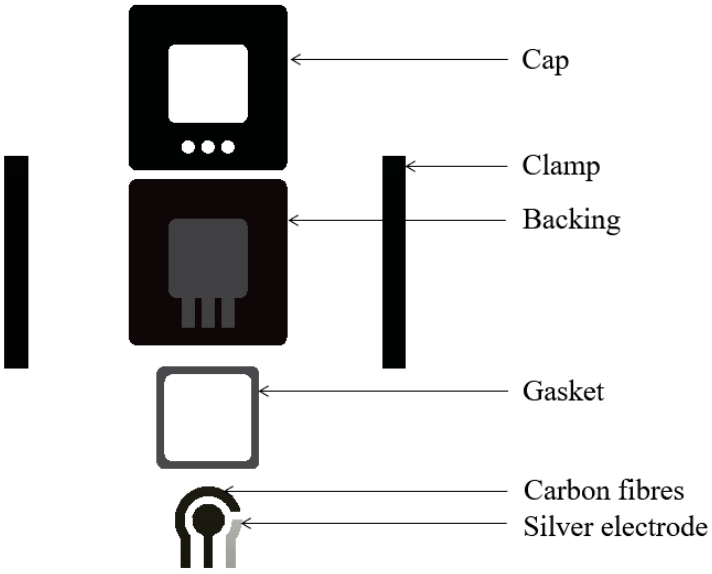

Figure 5.11: First sensor labelled view

The cap, clamps, and backing was made from opaque Perspex and the gasket was cut from a rubber slick road bicycle inner tube. All of the materials, except for the silver, were manufactured by the use of the laser cutter. The assembly is shown in Figure 5.12.

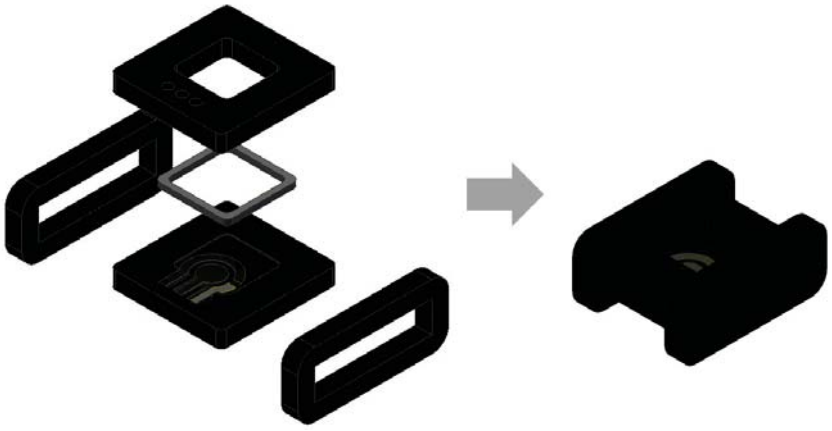

Figure 5.12: Components of first sensor

The purpose of the gasket was to keep the electrolytic liquid from flowing to the spring probes of the sensor electrical interface. The grooves in the backing provided compression relief for the fibres that had to pass under the gasket to the spring probes. The clamps proved to be an effective mechanism to lock the system in place. It applied just enough pressure to keep the liquid inside the desired area, and at the same time not crush the nanofibres. The pressure was a function of the clamp size and the depth of the gasket groove. The laser cutting provided a fine enough resolution to maintain a separation between the three different holes for the spring probes. Should the connection mechanism have become misaligned, the Perspex kept the spring probes apart. The final manufactured device is shown in Figure 5.13.

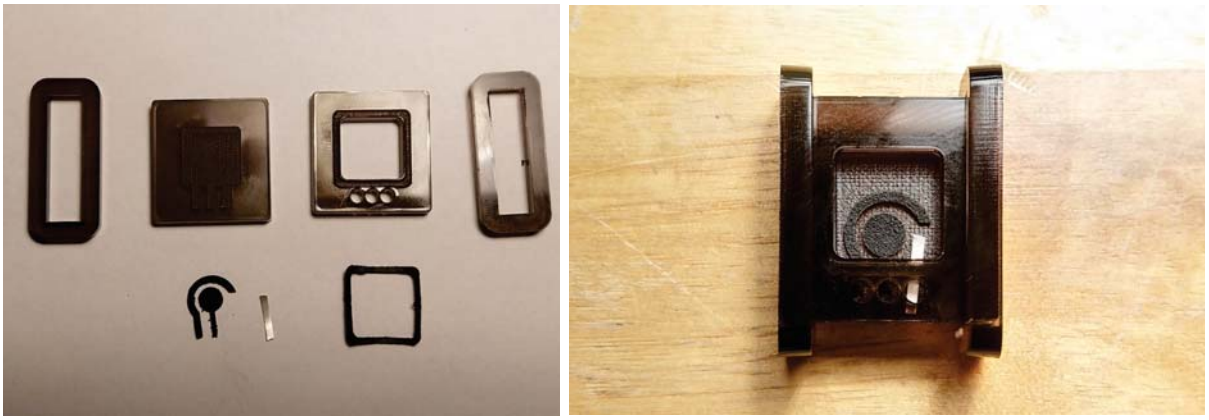

(a) Disassembled sensor (b) Assembled sensor

Figure 5.13: First manufactured sensor

The sensor manufacturing and assembly procedure was as follows:

Step 1: Lasercut Perspex casing

Step 2: Lasercut fibre electrodes

Step 3: Cut silver electrode with tin scissor

Step 4: Place and align the electrodes on backside

Step 5: Place and align gasket on top component

Step 6: Carefully place and compress top component on backside

Step 7: Slide on clamping components to maintain compression

Step 8: Place sensor in interfacing mechanism for testing

Sensor 2

The second sensor components are given in Figure 5.14. This sensor was made in different layers of DC Fix and double sided tape, mounted on a sterile glass slide. The stationary materials were all purchased from Uni-Stat, Stellenbosch.

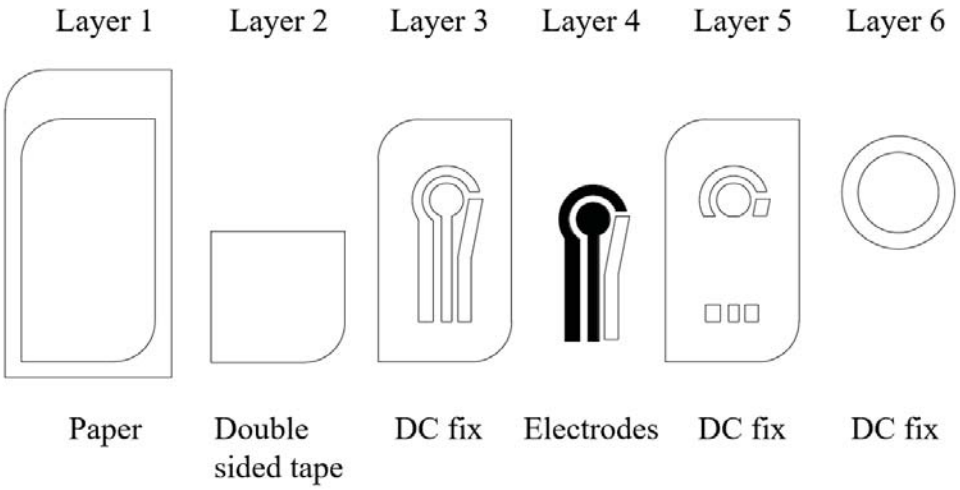

Figure 5.14: Second sensor assembly view

The layered assembly is given in Figure 5.15a. The first layer was made of paper, used only to label the sensor and had no influence on the working of the sensor. The second layer was double sided tape. This was used to temporarily secure the fibres while the sensor was assembled and help prevent fluid creep to the spring probes. The next layer was DC Fix. This layer compensated for the thickness of the electrodes before the top sealing layer was placed. The initial sensors were designed without this layer, but it was found that the electrolytic liquid easily seeped to the spring probes. This is shown by the yellow liquid in the section view of Figure 5.15b. Yellow was used because the electrolytic liquid used had a yellow colour due to the dissolved electrolytic liquid.

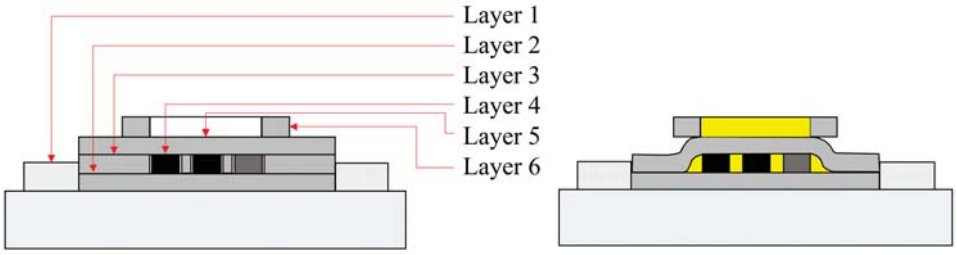

(a) Sensor 2 layering schematic (b) Sensor 2 without layer 3

Figure 5.15: Second sensor layering procedure

The purpose of layer 6, the circular layer, was to act as a barrier to keep the electrolytic liquid from straying away from the electrode contact areas. The surface tension of the liquid was, in addition to this layer, enough to fulfil this requirement. The process of assembly for these sensors is shown in Figure 5.16 where three of the sensors were fabricated on a single glass slide. Figure 5.16a shows the first paper layer on the glass slide. The layer was also used to locate the subsequent layers for a higher repetitive process. In Figure 5.16b sensor E1 shows layer 2 with the double sided tape unexposed. E2 shows the exposed double sided tape, while E3 has layer 3 placed on layer 2. Figure 5.16c shows the three completed sensors, with all of the subsequent layers in place.

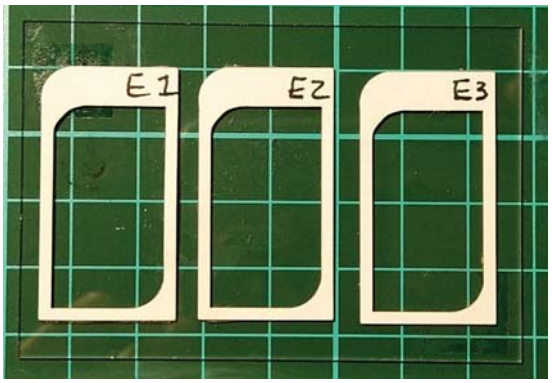

(a) Paper layer on glass slide

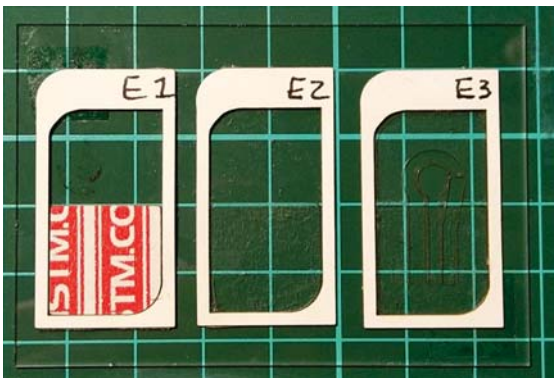

(b) Layers 2 and 5

(c) Completed sensors

Figure 5.16: Sensor 2 assembly procedure

The sensor manufacturing and assembly procedure was as follows:

Step 1: Apply a sheet of DC fix and double sided tape to a glass substrate

Step 2: Lasercut the different components

Step 3: Lasercut fibre electrodes

Step 4: Cut silver electrode with tin scissor

Step 5: Place and align layers 1,2, and 3 on glass backing

Step 6: Place and align the electrodes

Step 7: Place and align layers 5 and 6

Step 8: Place sensor in interfacing mechanism for testing

Sensor 3

The next sensor, sensor 3, was fabricated in a more simplistic fashion. Standard ceramic slides used in the lab for microfabrication were used as a backing material. The slides were wiped with acetone and then rinsed three times in deionised water before being left to dry on paper towels. The electrodes were placed on the clean ceramic backing and the electrode contact areas were covered with another ceramic slide. The circular transducing area was covered with a small Perspex button by merely placing it on the intended area. The exposed sensors and backing were then coated with a two step hydrophobic spray,

normally used to seal shoes from mud and water. The spray is NeverWet Liquid Repelling Treatment produced by Rust-Oleum, shown in Figure 5.17.

Figure 5.17: NeverWet by Rust-Oleum. [76]

The coating happened in two steps. The first coating was sprayed on and left to dry for 30 minutes. The second coating was sprayed on and it was also left for 30 minutes to dry. The coating configuration and post-sprayed sensor is shown in Figure 5.18. The layer proved to be a sufficient bonding agent to keep the electrodes from moving or lifting when in use. In effect, this sensor was the closest replication of the DropSens sensors.

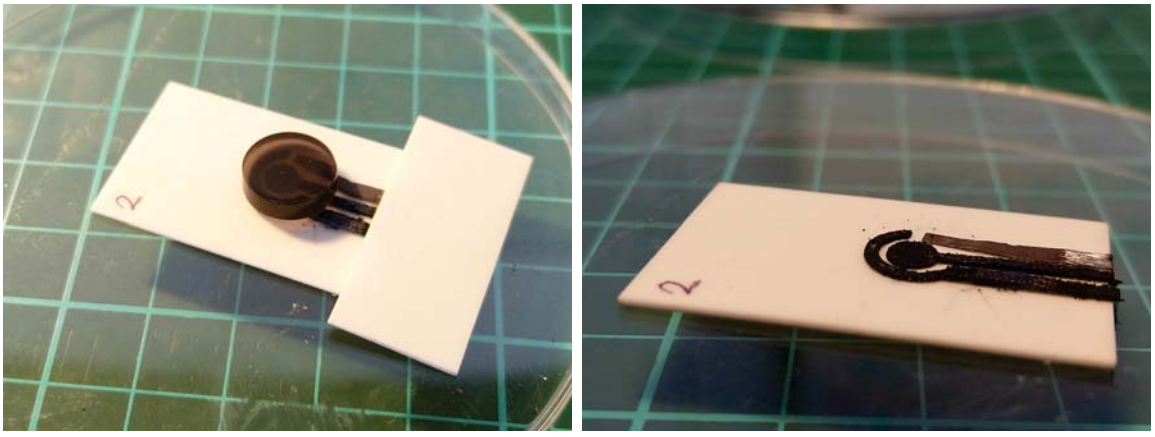

(a) Coating configuration (b) Coated sensor

Figure 5.18: Hydrophobic coating of sensor

The sensor manufacturing and assembly procedure:

Step 1: Lasercut fibre electrodes

Step 2: Cut silver electrode with tin scissor

Step 3: Place and align electrodes

Step 4: Place and align the covering layers

Step 5: Spray layer 1 of the hydrophobic layer

Step 6: Spray layer 2 of the hydrophobic layer

Step 7: Remove covering layers

Step 8: Place sensor in interfacing mechanism for testing

Sensor 4

The final sensor was made to work on the same principle as the first sensor, but with a different physical design. The sensor CAD design is shown in Figure 5.19. The fibres were extended to be longer and the clamping mechanism was made to be more versatile. The overall shape was changed, and the inside of the casing was coated with the hydrophobic spray.

Figure 5.19: Sensor 4 CAD design

The sensor components are shown in Figure 5.20. The materials and manufacturing methods of this sensor was the same as that of the first sensor. The pressure relief channels were modified to fit the electrodes shapes. This helped with the alignment of the electrodes to ensure more repeatable results.

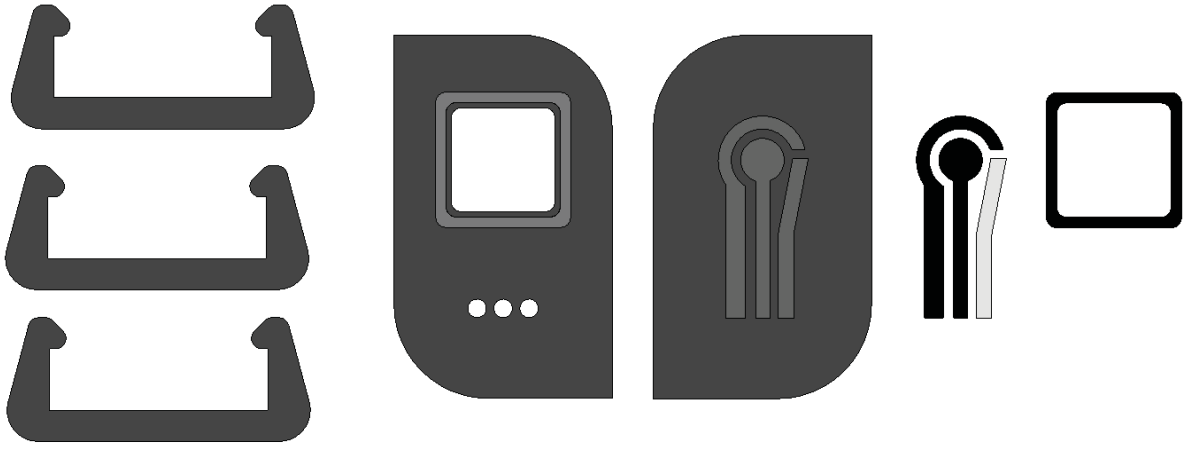

Figure 5.20: Sensor 4 components

The coated areas of the cap and backside is shown in orange in Figure 5.21a. The same procedure was followed as was when coating the third sensor casing, except the connection points were not covered. This was not necessary because the fibres were placed in the sensor casing after the coating took place. The clear sensor casing is shown in Figure 5.21 and the coated sensor casing in Figure 5.22

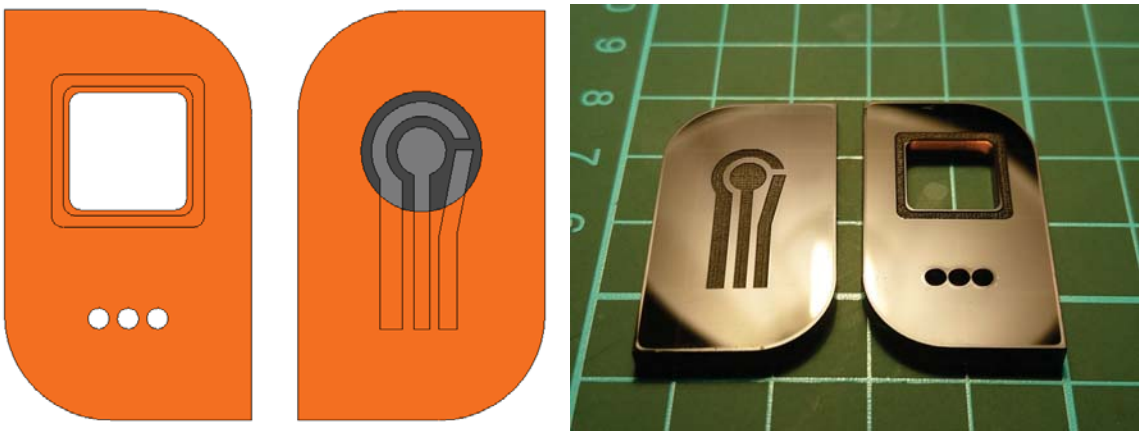

(a) Areas coated by hydrophobic layer

(b) Clean sensor casing

Figure 5.21: Hydrophobic coating of sensor

(a) Coated sensor casing

Figure 5.22: Hydrophobic coating of sensor

The purpose of the hydrophobic spray was to ensure that the spring probes were protected from the electrochemical reaction. The top and bottom coats of the spray was intended to ensure this characteristic when using the sensor. The assembly and manufacturing of the sensor was as follows:

Step 1: Lasercut Perspex casing

Step 2: Lasercut fibre electrodes

Step 3: Cut silver electrode with tin scissor

Step 4: Coat top and backside with hydrophobic spray

Step 5: Place and align the electrodes on backside

Step 6: Place and align gasket on top component

Step 7: Carefully place and compress top component on backside

Step 8: Slide on clamping components to maintain compression

Step 9: Place sensor in interfacing mechanism for testing

Summary

Before electrochemical testing, the four different sensors were critically evaluated to determine the hardware design advantages and disadvantages. This was to determine an unbiased validation of the assembly and manufacturing procedure. The categories of assessment were as follows: ease of assembly, manufacturing and assembly steps, assembly time, material attractiveness, types of materials used, sensor replication, and casing reusablility.

Sensor 1 was assembled with little difficulty. The alignment of the fibres were not very repeatable because there was no indication of where the fibres were to be placed. The time it took to completely manufacture and assemble one sensor took approximately 15 minutes. Two different materials were used for the casing: Perspex and rubber. These materials were easy to come by and not difficult to manufacture. The manufacturing and assembly of the sensor was highly repeatable. The casing was reusable, where only the carbon nanofibres were to be replaced between tests.

The fibre placement for Sensor 2 was done with ease, since the DC fix provided a pattern similar to the fibres. The fibres tended to spontaneously adhere to the different surfaces available, thus it was difficult to get the fibres in alignment with the pattern. It took approximately 90 minutes to fabricate and assemble a single sensor. This was due to the precise alignment required for the different layers and care that had to be taken to keep the layers from sticking and contaminating the central surfaces.

The materials used for the casing: paper, glass, DC fix, and double sided tape. The materials were procured from a local stationary shop. The casing was not reusable, and only the silver electrodes could be used again.

The materials used for Sensor 3 were ceramic slides and hydrophobic spray. The sensor manufacturing took approximately 75 minutes. The first 15 minutes were to cut and align the different electrodes. This was a time consuming process since there was no guidance as to where the electrodes were to place. This also hindered the sensor replication rate. The next 60 minutes were for the drying of the hydrophobic layer, 30 minutes per layer. The assembly procedure is as follows: The sensor casing was not reusable at all since all of the electrodes were partly covered with the hydrophobic layer. The materials were all easily attained.

Sensor 4 was the most complex sensor of the four. The assembly procedure for this sensor was the same as Sensor 1, with an additional step where the top and backside was covered in the hydrophobic layer. The electrode placement was a highly repeatable process since the grooves were cut in the same shape as the electrodes. The materials

that were used are Perspex, hydrophobic spray, and rubber, which were all standard materials that were easy to come by. The casing was reusable, but the hydrophobic layer was assessed after each use to inspect its integrity.

Chapter 6

Commercial sensor findings

This chapter contains a sample of the data gathered during the experiments discussed in Chapter 4 for the commercial DropSens sensor. The goal was to validate the biochemistry and electroreactive response of the working sensor. This chapter presents some of the raw data required to understand the different signals. It also includes a discussion regarding the nature of the data, a descriptive analysis, and notable unusual results obtained. The topic of data validity and reliability is introduced, and the goal of the chapter is reviewed before proceeding to the experimental results of the manufactured sensor. The comparison of the results of the different sensors are conducted in Chapter 8.

6.1 Brief overview

The experimental procedures were conducted in a step-by-step fashion, where the results of the experiments provided the basis for the next. The first experiments analysed the unmodified sensors in the 5 mM potassium ferricyanide electrolytic liquid. This included a cyclic voltammetry response and a square wave voltammetry response. Following this, electrodes were electrografted and the results were analysed with square wave voltammetry.

The electrografted carboxyl groups were activated with the EDC/NHS protocol and different concentrations of the capture antibody were immobilised to test for the sensor surface coverage saturation. This was validated with square wave voltammetry.

Further tests were done by incubating different concentrations of interferon gamma, the secondary antibody and the HRP label on sensors with immobilised capture antibodies. The interferon gamma and labelled sensors were analysed with SWV to determine if a change in concentration could be detected. The knowledge gained in this Section was utilised to make better assumptions and adjustments with the manufactured sensors to improve reliability and repeatability.

6.2 DropSens experimental results

This section presents samples of the unfiltered data gathered from the DropSens sensors in various stages of operation. As a note regarding the square wave voltammetry results, the starting current was neglected from the given graphs. An example with the starting

current is given in Figure 4.15, but for analysis this current was excluded because it had no known influence on the peak current and made it difficult to analyse the data visually. The SWV raw data was also moved to zero in some cases to suit the scale of the graph. The normalising algorithm employed the baseline method to compare the different data sets, thus the analysis was done from the unmoved data.

All biological elements that were validated with SWV were not used for further experiments since they were contaminated with the electrolytic liquid. They were washed in PBS and stored at room temperature in PBS until the end of the project. All experiments that validated the next step of the immobilisation or detection were conducted from clean carbon sensors until the relevant step.

6.2.1 Unmodified sensor response

The initial testing done upon receiving the DropSens sensors were to validate the sensor electrochemical responsiveness. Given in Figure 6.1, the sensor response relative to three voltammetry sweeps are given. The potential range is from 0.6 V to -0.6 V, starting 0 V, sweeping to 0.6 V and then -0.6 V, and back at 0.6 V after three cycles.

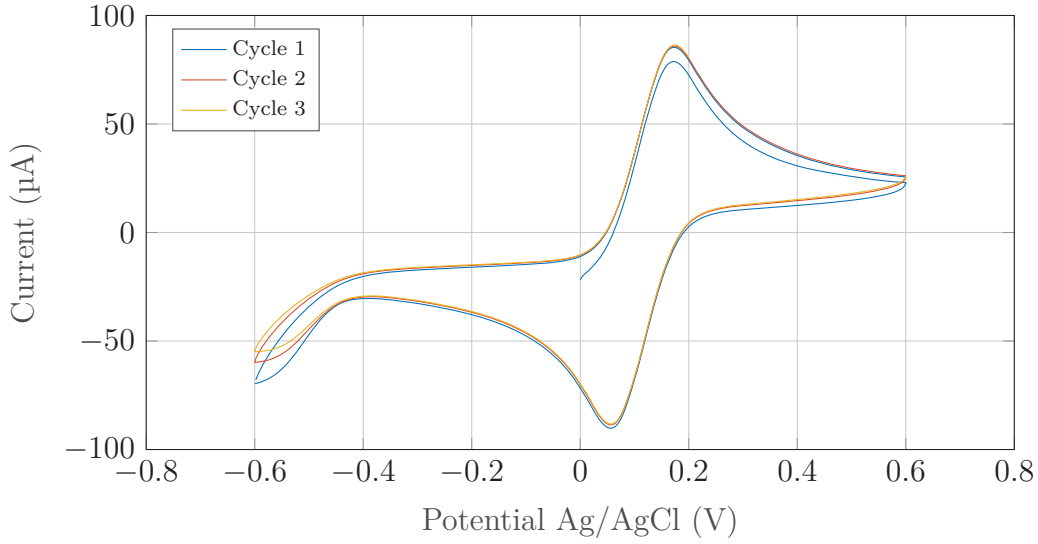

Figure 6.1: Unmodified DropSens sensor cyclic voltammogram

From the cyclic voltammetry response it can be concluded that the electrochemical cell is stable, with little changes in peak currents for successive cycles. The changing currents at the tail of the graph at -0.6 V can be attributed to the start of the reduction of the PBS buffer. The potential was given in Chapter 4 Section 4.2.1 as -0.69 V, according to the IUPAC convention.

This was followed by clean square wave voltammetry testing, given in Figure 6.2. Four different sensors were used to test the repeatibility of the findings. The scans were conducted from 0.3 V to -0.4 V in a single direction, with the potentiostat settings as described in Chapter 4.

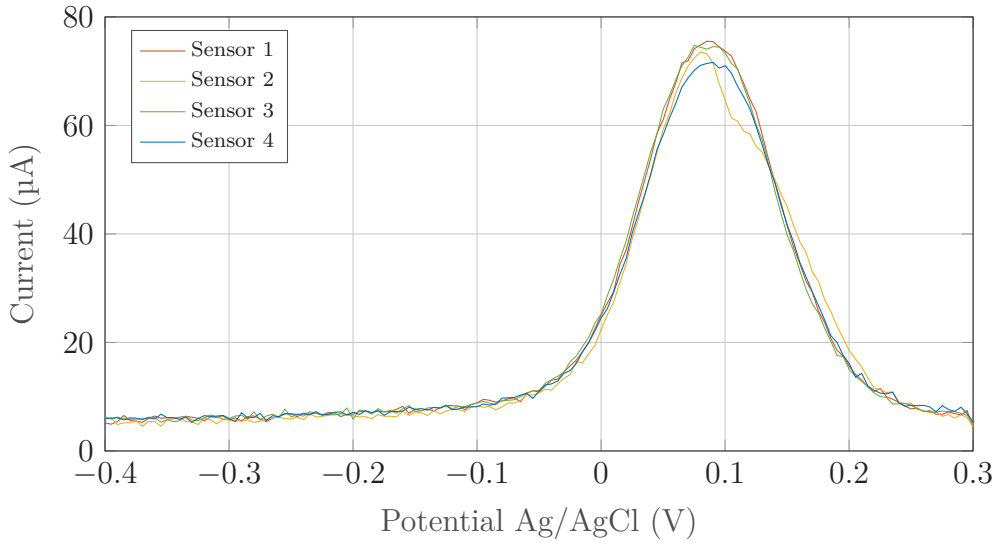

Figure 6.2: Unmodified Dropsens square wave voltammetry

The response for both Figures 6.1 and 6.2 visually indicated a stable and repeatable system, and proved the electrochemical activity of the cell setup because the form of the graphs were as expected. It was assumed that all the sensors would respond in an acceptable similar fashion, thus the following experiments were conducted without this initial unmodified test to prevent contamination.

6.2.2 Electrografting

The diazonium salt was prepared according to the protocol of Chapter 4. A droplet was placed on the electrodes of the sensors immediately afterwards. The sensor electrodes were swept from 0.2 V to -0.6 V, starting and finishing at 0.2 V. The first sensor was subjected to only a single sweep, given in Figure 6.3, to test the solution activity.

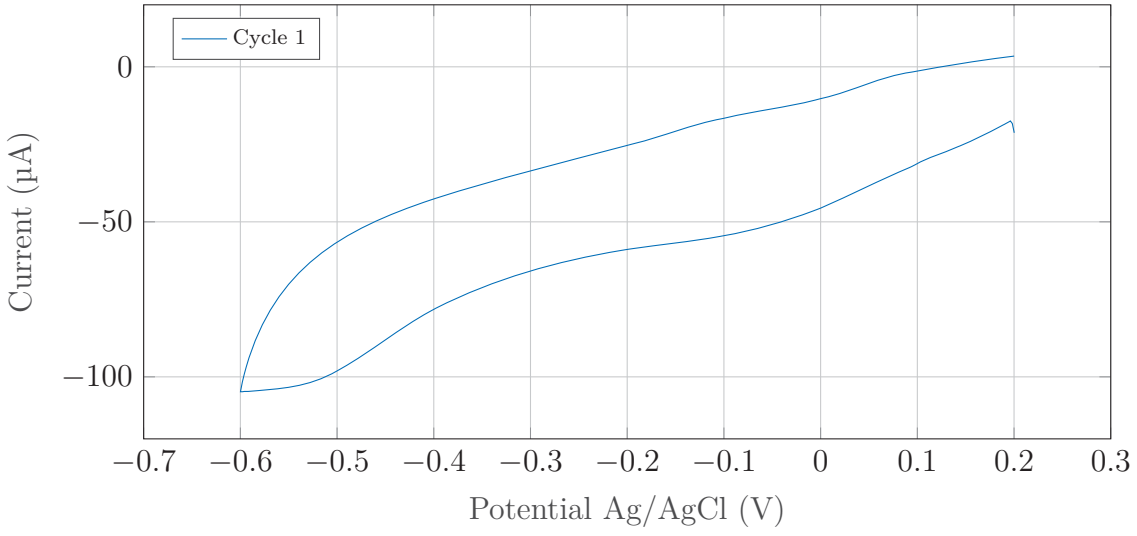

Figure 6.3: Single cycle Dropsens cyclic voltammogram electrografting response

The form of the voltammogram in Figure 6.3 indicated a possible successful electrografting cycle, since its form is similar to that found in literature. The next sensor was subjected to fifteen consecutive cycles to test for the amount of sweeps required for electrode surface saturation. The cyclic voltammetry data is given in Figure 6.4. The data can be interpreted by considering the highest peak current cycle to be the first cycle, and a decreasing peak current for each successive cycle.

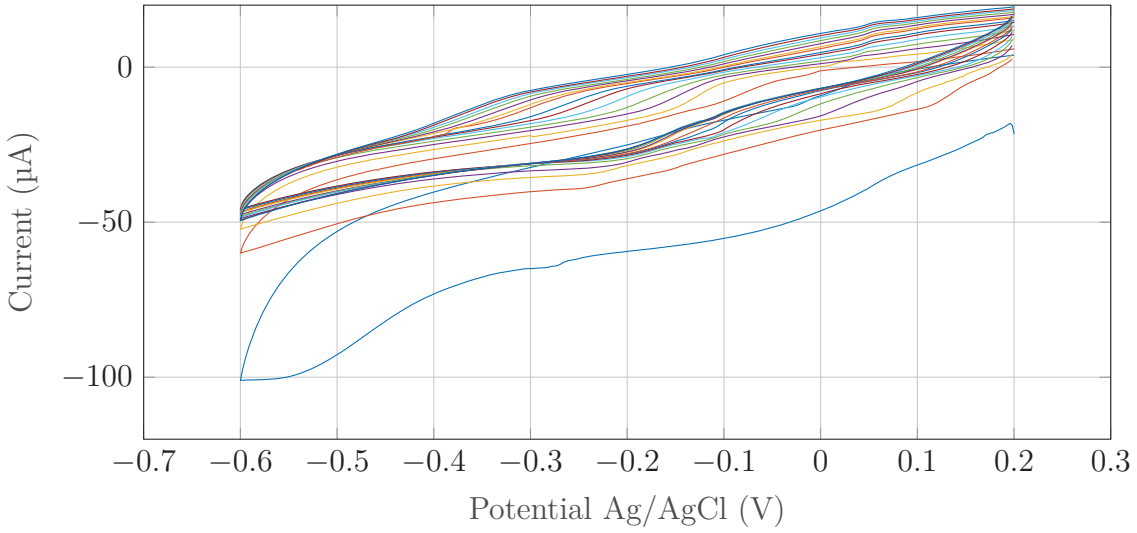

Figure 6.4: Fifteen cycle Dropsens cyclic voltammogram electrografting response

The difference in the peak values of the successive cycles were analysed, given in Figure 6.5. The current decreased with each cycle for the first seven scans. Thereafter all of the scans saw an increase in the peak current. The initial peak difference can be explained by the successful surface modification, with saturation reached after cycle 7. The near stabilisation, but growth in peak height might be attributed to the ionic chlorine molecules interacting with the positively charged working electrode, as shown in Figure 4.5. This element could be present in all of the cycles, but with a minuscule influence compared to that of grafting process.

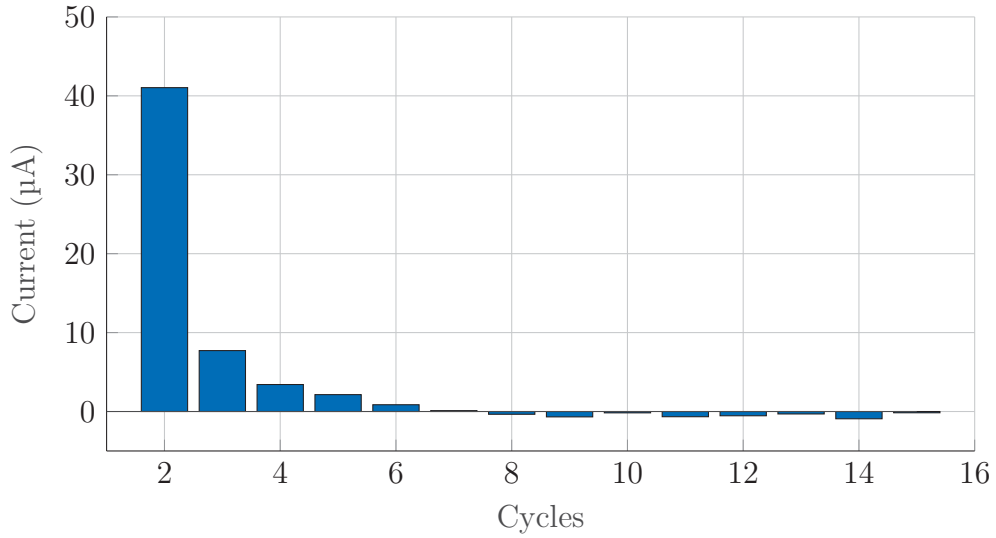

Figure 6.5: Current difference of the successive peaks of the electrografting

The validation of the electrografting was done by square wave voltammetry. An additional sensor was electrografted, but with four scans in total. The peak difference current of four scan was considered to be large enough to properly cover the surface of the electrode, but not yet at saturation. All of the electrodes were rinsed according to protocol, dried, and then placed in the electrolytic liquid. The resulting normalised current for the three different tests are given in Figure 6.6 and compared to an unmodified sensor. The peak currents are given in Table 6.1

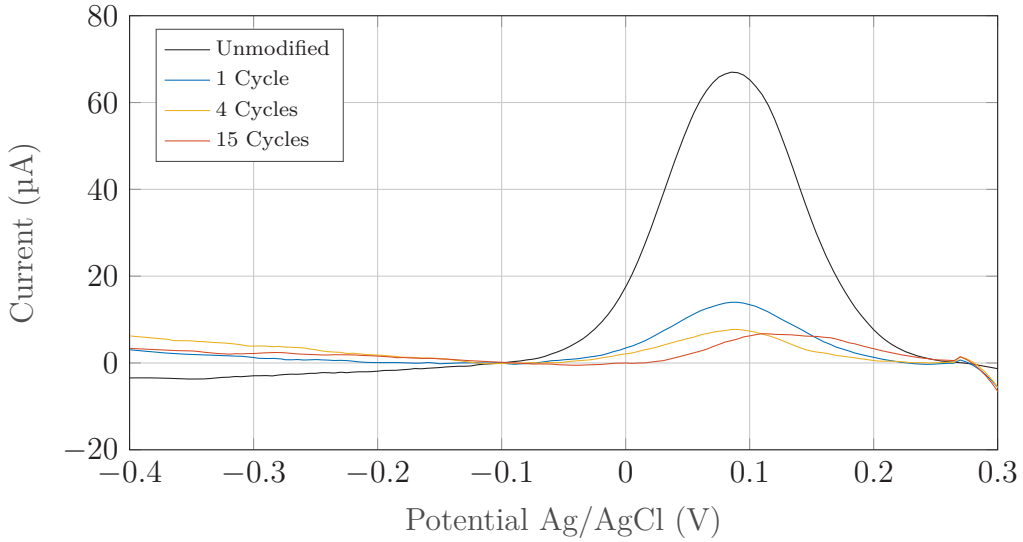

Figure 6.6: DropSens electrografting peak comparison with square wave voltammetry

Experiment	Current (µA)
Unmodified	67.00
1 Cycle	13.98
4 Cycles	7.72
15 Cycles	6.74

Table 6.1: Peak currents of the different electrografting experiments

The reason for a diminishing peak current might be explained by the diazonium salt that was chosen to be grafted to the surface of the electrodes. The carboxyl group would be in the dissociated form, COO^-, in the electrolytic liquid with a pH of 7. This means that by losing the H^+ the group becomes negatively charged and inhibits electron transfer to the electrode. Interestingly enough, the peak current between four and fifteen cycles did not differ by more than 1 µA. It means that the surface coverage between four and fifteen cycles does not differ significantly enough to motivate the use of more cycles. This, in conjunction with the peak changes of the electrografting peak currents and literature, justified the use of four cycles of electrografting per sensor.

6.2.3 Capture antibody

The sensors that were to be used for antibody concentration optimisation were electrografted with four potential cycles. The carboxyl groups were activated using the EDC/NHS protocol, and select concentrations of the capture antibody was placed on the working electrode of the sensors. This was incubated at 4°C overnight. The sensors were inspected by using square wave voltammetry. The unfiltered data is shown in Figure 6.7.

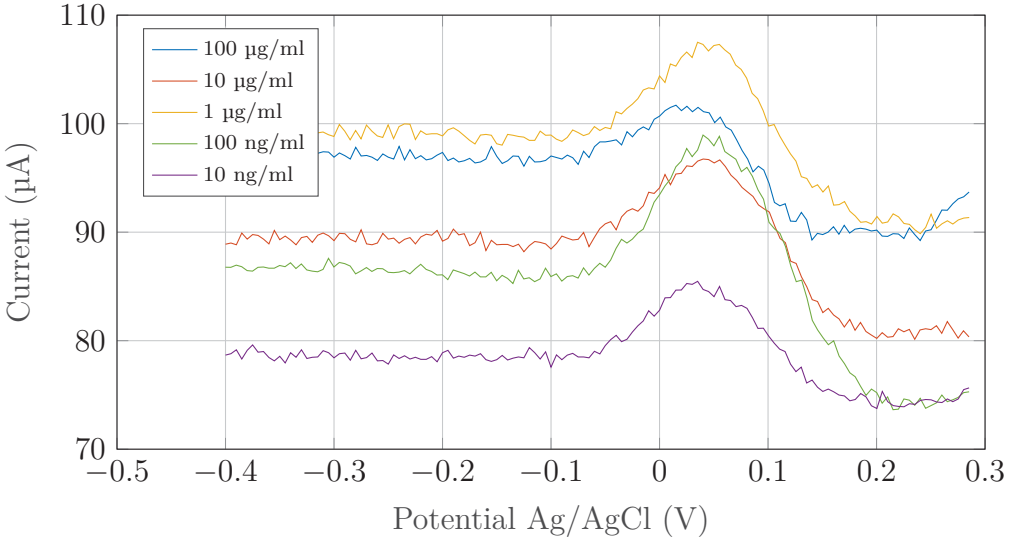

Figure 6.7: DropSens 5 mM ferricyanide SWV capture antibody validation

The validity of the sensing technique could be analysed by the results of the antibody immobilisation, because the biological matter that was attached to the surface of the sensor resulted in a change of the peak heights. It must be noted in Figure 6.7 it may seem that the settling current of the sweep may have been used to determine the concentration

of the antibody immobilised. This is not true, because if another set of SWV data were to be used, this level would differ. An example is given in Figure 6.8, where the data set of two different concentrations of the antibody is compared.

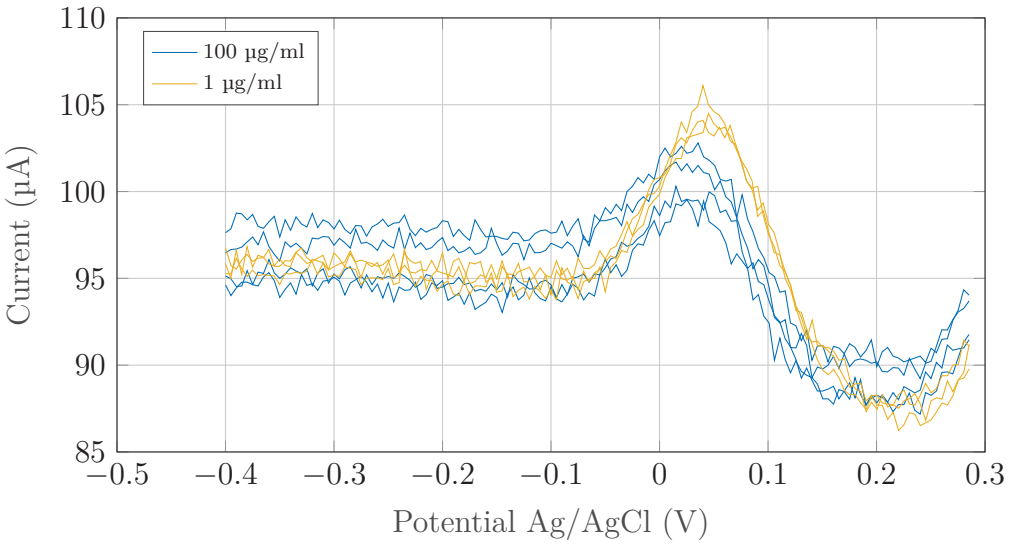

Figure 6.8: DropSens 5 mM ferricyanide SWV capture antibody validation for two concentrations

The key to analysing the data can also be observed in Figure 6.8. The peak difference between the different concentrations are clearly visible, and it is this characteristic that is used to determine the concentration of the target molecule. This is an example of data not yet normalised by the algorithm, and unless required for a detailed explanation, the filtered data was presented.

The normalised response of the different tests per concentration is given in Figure 6.9. It can be observed that the redox potential of the graphs not only differ from the unmodified graphs, but also between the different concentrations.

There are many different elements that may have an influence in the changing redox potentials. This could include contamination of the electrolytic liquid near the surface of the electrodes due to residue liquid from the incubation or from another source. Also shown by 3.5, the temperature of the liquid affects the half wave potential. This might be the case. In this study the influence of the half wave potential of the electrolytic liquid had no known effect on the results because the comparison between the tests were done purely through the peak current of the SWV experiments. This is also because the same electrolytic liquid was used for all of the SWV experiments. The indication that the peak current is independent of the half wave potential was also shown by 3.6. The normalising algorithm was analysed for its effect on the location of the half wave potential, but it indicated no effect, and out of principle it should not have an influence the potential.

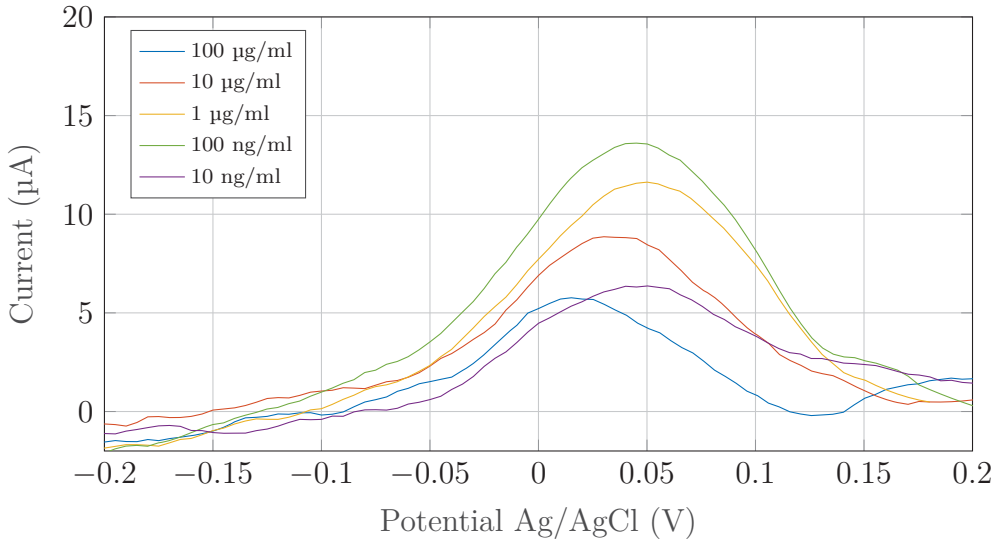

Figure 6.9: Normalised SWV response for different concentrations of the capture antibody immobilised on the fibre surface

The peaks are compared in Figure 6.10 relative to the concentration of the capture antibody used in the experiment. The test proved to yield interesting results, because if the most extreme concentrations is compared to the values in Table 6.1, it can be seen that the peak currents were lower than that of the electrografted fibres. This will be compared and discussed in Section 6.3. The chosen concentration for the capture antibody for successive tests was 2 µg/ml. The reason for this is partly shown by Figure 6.11 and Table 6.2.

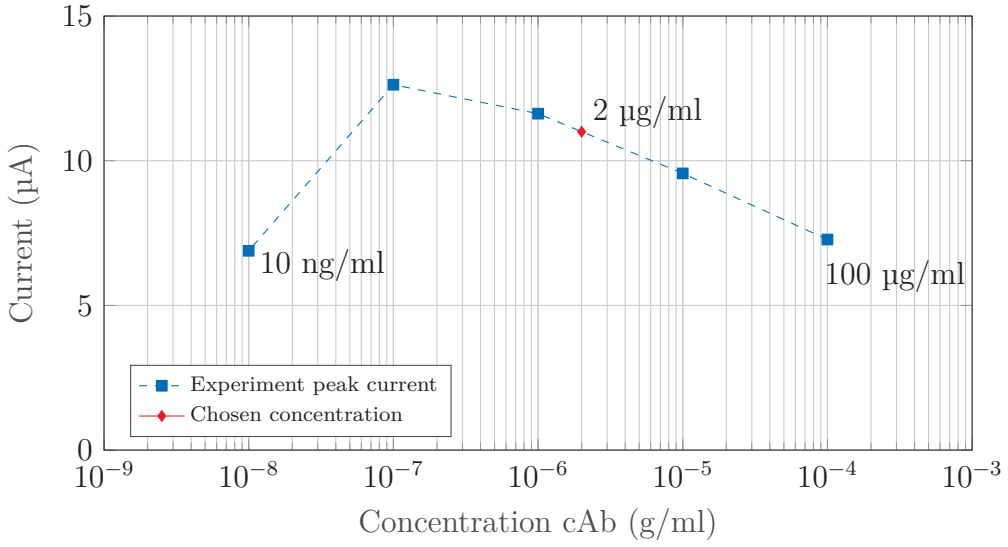

Figure 6.10: SWV peak comparison for different concentrations of the capture antibody immobilised on the fibre surface

The trend of the peaks were analysed in two different scenarios: the first considered n = 4 where the range of the points to calculate the line spanned from 100 µg/ml to 100 ng/ml. This is shown by the green line in Figure 6.11, $y = 0.30922 - 1.8115 \log(x)$.

The second was to consider n = 3, where the concentration of 100 ng/ml was also discredited as not in the linear working range. This is given by the red line in Figure 6.11, $y = -1.3872 - 2.175\log(x)$.

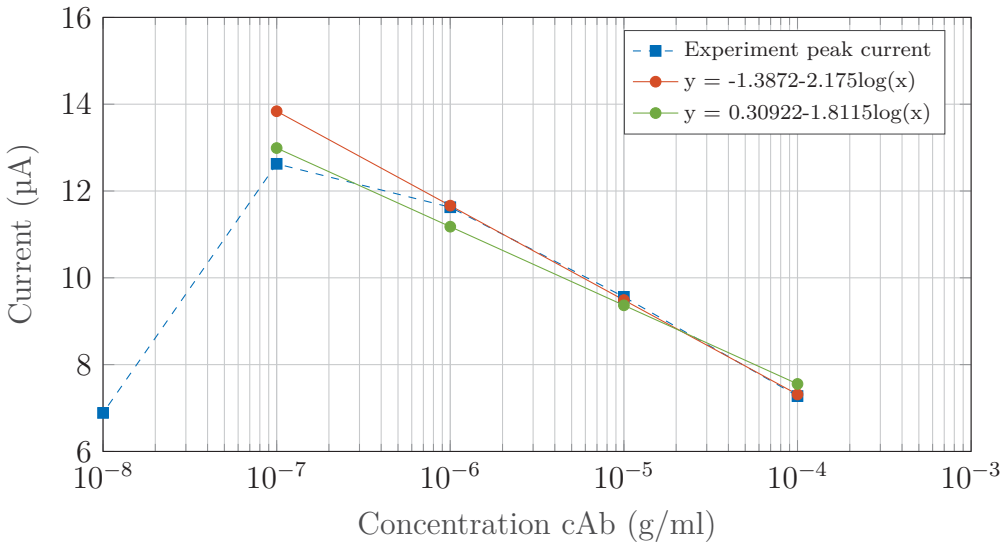

Figure 6.11: Different regression lines representing the SWV peak currents

The measured values are compared to the predicted values in Table 6.2. The average error for the first regression line is 0.321 µA with a maximum of 0.448 µA. In comparison the second regression line has an average error of 0.049 µA and a maximum of 0.073 µA, both nearly a decade smaller. Since the amount of data points is too low to calculate a descriptive R value, the table was used as an indication of the line of fit.

Concentration	Measured current (µA)	$y = 0.30922 - 1.8115\log(x)$		$y = -1.3872 - 2.175\log(x)$	
		Predicted (µA)	Error (%)	Predicted (µA)	Error (%)
100 µg/ml	7.276	7.555	3.834	7.31	0.503
10 µg/ml	9.561	9.367	2.033	9.49	0.766
1 µg/ml	11.626	11.178	3.854	11.66	0.315
100 n/ml	12.626	12.99	2.879	N/A	N/A
10 n/ml	6.887	N/A	N/A	N/A	N/A

Table 6.2: Regression line error comparison for capture antibody concentration

The choice regarding the concentration of antibodies used in the successive tests was based on the linearity of the response of the higher three concentrations. Theoretically, the highest amount of antibodies in the linear range would improve the sensitivity of the sensor because it would increase the probability of successful binding between the protein and the antibody. This said, for production efficiency and a decreased cost per sensor, the concentration used has to be as low as possible. The total amount of available antibodies also played a role in selecting this concentration, because of a limited supply. Coincidentally, the concentration used for an ELISA test fell within the bounds of the named restrictions, at 2 µg/ml, thus it was selected. This is indicated in Figure 6.10. It was decided that this concentration was to be kept constant for all of the successive tests.

6.2.4 Interferon gamma

The next step of the experimental process was to immobilise interferon gamma. The interferon was diluted in factors of 10 between 100 ng/ml to 10 pg/ml. The purpose of this test was to analyse if it was necessary to use a label molecule to amplify the response signal. The dilutions were made and incubated on sensors that had capture antibodies immobilised at a concentration of 2 µg/ml. The surface of the sensors were analysed again by SWV in the electrolytic liquid. A sample SWV curve of each of the different concentrations of the IFN-γ is given in Figure 6.12. The data was significantly noisier than that of the previous measurements, as seen in the shape of the data.

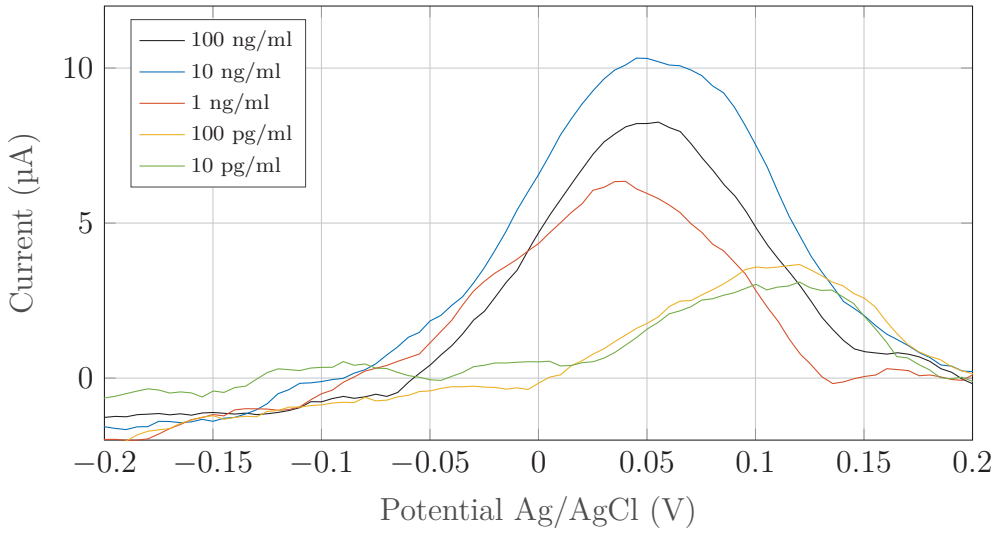

Figure 6.12: DropSens protein SWV response

Three sensors per concentration were tested and the peaks were compared. This is shown in Figure 6.13. The working range of this was identified to be between 10 ng/ml and 100 pg/ml. The sensor lower detection limit can be observed to be between 100 pg/ml and 10 pg/ml because of no significant peak increase in the peak response.

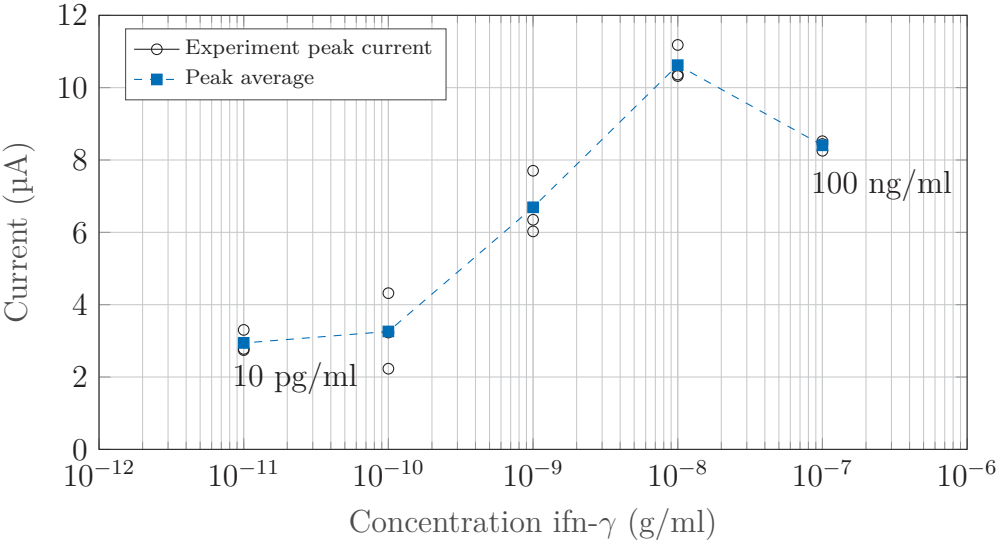

Figure 6.13: DropSens protein SWV peaks

The peak decrease at the upper detection limit will be discussed in Section 8.2.5 where it is compared to literature. The regression line for the working range was calculated to be $y = 39.987 + 3.681 \log(x)$, with an R-squared value of 0.949 and a root mean squared error of 0.789 µA.

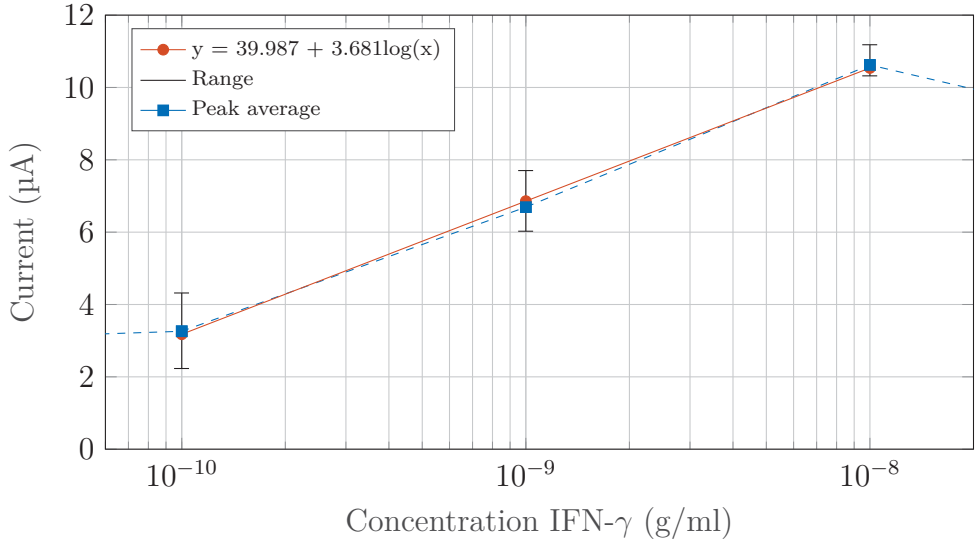

Figure 6.14: DropSens protein calibration curve

The results were significant, because without the use of a label the sensor had a working range to detect interferon gamma. This range was at a concentration of 10 ng/ml to 100 pg/ml. The trend of the line fits the explanation where the current increases as the concentration of the protein increases. This is due to the negative electrolytic liquid being attracted to the surface because of the positively charged protein. This may also account for the amount of noise recorded with these experiments, due to the irregularity of the charge on the surface.

6.2.5 Horseradish peroxidase

The final experiments were conducted by labelling the captured interferon gamma with the monoclonal biotinylated antibody and HRP. This was done to test if a label would have an effect on the peak response of the SWV graphs and hopefully increase the sensor working range. Figure 6.15 gives the normalised data from a set of sensors where the concentrations ranged from 100 ng/ml to 10 pg/ml and an electrolytic liquid of 5 mM potassium ferricyanide.

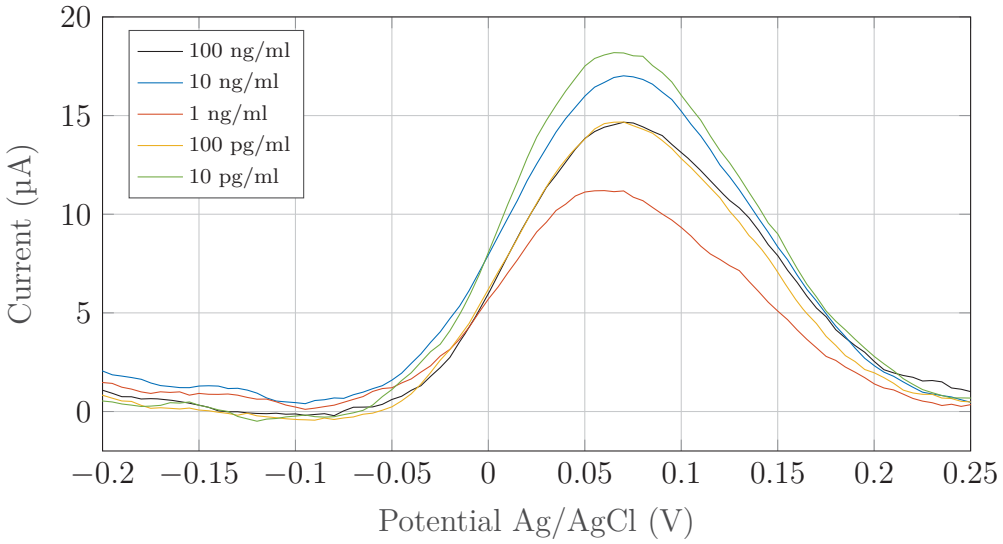

Figure 6.15: DropSens HRP labelled protein SWV response

The response of the labelled protein proved to be not as noisy as the unlabelled sensor. The peak responses are given and compared in Figure 6.16. An interesting phenomena is observed when looking at the general trend of the data. The peak current at a protein concentration at 1 ng/ml is lower than that of the higher concentrations, but also of the lower concentration.

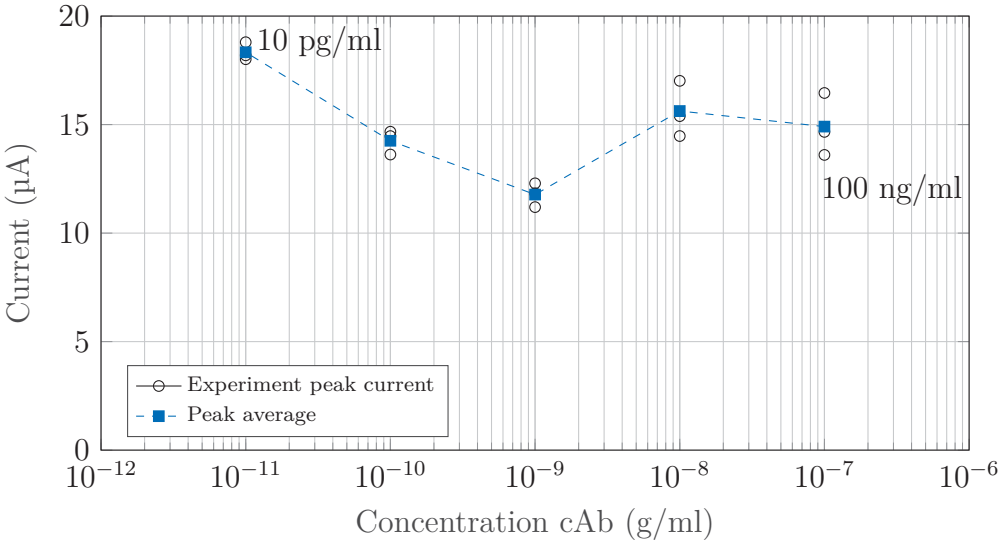

Figure 6.16: DropSens HRP labelled protein SWV peaks

It was decided that this response had to be addressed by conducting a negative control test to analyse the effect HRP would have if the labelled capture antibody could not bind to the target protein. To illustrate this, if the response was due to an unknown activity of HRP adhering to the fibres, for example being adsorbed due to ungrafted areas, this response might be repeated in the absence of the protein. The DropSens sensor stocks were unfortunately depleted by the time the analysis was made, but this was validated with the manufactured sensors. The complete description is given in Section 7.4.5. The conclusion was as hoped for, the HRP had no effect on the response if not bound to the

protein. This meant that the response could only be because of the HRP and that it could be expected to be repeated. The repetition of this result was observed when the effect of H_2O_2 on the peak currents was tested, discussed in Section 6.2.6.

The approximate linear region of 1 ng/ml to 10 pg/ml was used to model a linear regression line. The calibration curve for the peak values is given in Figure 6.17 with $y = -17.9994 - 3.2787\log(x)$. The R-squared value was found to be 0.958 with a root mean squared error of 0.638 µA.

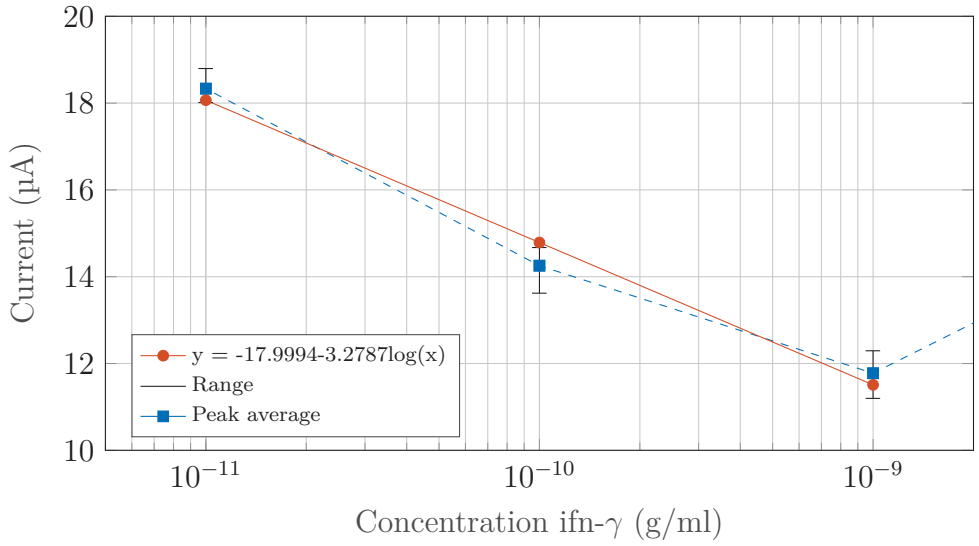

Figure 6.17: DropSens HRP labelled protein calibration curve

It can be observed that the trend of the line is in the opposite direction of the unlabelled response given in Figure 6.17. The conclusion here was that instead of attracting the charged electrolyte to the surface of the electrodes, the HRP either repels or interacts with the electrolyte. The latter is less probable, because a mediator such as H_2O_2 is required to spontaneously react with the HRP so that it in turn can be reduced to interact with ferricyanide.

6.2.6 Horseradish peroxidase with H_2O_2

The experiments were repeated exactly the same as before, but with the final test, 5 mM H_2O_2 was added to the electorlytic liquid before recording the SWV response. The normalised voltammograms are given in Figure 6.18.

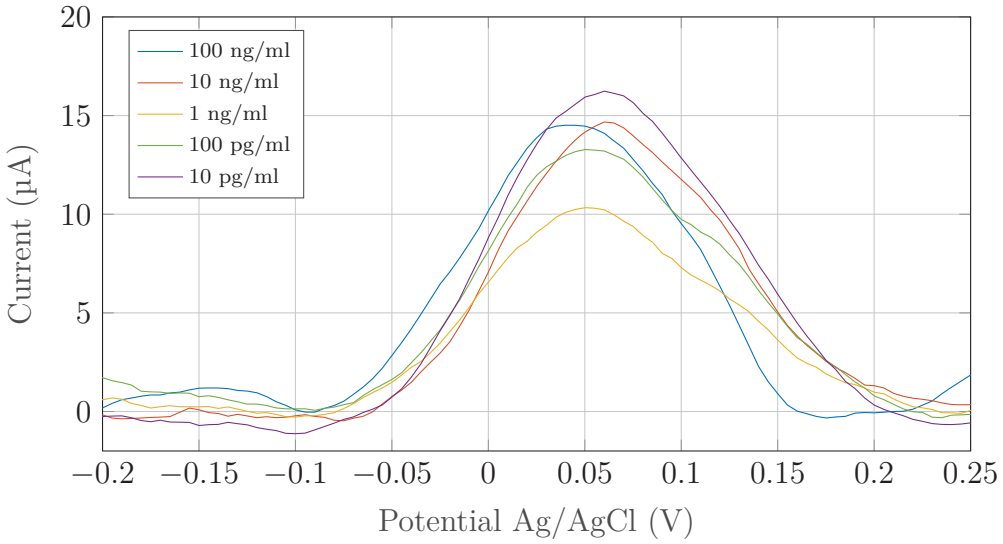

Figure 6.18: DropSens HRP labelled protein with H_2O_2 SWV response

The peaks were compared for the different concentrations of interferon gamma in Figure 6.19. The results were visually similar, meaning that the response is due to a mechanism between the interaction of the label and the electrolytic liquid. It must be noted that n = 1 for the concentration of 10 pg/ml and n = 2 for 100 pg/ml. These sensors were not tested due to a miscount and this was only realised when analysing the data. The spread of the measurements in and outside the linear region differ significantly. This effect most probably will be less notable when the data points are increased above the amount used in the experiments.

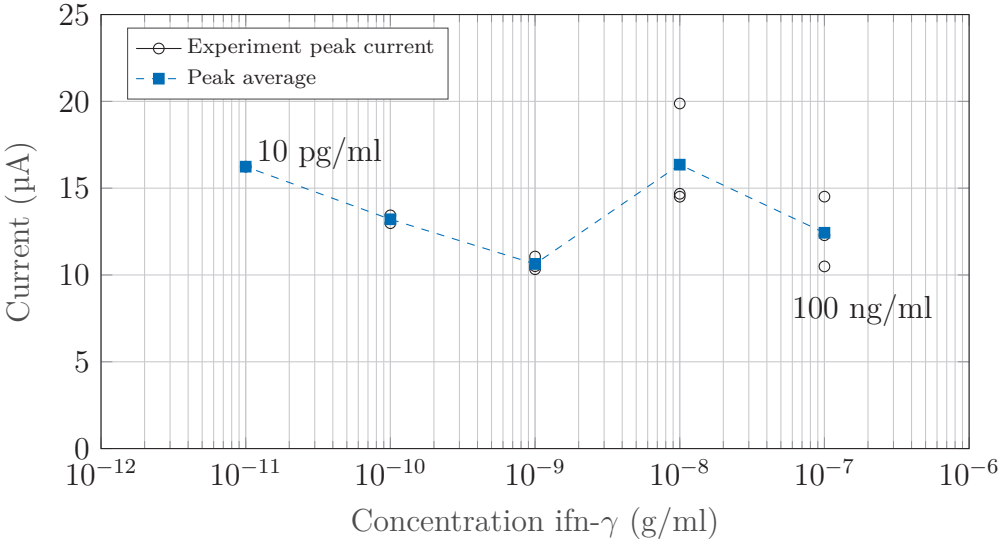

Figure 6.19: DropSens HRP labelled protein with H_2O_2 SWV peak current

The linear region for the sensor was 1 ng/ml to 10 pg/ml. The regression line calculated for this region was $y = -17.1365 - 3.0673\log(x)$ with an R-squared value of 0.977 and a root mean squared error of 0.414 µA.

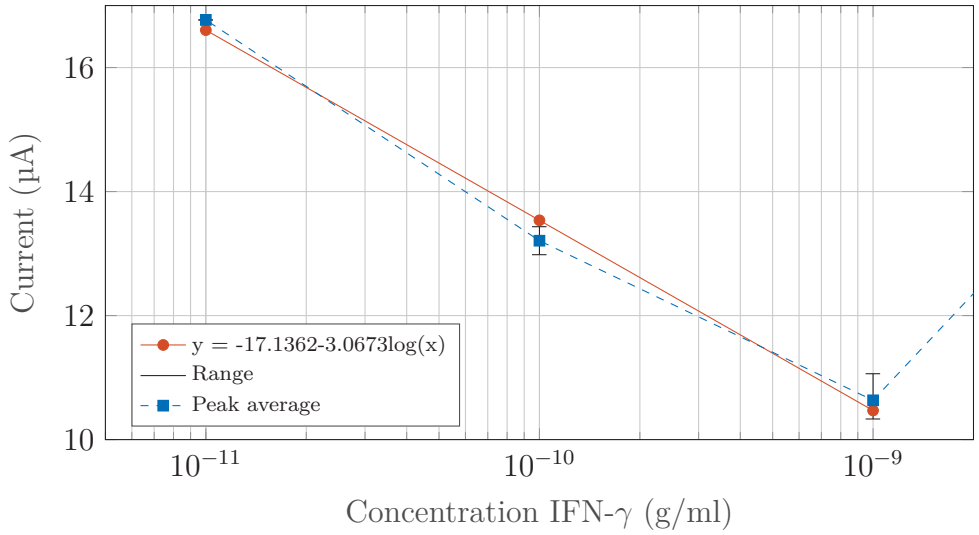

Figure 6.20: DropSens HRP labelled protein with H_2O_2 SWV calibration curve

The explanation for the trend of the regression line is similar to the previous experiment without H_2O_2. With all the data presented that was gathered for the DropSens sensors, the a detailed analysis of the comparison of the different components can be made.

6.3 Descriptive analysis

This section does a final evaluation of the results and compares the relevant methods.

6.3.1 Effect of H_2O_2

The intended effect of the H_2O_2 in the electrolytic liquid was to act as an amplifier, providing an additional electron that might be transferred to the working electrode without the necessity of the flow from the counter electrode. The peak response for the normal and the H_2O_2 are given in Figure 6.21.

The current differences are as follows: 1.14 µA for 1 ng/ml, 1.05 µA for 100 pg/ml, and 1.56 µA for 10 pg/ml. It was concluded that the HRP did not act as hoped for, but instead it is suspected that there was a cyclic reaction that was happening alongside the main electron transfer between the electrodes. When looking back at 4.2 to 4.4, this reaction might have been induced. It did not aid to the transfer, but instead added an additional step to get the electron to the electrode, explaining the decrease in the peak heights.

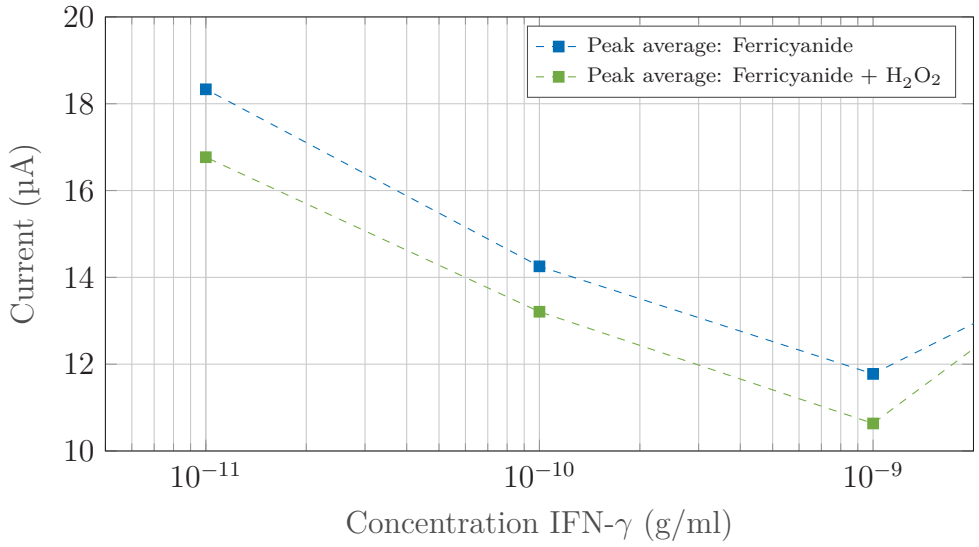

Figure 6.21: DropSens HRP labelled protein with H_2O_2 SWV peak current compared to the normal electrolytic liquid

6.3.2 SWV of different stages

The SWV peak currents for the different phases of the project is given in Figure 6.22. The linear regions of the unlabelled and labelled protein overlapped between 1 ng/ml to 100 pg/ml, thus a 1 ng/ml was chosen to indicate the change between the stages. The different effects can be directly compared. There is a high peak current when using the unmodified sensor surface in comparison with the subsequent tests. This is due to the large surface area available for the electron transfer of the electrolyte. The electrografted sensors exhibit a lower peak current due to the dissociated form of the carboxyl group in the PBS buffer that inhibits the electron transfer.

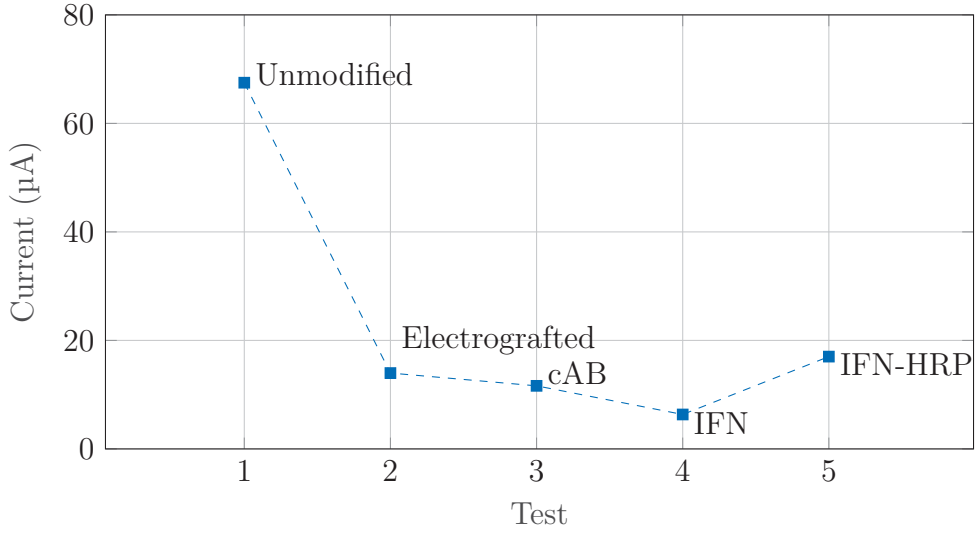

Figure 6.22: Comparison of SVW peaks of sequential surface morphologies for a protein concentration on 1 ng/ml

As a final comment on the electron transfer dynamics between the protein and the electrolyte and the label and the electrolyte, it might be explained by the isoelectric points of the specific molecules. In the case of interferon gamma, the isoelectric point for the protein is 9.7 [77]. This means that in the buffer at a pH of 7.4 the interferon is positively charged. This explains the increase in current as the protein increases. As for the labelled protein, something that has not yet been considered is the biotin and streptavidin link from the HRP to the captured antibody. The isoelectric point for biotin is 3.5, and the isoelectric point for streptavidin can range from 5 to 7.5 [78]. This means that both the streptavidin and biotin are negatively charged at a ph of 7.4. Taking into account the molecular mass of the molecules, (streptavidin 60 kDa and biotin 244.3 Da) it might be concluded that the streptavidin is largely the contributor to the negative charge. The protein has a molecular mass of 20.4 kDa, which means the streptavidin is much larger and could have a proportionate influence on the charge at the surface. HRP (40 kDa) on the other hand has a isoelectric point of 7.2 [79], which means in the buffer it has a small negative charge. If the negative charge of the streptavidin is the dominating force, this would explain the decrease in current as the concentration is decreased.

6.4 Conclusion

This chapter discussed the experiments that were conducted to determine the viability of detecting interferon gamma with an electrochemical cell using square wave voltammetry. A commercial sensor was used to conduct these tests.

The electrochemistry theory was validated and it was found that the sensor performed as expected. The different sensing configurations were tested: unlabelled interferon gamma, HRP-labelled interferon gamma, and HRP-labelled interferon gamma with H_2O_2. All of the methods were able to detect different concentrations of interferon gamma, but the H_2O_2 tests did not add to the response of the system. It was concluded that the labelled and unlabelled interferon gamma methods both looked promising, and this was to be used when developing the home-based sensors.

In this study, the working range of the labelled and unlabelled principles were 1 ng//ml to 10 pg/ml for the former, and 10 ng/ml to 100 pg/ml for the latter.

Chapter 7

Manufactured sensor findings

The experimental findings presented in this chapter was conducted with completed in the same fashion as in Chapter 6, but with the sensors that were manufactured in-house. The goal of this chapter is to highlight only the additional commentary regarding the results. A comparison of the different sensors can be found in the following chapter, Chapter 8.

7.1 Brief overview

This chapter discusses the selection of the preferred home-built sensor configuration. The electrochemical stability of the sensor was validated by cyclic voltammetry and square wave voltammetry in the pure electrolytic liquid. The sensors were electrografted and characterised. The immobilisation of the antibody and detection of labelled and unlabelled interferon gamma was conducted and the peak currents are compared in this chapter.

7.2 Sensor selection

The four manufactured sensors were tested with the electrolytic liquid to determine the repeatability of their electrochemical activity. It was quickly found that the electrolytic liquid had a tendency to creep through the fibres towards the spring probes. When in contact with the electrolytic liquid, the probes started to take part of the redox process, dissolving into the electrolyte. The metal ions would then contribute to the measured current. A short operation and hardware summary of the sensors are given:

Sensor 1: The sensor had the advantage of being compact and the easiest to assemble of the four sensors. Its lifetime was short-lived because of the tendency of having electrolytic liquid seep to the spring probes. It was difficult to align the electrodes because there was no visual way to repeatedly place the electrodes. The results were too inconsistent to provide the basis for a stable sensor.

Sensor 2: The sensor proved to yield more repeatable results than the first sensor, but the rate of manufacturing the sensors proved to make it undesirable. The alignment of the different made it a consuming process. The electrolytic liquid had a tendency of running off the electrodes during the experiments due to the small ridge keeping the liquid in place.

Sensor 3: The hydrophobic spray that coated the fibre tracks leading up to the transducer area seemed to inhibit electrical conductivity. None of the developed sensors worked. One advantage of this sensor was the fact that it kept the electrolytic liquid in place.

Sensor 4: Based on the design of Sensor 1, and having the advantage of the hydrophobic characteristics of Sensor 3, this sensor provided a simple and robust way of making the desired electrochemical cell. The electrolytic liquid did not seep through the gasket area, and if it did so, it was hindered by the hydrophobic layer.

With the obvious selection, Sensor 4 was developed by fabricating 25 different casings. The electrodes were replaceable and the hydrophobic layer was completely removed for thorough cleaning before reuse.

7.3 Additional modifications

It was found that by using pure silver it released silver ions into the electrolytic solution. This meant that the reference electrode was taking part of the reaction, which was not a desired attribute. A sensor with transferred silver can be seen in Figure 7.1.

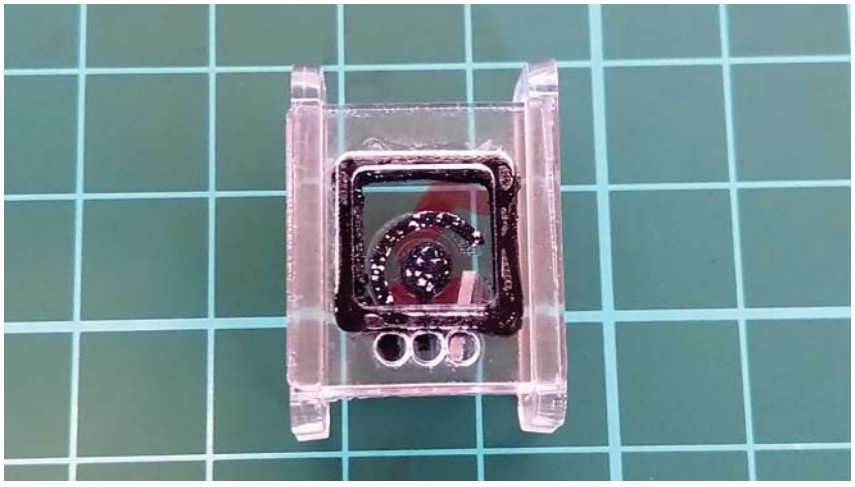

Figure 7.1: Silver ions transferred to the different electrodes

This was countered by coating the silver in chlorine to create a silver/silver chlorine reference electrode. This was done by placing the silver in 3.5% m/V sodium hypochlorite for 10 minutes. The sodium hypochlorite used was normal household bleach purchased at a supermarket. A used and refurbished silver reference electrode is given by Figure 7.2.

Figure 7.2: A used and refurbished silver electrode coated in chloride

Whenever a reference electrode was refurbished, the outer layer was sanded down with fine sanding paper. The electrode was washed with normal water, acetone, and then deionized water. The clean electrode was fully submerged in the sodium hypochlorite for ten minutes and then washed with deionized water. The end of the electrode was sanded to provide a contact point for the spring probe.

7.4 Manufactured sensors experimental results

The manufactured sensors were tested with the same methodology as followed for the DropSens sensors, with a few adjustments to suit the nature of the sensors.

7.4.1 Unmodified sensor response

The electrochemical activity of the sensor was evaluated by doing a cyclic voltammetry experiment in the electrolytic liquid. The response can be seen in Figure 7.3.

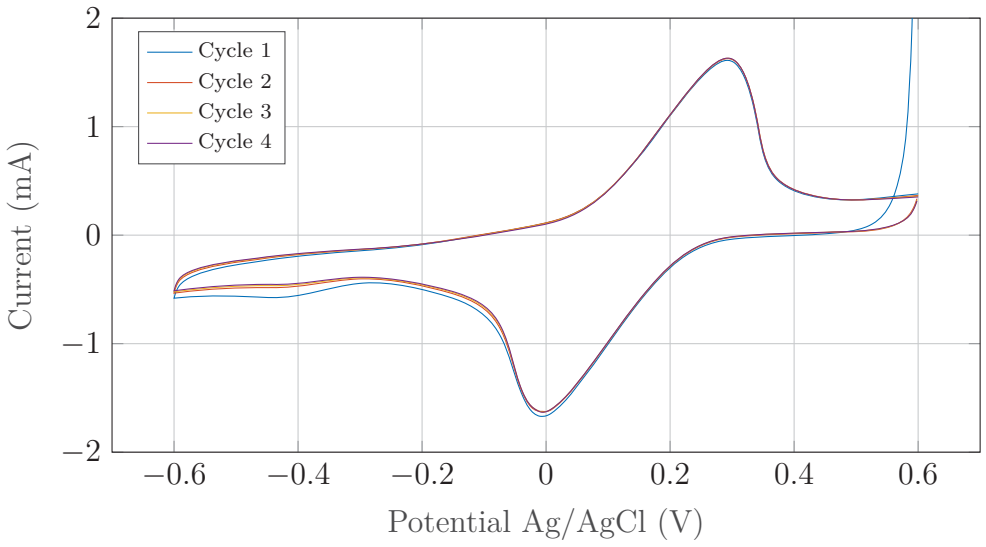

Figure 7.3: Unmodified sensor cyclic voltammetry response

The sensor response seemed to be visually stable because of no drifting. The square wave voltammetry test was conducted, and the result is given in Figure 7.4

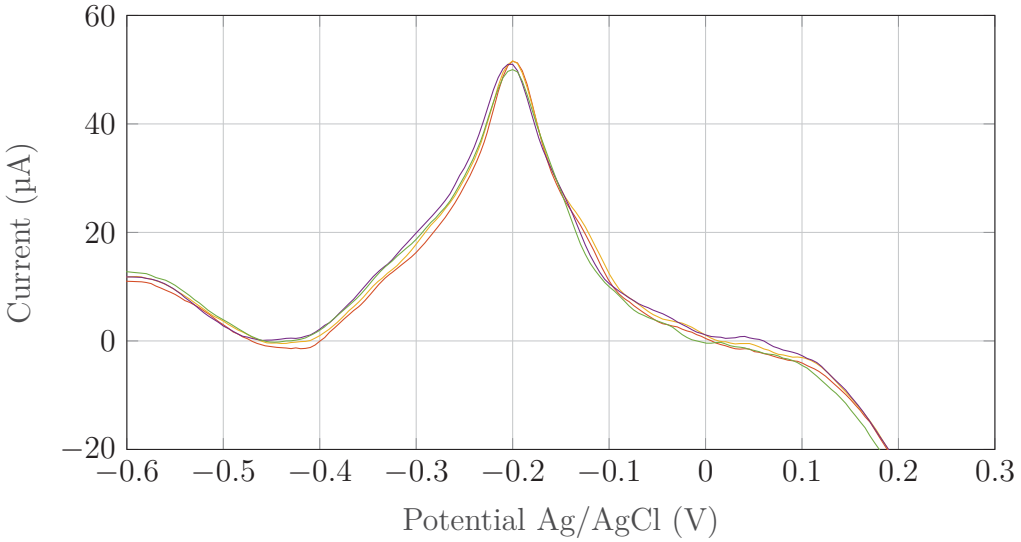

Figure 7.4: Unmodified sensor square wave voltammetry response

The results of both Figure 7.3 and 7.4 indicated a stable sensor. The peak for the SWV was very well defined. This was because the frequency at which the SWV was performed was increased to 50 Hz. The effect was studied by increasing the frequency from 10 Hz to 50 Hz. This can be seen in Figure 7.5. The main effect of increasing the frequency was the settling current at which the electrolyte stabilised. The data for this was collected using a stable sensor of Sensor 2, which might be the reason for the peak shape difference.

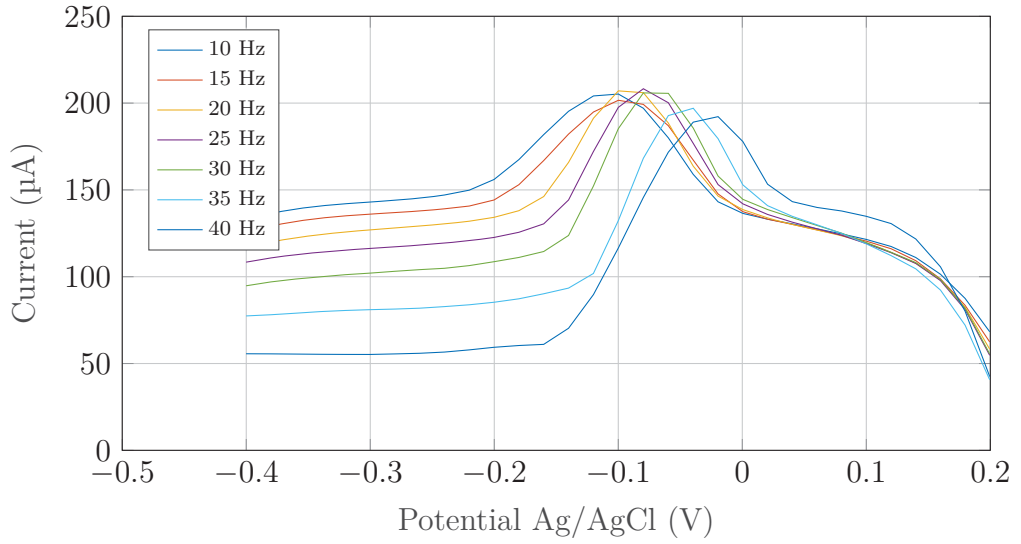

Figure 7.5: Manufactured sensor SWV frequency increase response

The effect of the increase in frequency was studied for Sensor 4 by measuring the response of the sensor at the usual 25 Hz, and then one at 50 Hz. The unfiltered response is given in Figure 7.6

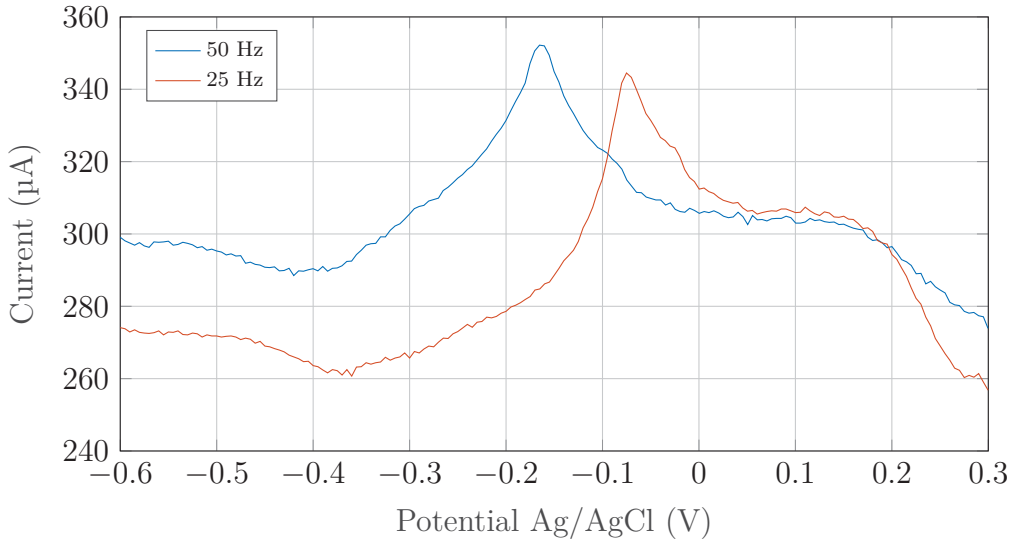

Figure 7.6: Unmodified sensor SWV frequency change effect unfiltered

The effect of the normalising algorithm was also tested on the increased frequency, so analyse if the peaks for the different frequencies differed in some way. If the magnitude of the peaks varied, then a comparison to the DropSens results in Chapter 6 would not be valid. The two normalised responses can be seen in Figure 7.7.

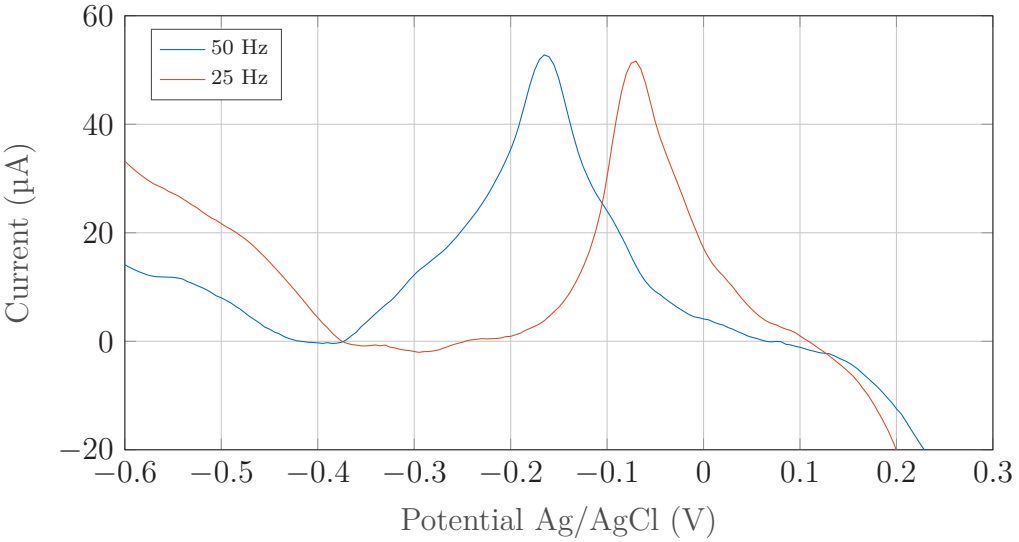

Figure 7.7: Unmodified sensor SWV frequency change effect normalised

It can be observed that the magnitude of the peaks are relatively the same. It was concluded, from these results, that the peaks were comparable. The increased frequency provided data that was easier for the algorithm to interpret and provide meaningful results. An interesting phenomena that can be seen in the response of Figure 7.7 is the difference in the half wave potential. The half wave potential moved to a more negative value. This is clearly illustrated in Figure 7.5 where the decrease in the half wave potential corresponds with the slow increase in frequency.

The effect of increasing the pulse size was also analysed. The response was as expected,

where the peak current grew as the pulse size increased. This is shown for 1 mV to 30 mV pulse size in Figure 7.8.

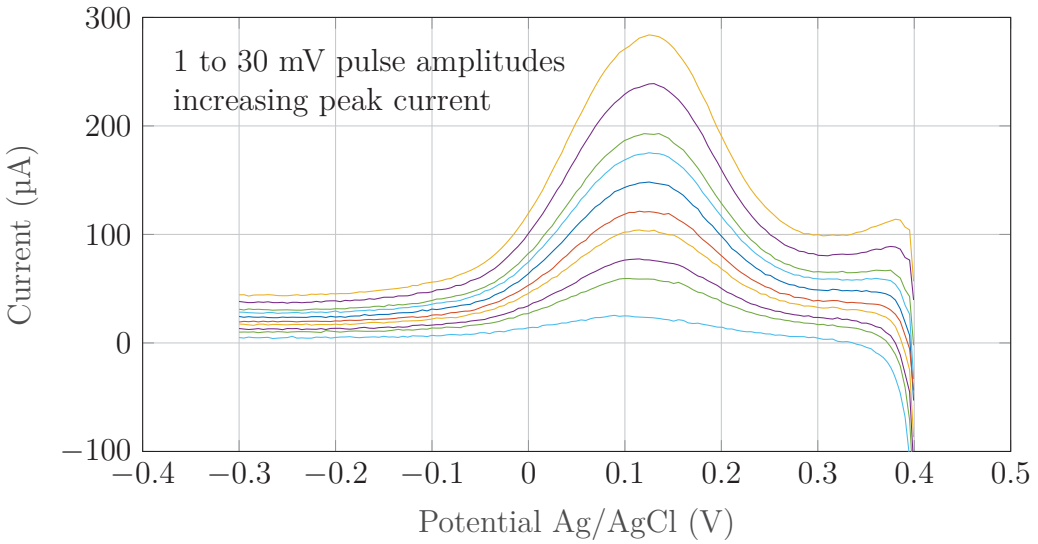

Figure 7.8: Manufactured sensor SWV pulse increase response

It was decided to keep the pulse size the same as for the previous experiments, since it had a definite effect on the peak current. If this was changed, the results would not be comparable with that found with the DropSens. The only modification was the frequency of the SWV, and as previously stated, had no known effect on the peak heights.

7.4.2 Electrografting

The next step was to electrograft on to the fibres. It was not necessity for a single cycle, since the parameters had already been established. The electrografting process can be seen in Figure 7.9.

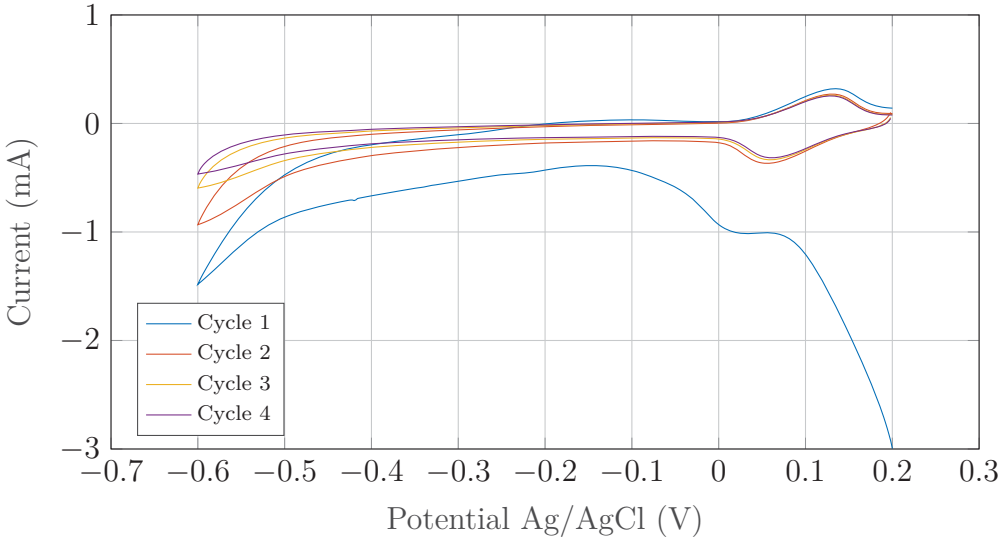

Figure 7.9: Manufactured sensor four cycle electrografting

The initial current for the sensors was different from what was expected. This might be to chlorine ions still in the vicinity of the reference electrode. If this was the case, the stray ions became depleted before the end of the first cycle. Another difference was the additional oxidation and reduction peaks that occured above 0 V. This was not considered to be a problem, since it seemed to reverse itself in every cycle. The grafting was also successful due to the change in peak currents at -0.6 V, indicating a surface morphology change. The electrografted fibres were tested with SWV. The response can be seen in Figure 7.10.

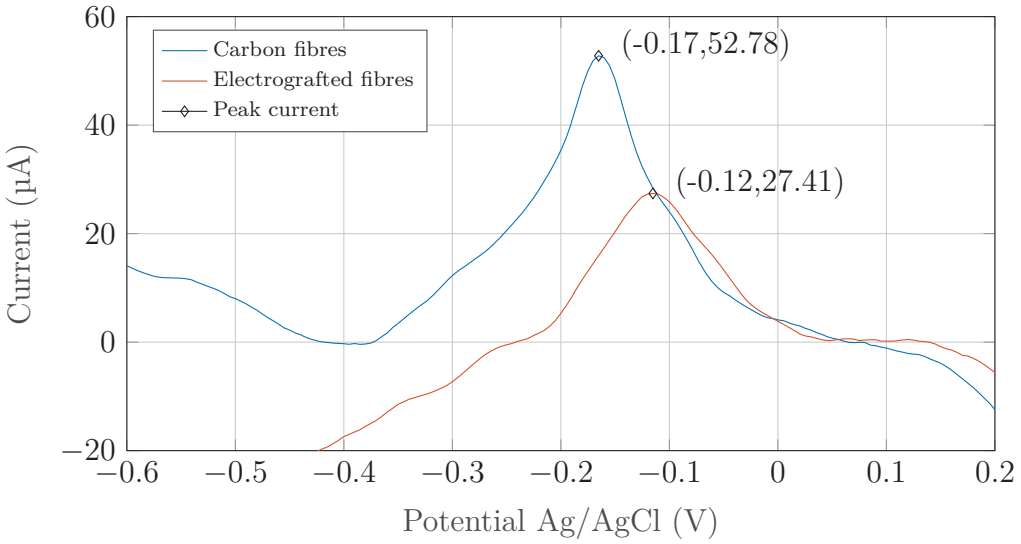

Figure 7.10: Manufactured sensor electrografting SWV peak comparison

The peak current changed from 52.78 µA to 27.41 µA after the electrografting process. The decrease in current happened as expected, with the newly formed carboxyl groups grafted to the sensor surface.

7.4.3 Interferon gamma

The carboxyl groups were activated according to the NHS/EDC protocol. The capture antibody was incubated on the sensor overnight at the predetermined concentration of 2 µg /ml. It was decided to keep this constant because an increase in antibody would mean more binding sites for the protein, thus changing one of the critical factors that would make the comparison with the commercial device invalid. Additionally, the response for a sensor with this concentration antibody was known, if the manufactured sensors failed to work, this factor could have been to blame. The concentrations for the protein was determined by the response of the commercial sensor. The range that was used spanned from 10 ng/ml to 1 pg/ml, with n = 3 per concentration. The unfiltered response for the captured protein is shown by Figure 7.11.

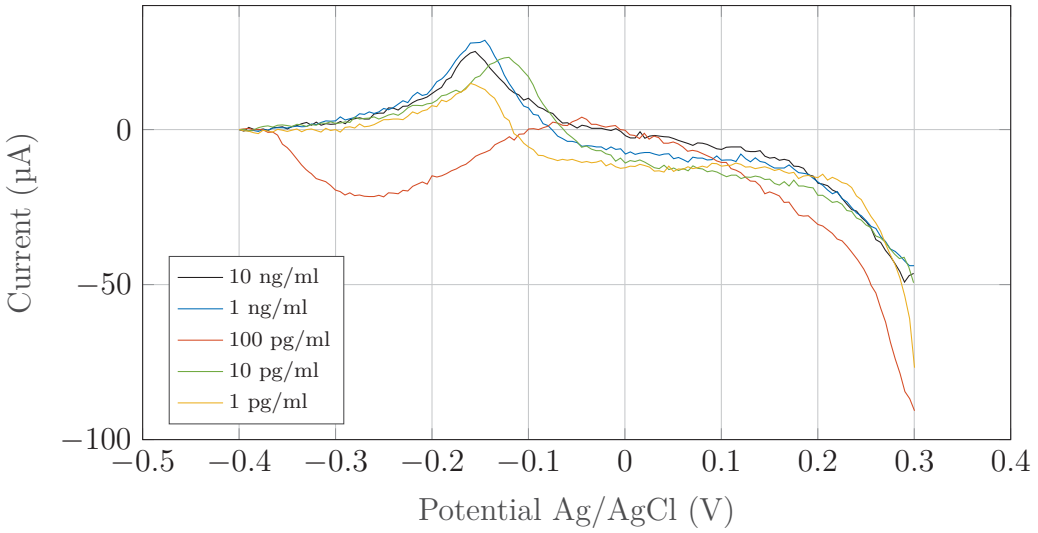

Figure 7.11: Manufactured sensor captured protein unfiltered SWV current response

The data was given in the unfiltered form to illustrate the response curve for the 100 pg/ml test relative to the rest. All three of the 100 pg/ml tests failed to generate a peak. This might be due to contamination or an erroneous dilution. The results for this concentration were omitted. The normalised response for the remaining concentrations is given by Figure 7.12.

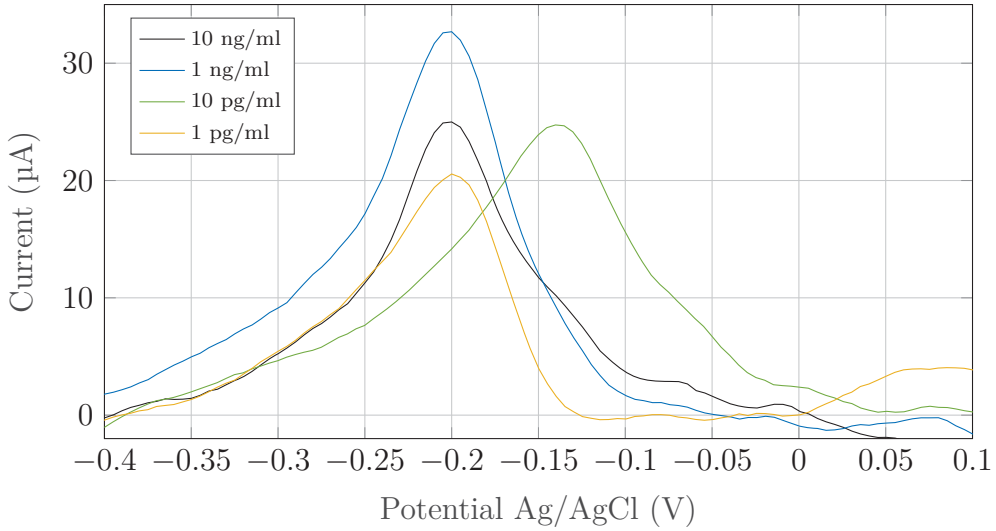

Figure 7.12: Manufactured sensor captured protein SWV current response

The peak currents are compared in Figure 7.13. The general trend of the data is again positive as the concentration of the interferon is increased. The same effect can be observed where the sensor saturation is surpassed and the peak current decreases.

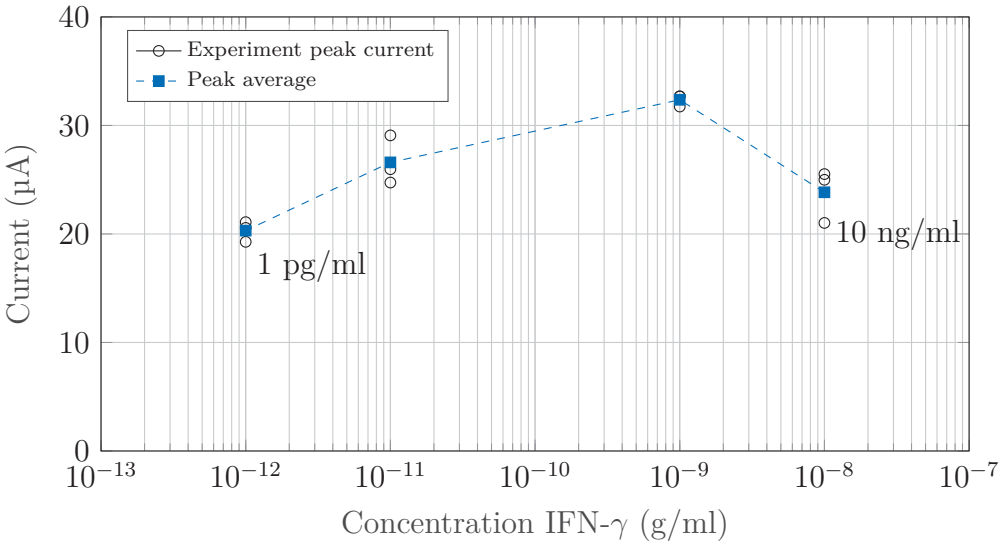

Figure 7.13: Manufactured sensor captured protein SWV peak currents

The linear range for the sensor was 1 ng/ml to 1 pg/ml. This is described by a calibration curve of $y = 67.564 + 3.857\log(x)$, with an R-squared value of 0.903 and a root squared mean error of 1.78 µA. These values might have been improved if there were data for the concentration of 100 pg/ml, which in turn might have improved the fit of the linear regression.

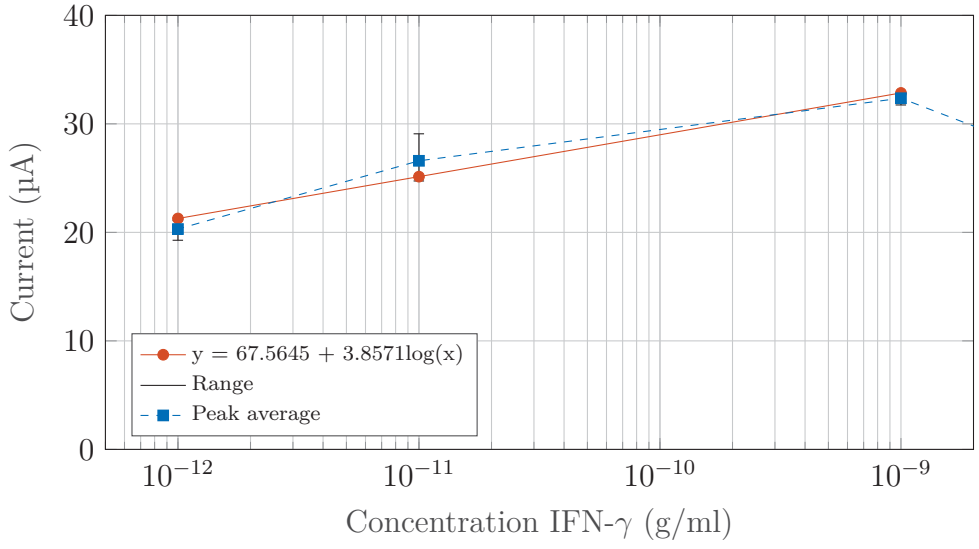

Figure 7.14: Manufactured sensor captured protein SWV peak calibration curve

7.4.4 Horseradish peroxidase

The final test was to analyse the effect that the HRP-labelled antibody had on the response of the sensor. The protocol was followed as before, and three sensors per concentration was tested. The concentration test range was from 10 ng/ml to 10 fg/ml. This range was chosen because with the DropSens sensors the lower detection limit was not reached, thus motivating the approach to test the detection for even lower concentrations of the protein. The SWV curves for a single test per concentration is given in Figure 7.15.

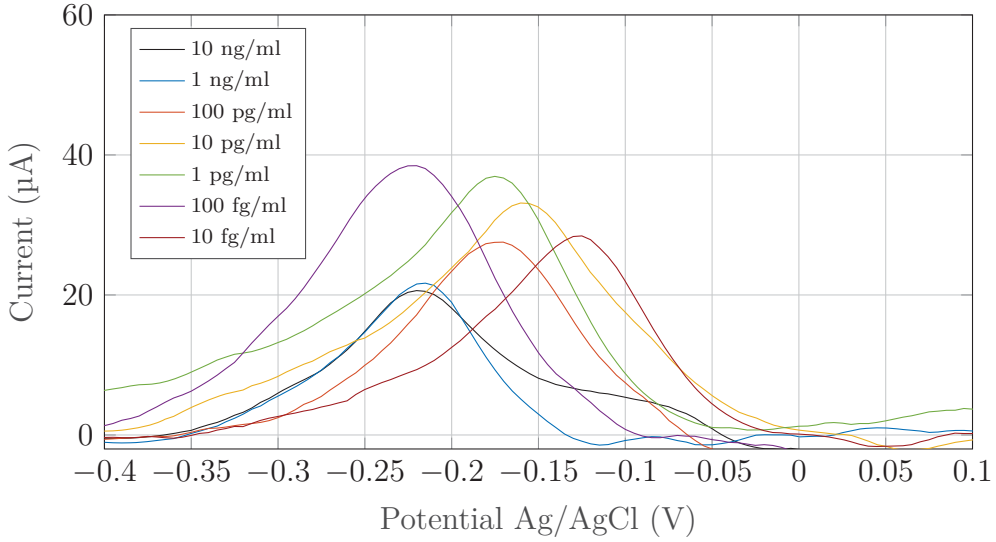

Figure 7.15: Manufactured sensor captured labelled protein SWV response

The half wave potential of the differed more than the previous tests. Again this was no real concern, but it indicates that there was another mechanism influencing this potential. The most probable was the temperature of the surrounding environment. The tests were conducted next to another experiment that produced humid air when operational. The effect of the changing potential theoretically has no influence on the peak currents, as shown by 3.6. The peak currents are compared in Figure 7.16.

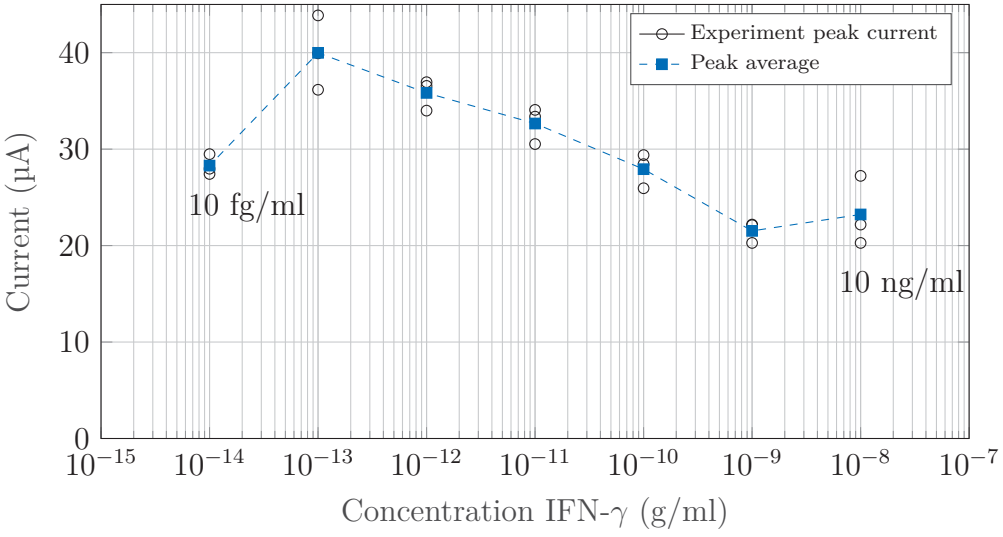

Figure 7.16: Manufactured sensor captured labelled protein SWV peaks

The same trend in the data can be observed where a decrease in the labelled protein meant an increase in the peak currents. The linear working range of the sensor was observed to be from 1 ng/ml to 100 fg/ml. The calibration curve is given in Figure 7.17 as $y = -17.727 - 4.483\log(x)$. The R-squared value of 0.908 was calculated with a root mean squared value of 2.16 µA.

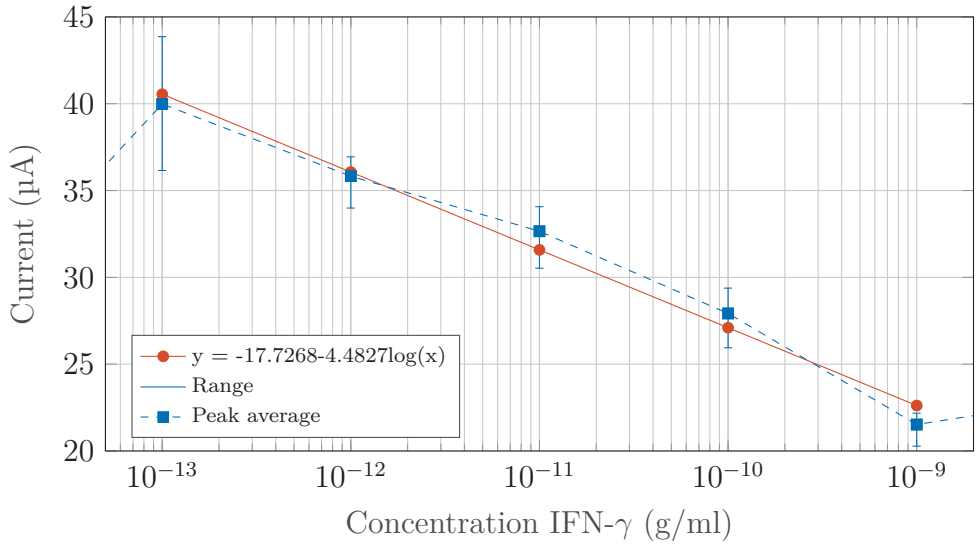

Figure 7.17: Manufactured sensor captured labelled protein SWV peak calibration curve

7.4.5 Negative control

Negative control tests were conducted to monitor the specificity of the sensor and to validate the sensing mechanism of the electrolyte-protein and HRP interaction.

The interaction was analysed by using a different capture antibody. The original anti-equine interferon gamma antibody (cAB) was replaced with an anti-human interferon gamma antibody (cAB2). The rest of the chemicals were kept the same. The cAB2 was immobilised to the sensors, and the equine interferon gamma was incubated with a concentration range of 10 ng/ml to 10 fg/ml. Following this, the equine label antibody was incubated on the sensors, followed by the streptavidin HRP, according to protocol. This was washed and tested as before. The goal of this change in the experiment was to analyse if the HRP was binding specifically to the biotinylated label antibody. If this were the case, the response of Figure 7.16 would be replicated by using the unmatched capture antibody, and the response curves for the HRP-labelled protein would be disqualified as a detection curve for interferon gamma. The recorded response for this experiment is given in Figure 7.18. This is compared to the linear working range of the two sensing techniques, and the response of having only a capture antibody immobilised on the surface.

It can be observed that the response of the control test was repeatable for the different concentrations of the protein. This means that the label did not spontaneously bind to anything else but the protein and the principle on which the detection was based was valid. There was a general increase in the peak current, compared to the sensor with only the capture antibody linked to it. This might be attributed to nonspecific adsorption of the different molecules on the sensor surface. It did however show that the lower detection limit of the unlabelled protein was at its extreme. It also explains the upper detection limit of the HRP-labelled protein, since the sensor reached a saturation point after 1 ng/ml, as seen in Figure 7.13.

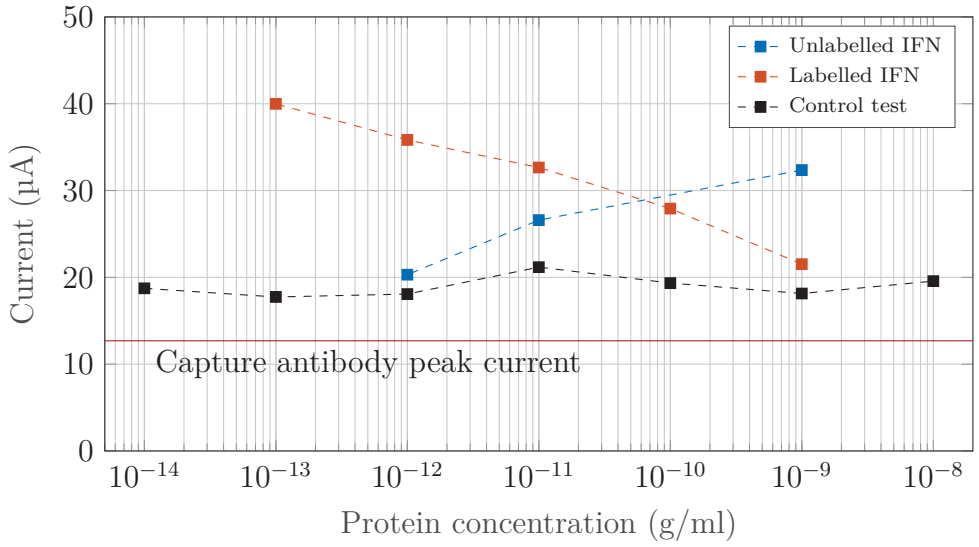

Figure 7.18: Response for negative control of using an unmatched capture antibody relative to the sensor linear response

The second negative control test that was conducted was to analyse the specificity of the chosen biorecognition element. C-reactive protein (CRP) was chosen as the reference protein. CRP is a nonspecific inflammatory biomarker that is sometimes suggested to be part of the proteins that may be used in conjunction with other to help diagnose TB [80]. A concentration of 10 pg/ml was incubated on three sensors. The response is given by Figure 7.19, where it is compared to the response of a labelled and unlabelled protein of 10 pg/ml.

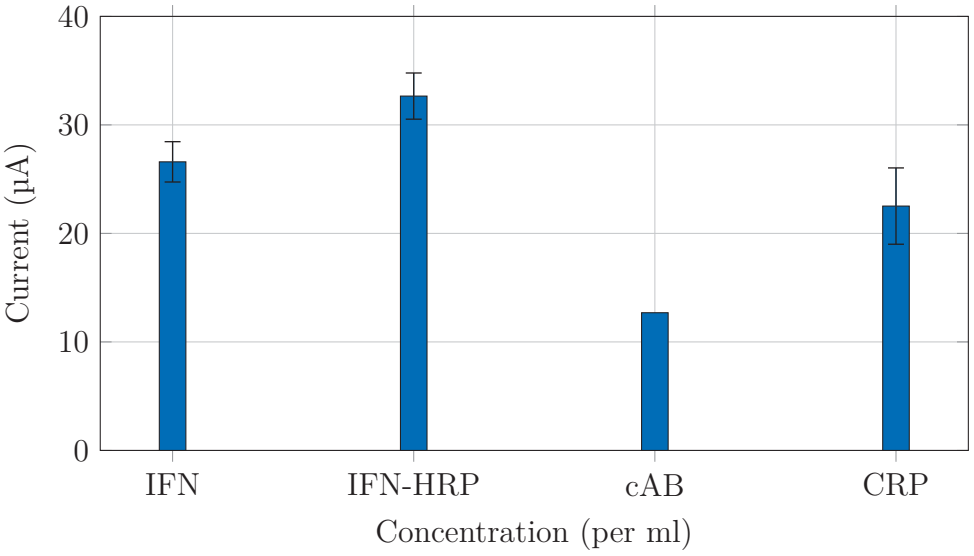

Figure 7.19: Negative control peak responses for 10 pg/ml proteins (IFN and CRP)

This yielded an interesting result, because the specificity of the sensor at 10 pg/ml is still maintained because the responses do not overlap. When comparing this with the lowest peaks of both tests, the specificity changes. This can be seen in Figure 7.20

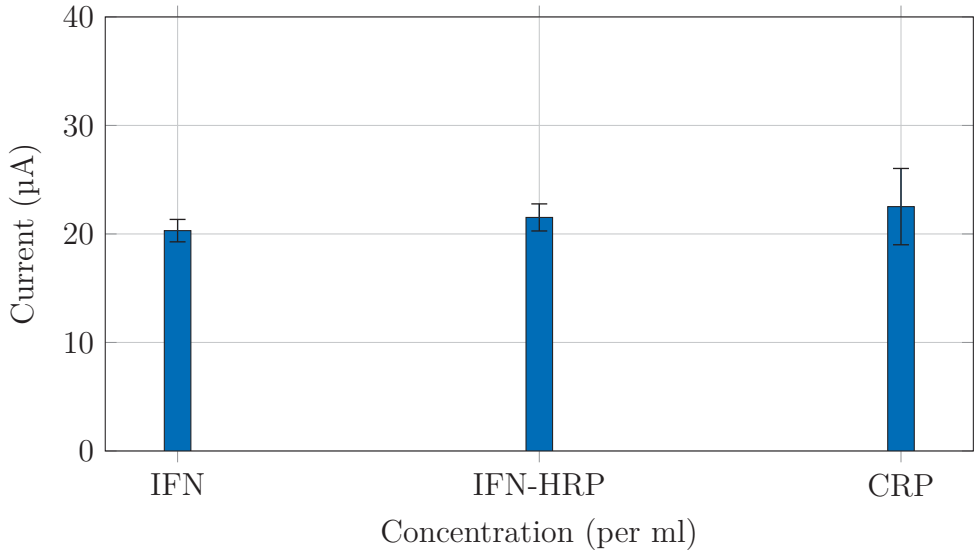

Figure 7.20: Lower peak response relative to the negative control of CRP

This means that the sensors are less specific at their lower extremes. This could be improved if the spread of the data is also considered as an indication of specific bindings. If the total of the three tests are accounted together, the CRP data ranges with a maximum of 3.516 µA from the mean, whilst the unlabelled and labelled ranges were 1.03 and 1.2 µA, respectively. This might be explained by the absorbance of the CRP, instead of the stronger affinity binding to the antibody.

7.5 Conclusion

This chapter discussed the selection of the manufactured sensor and the additional changes that were made to the designs. The electrochemical activity of the manufactured sensor was tested and validated before immobilising the capture antibody to the electrografted surface. Different square wave voltammetry settings were compared to find the suitable settings for analysis of the sensors.

The system was able to successfully detect unlabelled and labelled interferon gamma. The former having a linear working range of 1 ng/ml to 1 pg/ml of the protein, and the latter a linear working range of 1 ng/ml to 100 fg/ml. The sensing mechanism was successfully validated with a negative control test, and the the specificity was analysed by using C-reactive protein and comparing it with the original results.

Chapter 8

Discussion

This chapter compares and discusses the important experimental results of the commercial and the home-built sensor. This is then in turn compared to literature for validation and analysis of the sensor performance.

8.1 Brief overview

The performance of the home-built and commercial sensors are compared by analysing the results of the experiments discussed in Chapter 6 and Chapter 7. This includes the unmodified sensor response, the electrografting results, the different types of detection, concluded with a summary. The performance of the normalising algorithm is discussed, followed by a review of the project objectives. A post hoc-analysis concludes this chapter.

8.2 Experimental results

This section directly compares the different aspects of the commercial and home-built sensor. Aspects such as stability, peak current magnitude, working range, and linear regression are compared and discussed.

8.2.1 Unmodified response

The average of three cyclic voltammetry peaks for the electrolytic response of the sensors are given in Table 8.1. The response of the fabricated sensor was approximately 19 times larger than that of the commercial sensor. This can be attributed to the larger surface area of the electrodes used in the home-built sensor. The stability of both sensors can be illustrated with the peak heights, since the reduction peak almost completely reverses the effect of the oxidation peak in both cases. This effect indicates the consistency electrolytic liquid used, since both sensors were not available at the same time they were not tested with the same batch of the diluted potassium ferricyanide.

Peak	**Oxidation**	**Reduction**
DropSens (µA)	85.38	-90.22
Home-built (µA)	1629.03	-1629.0

Table 8.1: Cyclic voltammetry peak comparison for the commercial and home-built sensor

Looking back at the Randles-Sevcik equation discussed in the Chapter 3, given as

$$i_p = 0.4463nFAC^0\left(\frac{nFvD_o}{RT}\right)^{\frac{1}{2}}, \tag{8.1}$$

where the peak current is a function of two changeable variables, which is the area (A) and the square root of the scan rate (v). If the assumption is made that the other variables were kept consistent for the experiments the ratio of the area difference can be calculated using

$$\frac{i_{p1}}{A_1} = \frac{i_{p2}}{A_2}, \tag{8.2}$$

the area ratio is then found to be equivalent to the peak current ratio: 19.16 for the oxidation peaks and 18.06 for the reduction peaks. The lower area calculation for the reduction peaks might be due to the additional changing oxidation peak at -0.6 V for the DropSens sensor.

8.2.2 Electrografting

The electrografting response peak heights for the different sensors are given in Table 8.2. When the regression of the peak current ratio is taken into consideration, the initial ratio was 19.04 and the final ratio 12.90. The initial peak corresponds to the cyclic voltammetry response, giving credit to the assumption that the experimental conditions were approximately the same. The final ratio of 12.90 may be an indication that the home-built sensor underwent a more effective electrografting process, diminishing the peak current with an increased carboxyl group count.

Cycle	**1**	**2**	**3**	**4**
DropSens (µA)	-77.70	-48.65	-39.69	-36.13
Home-built (µA)	-1483	-933.20	-595.20	-466.20

Table 8.2: Electrografting peak current decrease comparison

8.2.3 Unlabelled protein detection

The linear regions of the unlabelled protein detection is given in Figure 8.1 for both the commercial and home built sensors. The working range for the DropSens sensor was found to be 10 ng/ml to 100 pg/ml. The home built sensor had a linear working range from 1 ng/ml to 1 pg/ml. In the overlapping region, the average peak current of the home-built sensor was 4.84 times higher than that of the commercial sensor.

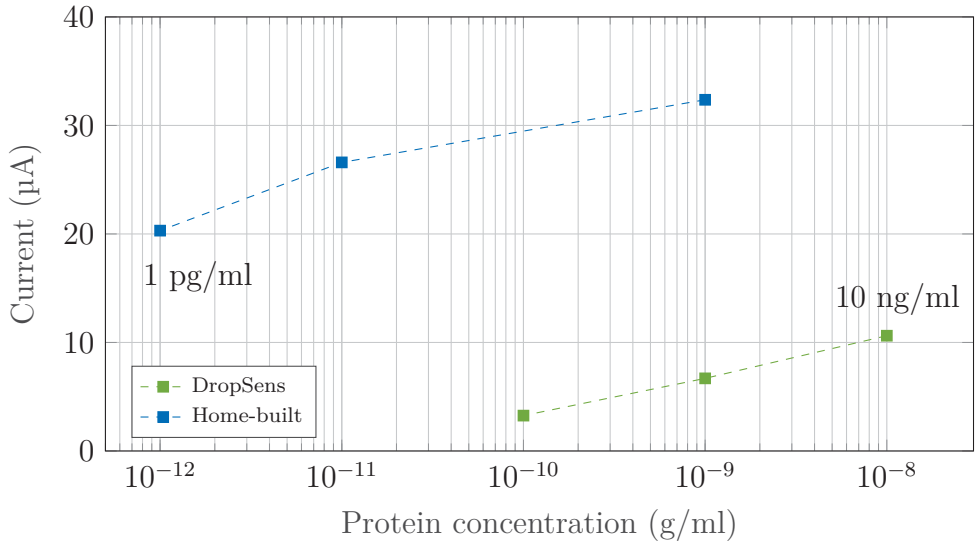

Figure 8.1: SWV peak response for the different sensors for different concentrations of the unlabelled protein

The RMS value for the of the home-built sensor was 1.78 µA, and for the DropSens 0.789 µA. This indicates that the spread of the data relative to the average for the DropSens was lower than that of the home-built sensor. This could be expected, since the DropSens is machine produced and would have less inconsistencies. None the less, the RMS value for the home built sensor can still be considered to be low since the peak currents were much higher than the DropSens peak currents, increasing the signal to noise ratio.

The linear regression line for the home-built sensor was calculated to be

$$y = 67.5645 + 3.8571 \log(x) \tag{8.3}$$

and for the DropSens

$$y = 39.987 + 3.681 \log(x). \tag{8.4}$$

The ratio of the gradient of the regression of the different sensors was calculated to be 0.954 (DropSens/Home-built). This means that the trend of both sensors were closely correlated. The only main difference was the amplified current of the home-built sensor. If the ratio was calculated to be 1, the lines would have followed a perfect path together, indicating that the change in concentration had the same effect on both sensors. The DropSens sensor was not tested up to its lower limit.

8.2.4 Labelled protein detection

The linear response regions of the home-built and commercial sensors are given in Figure 8.2. The working range for the home-built sensor is given with an upper detection limit of 1 ng/ml and a lower detection limit of 100 fg/ml. The DropSens upper detection limit was found to also be 1 ng/ml. The lower detection limit was not reached for this sensor. It was due to the fact that there were only a limited amount of sensors available for testing, and the DropSens sensors were used to also investigate the effect the H_2O_2 had on the peak currents.

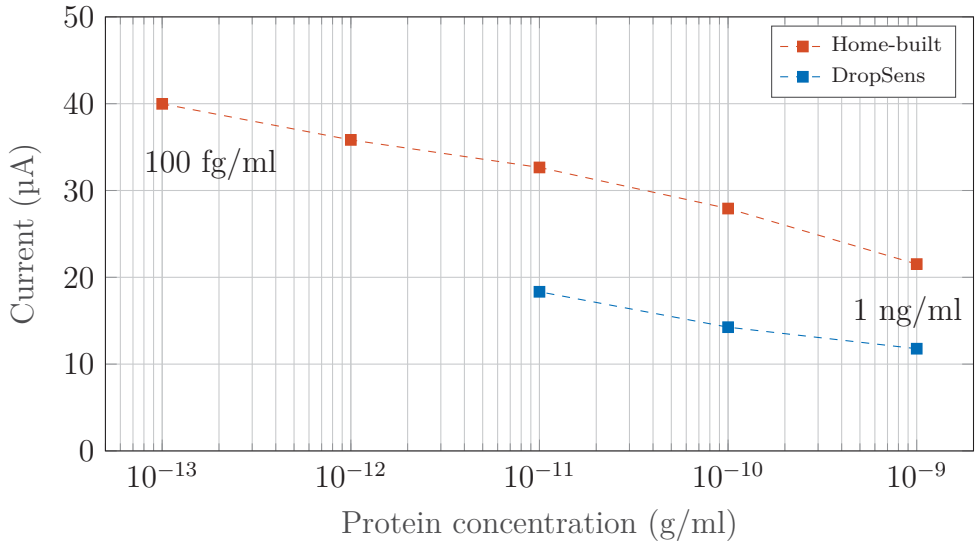

Figure 8.2: SWV peak response for the different sensors for different concentrations of the labelled protein

The regression line for the home built sensor was calculated to be

$$y = -17.7268 - 4.4827 \log(x), \tag{8.5}$$

and for the DropSens

$$y = -17.9994 - 3.2787 \log(x). \tag{8.6}$$

The ratio of the gradients was calculated to be 0.7314 (DropSens/Home-built). The gradient of the lines differed more significantly than that of the unlabelled response. This means that the regression lines diverge, and the change in concentration does not have the same magnitude change in current for the different sensors. For every 1 µA change in current for the home-built sensor would be equivalent to 0.7314 µA change in the DropSens response. This means that when the protein concentration is changed, the response of the different sensors would not equal in magnitude. Theoretically, the higher current change means that the saturation of the sensor would be reached earlier. This unfortunately could not be validated.

The RMS value for the home-built sensor peak current response was calculated to be 2.16 µA. The DropSens had a RMS value of 0.638 µA. This means that the average repeatability of the DropSens was higher than that of the manufactured sensor. The current amplification for the overlapping region was calculated to have an average value of 1.86.

8.2.5 Literature review

This section does a comparison to the work found in literature to validate the final findings. The main findings can be compared to Eissa *et al.*, Zhang *et al.* and Fethi *et al.* due to their work on DropSens electrochemical sensors, the immobilisation technique used, and the relevancy to tuberculosis.

Eissa *et al.* electrografted diazonium salt to a similar DropSens SPE modified with nanofibres. The response for the electrografting Figure 8.3

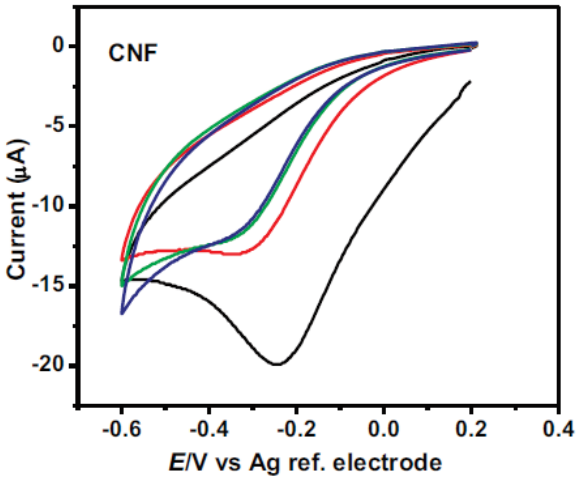

Figure 8.3: Electrografting of diazonium salt on DropSens carbon nanofibres [41]

This is similar to the electrografting experimental results of the DropSens sensor, seen in Figure 8.4. The shape of the graph is not an exact replication because the current was much higher in the findings of this study. There is no apparent reason why this should be, because the method was done according to the protocol described by Eissa *et al.* As seen before, the peak current for a cyclic voltammogram is subject to the area of the electrodes. It might be that the manufacturer improved the nanofibre composition by the time this study was done. Eissa *et al.* dis not supply any information regarding the temperature at which the experiments were conducted.

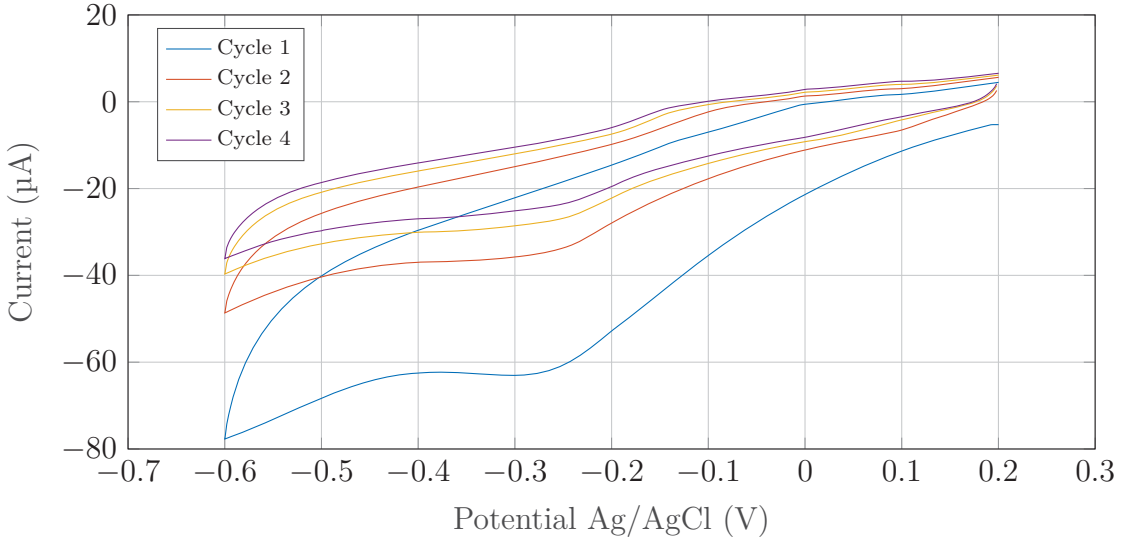

Figure 8.4: Four cycle Dropsens cyclic voltammogram electrografting response

Both Eissa *et al.* and Fethi *et al.* developed an unlabelled electrochemical biosensor using DropSens sensors. Fethi *et al.* used a gold screen printed electrode sensor. Both used square wave voltammetry as the voltammetry technique. The responses of the unlabelled protein SWV peaks are given in Figure 8.5.

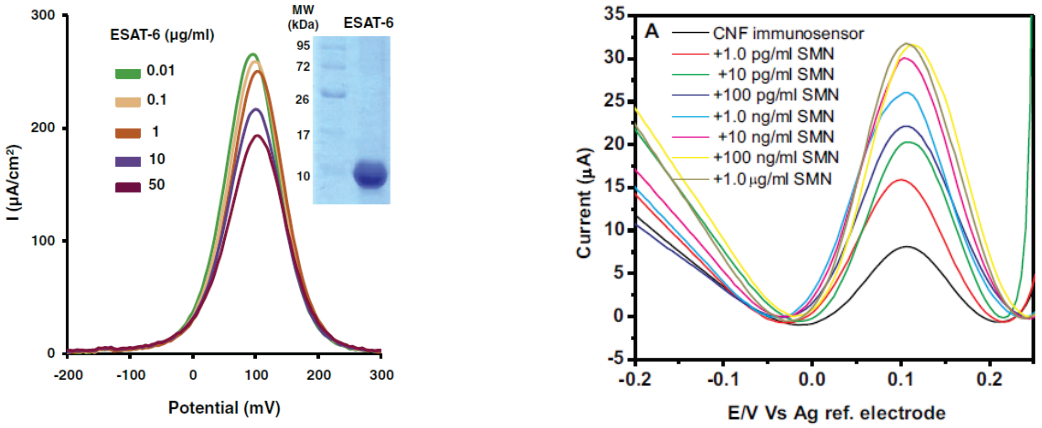

(a) ESAT-6 protein peak response [40]

(b) SMN protein peak response [41]

Figure 8.5: Unlabelled protein SWV peaks for Fethi *et al.* and Eissa *et al.*

The work on SMN found that their sensor had a linear range from 1 µg /ml to 1 pg/ml, with increasing SWV peaks as the protein concentration increased. The ESAT-6 work found their gold electrodes has a linear working range between 50 µg /ml and 10 ng/ml, with the peaks increasing as the protein concentration decreased. This might be explained by the isoelectric point of ESAT-6 being 4.69 [81]. This means that the protein is negatively charged in the reported buffer pH of 7.2, repelling the charge carriers. Similarly the SMN isoelectric point is 8.0 [82], which means it had a positive charge in the reported buffer pH of 7.4. This proves the explanation that the interferon gamma used in this study acted as an attraction for the electrolytic liquid, as explained in Chapter 6. It also validates the findings where the current increases as the protein increases.

The linear range of the unlabelled sensor that was developed in this work was found to be form 1 ng/ml to 1 pg/ml. The sensor had a lower detection limit than that of Fethi *et al.*, but lacked the dynamic range of the SMN detection limits.

Zhang *et al.* developed a disposable indium tin oxide electrochemical biosensor for HRP-antibody-conjugated nano gold labelled interferon gamma using differential pulse voltammetry. This work compared the effect of using an HRP-labelled antibody and an HRP-labelled antibody gold conjugate. The regression lines of the normalised peak currents are given in Figure 8.6a

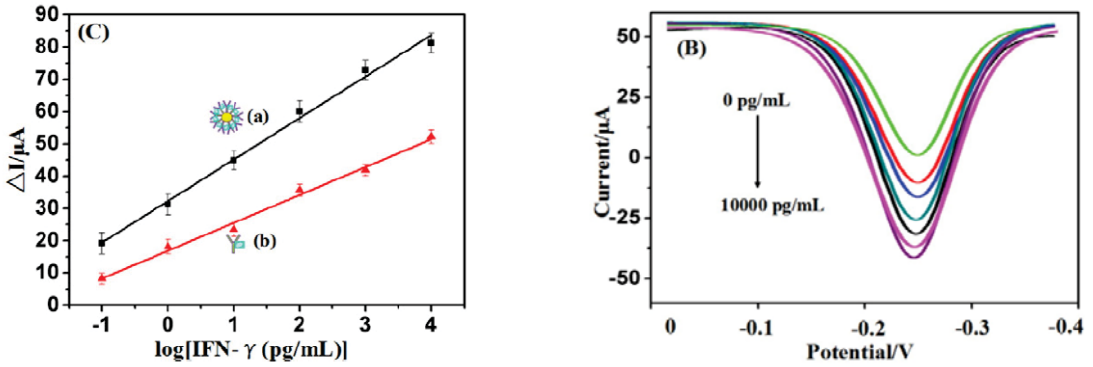

(a) HRP conjugate calibration curve

(b) DPV measurements of interferon gamma

Figure 8.6: HRP-labelled protein DPV peaks for Zhang *et al.*

The regression line for the gold conjugate tag was given to be

$$y = 32.28 - 12.862 \log(x), \tag{8.7}$$

with a lower detection limit of 0.048 pg/ml. For the HRP-antibody tag

$$y = -16.991 + 8.6010 \log(x), \tag{8.8}$$

with a lower detection limit of 0.36 pg/ml. The concentrations were all given in pg/ml. The paper stated that the sensor had a linear detection range of 100 fg/ml - 10 ng/ml. This is comparable to that found in this work for the HRP-labelled interferon gamma.

The DPV measurements of Zhang *et al.* can be seen in Figure 8.6b. Because of the principle DPV analyses its measurements, the peak response is always in the opposite direction than that of SWV. Looking at the linear regression of this study, it can also be seen that it is in the opposite direction as found by the experimental results in this thesis. This substantiates the response where the peak current of the SWV increases as the concentration of the label decreases due to a decrease in protein concentration.

As a final note, the literature only provides the linear response of the sensors. This might be due to the saturation effects found in with all of the sensors where instead of the usual levelling at saturation, the response changes direction and may even seem erratic. The conclusion drawn from this is that the selection of the linear range was also done by literature. The effect causing this is unknown, since the literature completely ignores it. It might be to additional adsorption, or hindrance due to an excess of molecules. The results correspond well with what had been presented in literature.

8.3 Algorithm review

The algorithm used to analyse the data performed as expected. It improved the time it took to analyse the data and ensured that the data was not manipulated to fit a desired outcome. It does, however, require a more dynamic and user friendly method of interaction with the user. Currently only the developer knows how to implement the code and if this knowledge were to be transferred to a subsequent project, more refinement would be required. None the less, the method of normalisation ensured the success of this project.

8.4 Project objectives

The project successfully met both the primary and secondary objectives, namely:

Primary objective: Investigate the possibility of the detection of interferon gamma and develop a protocol for this method.

A commercial sensor was used to successfully develop a protocol for the detection of varying concentrations of interferon gamma. Different sensing techniques were compared and two were found to be viable for the detection of the protein. The primary objective was then expanded and applied on home-built sensors.

Secondary objective: Build a home-based sensor to match or improve on the findings of the commercial sensor. The materials and fabrication methods should be kept as simple and straightforward as possible.

The secondary objective was also met by fabricating and testing a home-built sensor. The sensor response was comparable with the commercial sensor response at a fraction of the price. The components used were manufactured in-house. All of the materials used were commercially available and were modified in-house to fulfil the desired purpose. A summary of the projected cost can be found in Appendix C. It was projected that the total cost of a single sensor was R14.75. The DropSens sensors were purchased at R100.00 per sensor, thus this is a significant improvement in regards to the cost.

8.5 Post-hoc analysis

This project was very successful in evaluating the electrochemistry of the biosensor. There exists a need for a proper comparison of the range of detection of the DropSens sensors. The effects of all of the parameters of the square wave voltammetry technique has to be tested in isolation. This would help interpret the peak responses when the conditions of the electrolytic liquid is not well known.

The range of the sensors were successfully evaluated, but smaller variations in the concentration change of the interferon gamma has to be done to fully understand the nature of the response. This study had a limited supply of the protein and the commercial sensor. If this effect was to be studied then a larger supply of the materials would be required.

This study did not take into account the effect of the room temperature when the experiments were conducted. Temperature plays a large role in electrochemical systems and cannot be neglected when looking at something as sensitive as biosensing.

Chapter 9

Conclusion

This chapter concludes the the project with a summary and the final conclusion. The project implications are discussed, followed by a short review of the limitations of the results. The possibility and opportunities for future work are described at the end of the chapter.

9.1 Thesis summary

This thesis set out to analyse the possibility of developing a biosensor to aid in the diagnostic knowledge of tuberculosis. It was decided that the purpose of the biosensor would be to attempt to determine the concentration of the cytokine, interferon gamma.

The primary objective of the project was to analyse the biochemistry required to be able to determine different concentrations of interferon gamma. The secondary, and subsequent objective was to attempt to develop a biosensor in-house to determine the concentration of interferon gamma in a buffer.

The first objective was fulfilled by using a commercial electrochemical sensor and an electrolytic liquid to determine the concentration of the protein. This was done by modifying the surface characteristics of the sensor with the presence of the protein to affect the current response of the electrochemical system. Three different types of changes were tested: using a label free protein to bind to an antibody on the surface, adding a label to the bound protein to change the response further, and lastly changing the properties of the electrolytic liquid by adding hydrogen peroxide.

Of the three methods, the former two worked to such an extent that they were both used in the development of the home-built sensor. The home-built sensor that was developed had the same properties as the commercial sensor. This was chosen so that the responses of the two could be compared to a certain surety.

The home-built sensor was manufactured from off-the-shelf commercial products. The working range of the final unlabelled sensor was found to be 1 ng/ml to 1 pg/ml of the protein. The labelled method had a working range of 1 ng/ml to 100 fg/ml. These results were finally compared to literature and it was found that both methods matched or outperformed existing work.

9.2 Final conclusions

This project was successful in truly developing a low cost electrochemical biosensor from commercially available materials. The production of the sensors were repeatable and effective. The sensors had a linear working range comparable with literature that used commercial sensors. It goes without saying, but the results in this project look extremely promising, and with more optimisation the response curves can be improved. It was the first time, known to the author, that a biosensor was developed with this hardware methodology in combination with the sensing mechanism.

9.3 Project implications

This project is the first step towards an electrochemical method to diagnose tuberculosis. Human lives become part of statistics in epidemics such as with TB. In the world of today where the means exists to rid people of unnecessary suffering it is our duty to act on it.

9.4 Limitations of results

The use of the developed biosensor is currently limited to a laboratory environment. The potentiostat is a large device that requires a stable power supply to operate. This aspect limits the use of the sensor significantly.

The current use of the sensor as a biosensor is limited to proteins in a buffer. The effect of whole blood tests is still a long way down the line due to the complexity of the interaction of blood with biological matter.

The ideal detection method would be to be able to detect the protein just as it is, without the use of a label. Currently, labels are used in many antigen-based assays. This however is not ideal. The range of the sensor was more limited without the use of a label molecule.

9.5 Future research

Future work would include the development of a potentiostat that suits the requirements of the electrochemical cell. There exists many different types of potentiostats in literature, but all have a limitation of some sort. The first step in the development of such a system would be to completely understand the electrochemical reaction that would be monitored. If the device was developed as cheap as possible, then it would be wise to optimise it for a single type of experiment with different parameters.

The second aspect that requires a plenty of attention is the normalising algorithm. If the sensor system were ever intended to be used outside a laboratory environment, then the algorithm that is used to analyse the data needs to be as robust as possible so that it can interpret the data and adapt to the environmental conditions without any presetting or post-processing required from the user.

The method of application of the buffer and electrolytic liquid can be optimised. A transducer like this is not limited to the current design of liquid pipetting. This can be

optimised with microfluidic channels or lateral flow paper. The biorecognition element can also be changed to test the response of different proteins and DNA.

Appendix A

Laser calibration

The laser used to fabricate the different components is a 40W TS4040 CO_2 laser system produced by Jinan Transon CNC Equipment, China. The laser was calibrated in two steps: beam orientation, and beam focus. The laser cutting machine is shown in Figure A.1.

Figure A.1: 40W TS4040 CO_2 laser system

The technical specifications for the laser system is given in Table A.1.

Table A.1: Technical specifications for the TS4040 laser cutting system

TS4040 Technical Specifications	**Parameter**
Spot diameter	0.3-0.5 mm
Supplied power rating	40 W
Maximum cutting speed	300 mm/s
Power dissipation	141.47 - 50.92 W/mm^2
Working area	400x400 mm
Control system	On-board DSP
Graphic input	BMP, PLT, DST, DXF, AI

Figure A.2 shows a labelled graphical representation of the laser beam setup.

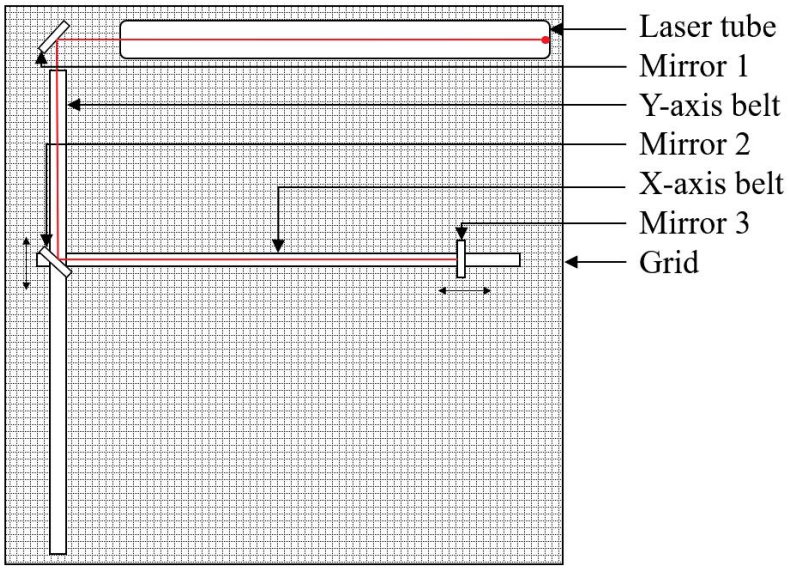

Figure A.2: Top view of laser system

To calibrate the beam orientation, the mirror system was aligned. This was done according to the process shown in Figure A.3. The first mirror was aligned, circled in Figure A.3a, relative to the next mirror, circled in Figure A.3b. This was done manually by placing adhesive tape over the second mirror and moving the first mirror while pulsing the laser beam. Mirror 2 was then moved between position B and C, again while pulsing the laser. If only a single hole appeared in the adhesive tape, the first mirror was successfully aligned. This process was repeated for the third mirror, but it was moved between position D and E. The third mirror is mounted to direct the beam towards the grid through the collimator.

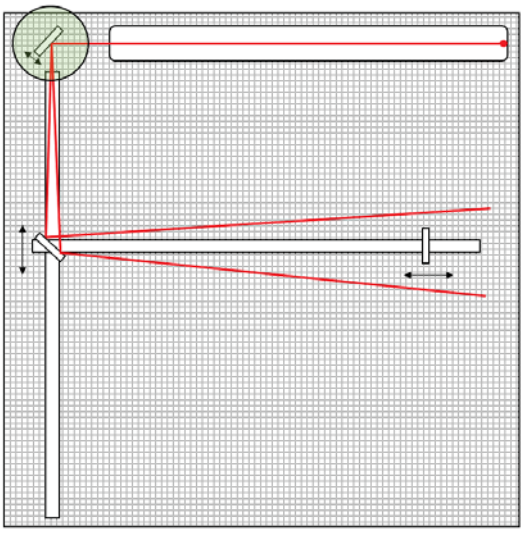

(a) Mirror 1 alignment

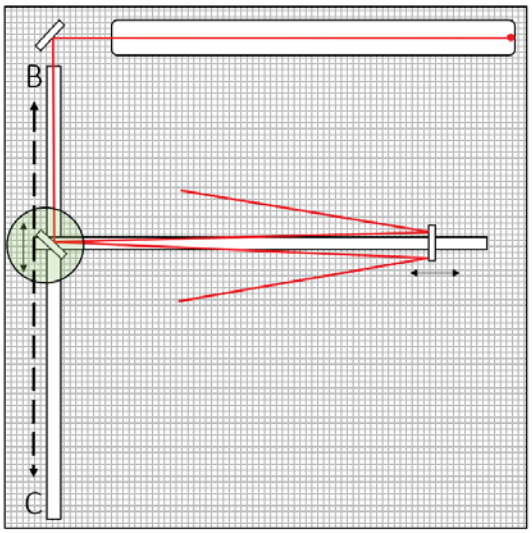

(b) Mirror 2 alignment

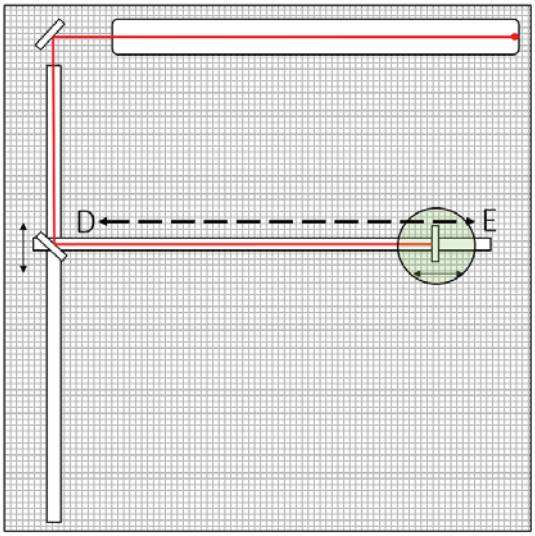

(c) Aligned system

Figure A.3: Alignment of laser mirror system

Appendix B

Gamry Interface 1000 specification sheet

This appendix contains the specification sheet of the potentiostat used in the experiments of the project.

THE GAMRY DIFFERENCE

Gamry Instruments provides you with the complete solution to get the answers you need. We carefully consider every detail of system design. Everything from board layout, component selection, signal processing, and all the way down to the tip of our smart cell cables, is designed to deliver maximum performance. Our software is intuitive and easy to use yet powerful enough underneath to allow you to customize experiments and interfaces to suit your needs. This combination of features and capabilities give you the maximum amount of performance at incredible value.

SPECIFICATIONS

	Interface 1000T	Interface 1000B	Interface 1000A	Interface 1000E
Cell Connections	2, 3, 4			
Floating	Yes			
System				
Maximum Current	± 100 mA	±1 A		
Current Ranges	6	9		
Current Ranges (with Gain)	8	11		
Minimum Current Resolution	0.3 pA	3.3 fA		
Minimum Voltage Resolution	1 μV			
Maximum Applied Potential	± 5 V	± 12 V		
Rise Time	1 μs			
Noise and Ripple	<20 μV rms			
Minimum Timebase	1 ms	10 μs		
Maximum Timebase	750 s			
Minimum Potential Step	12.5 μV			
EIS Measurement				
Frequency Range	100 mHz - 10 kHz	–	–	10 μHz - 1 MHz
Impedance Accuracy	99%	–	–	See Accuracy Contour Plot
Maximum AC Amplitude	2.33 V rms	–	–	2.33 V rms
Minimum AC Amplitude	17.8 μV rms	–	–	17.8 μV rms
Control Amplifier				
Compliance Voltage	± 20 V			
Output Current	> ± 1 A			
Speed settings	3			
Unity Gain Bandwidth (typical)	980, 260, 40, 4, 0.4 kHz			
Electrometer				
Input impedance	$> 10^{12}$ Ω			
Input current	< 20 pA			
Bandwidth (-3 dB) (typical)	> 15 MHz			
Common Mode Rejection Ratio	> 80 dB (10 kHz), > 60 dB (1 MHz)			
Applied Potential				
Accuracy	± 1 μV ± 0.2% of setting			
Resolution	12.5 μV, 50 μV, 200 μV/bit			
Potential Scan Range	± 0.4 V, ± 1.6 V , ± 6.4 V			
Measured Potential				
Accuracy	± 1 μV ± 0.3% of setting			
Resolution	400 μV, 100 μV, 10 μV, 1 μV/bit			
Applied Current				
Accuracy	± 5 pA ± 0.3% of setting			
Resolution	0.0033% full-scale/bit			
Measured Current				
Accuracy	± 5 pA ± 0.3% of setting			
Resolution	0.0033% full-scale/bit			
Bandwidth (current range dependent)	> 10 MHz (100 mA - 100 μA ranges) > 1.5 MHz (10 μA range) > 150 kHz (1 μA range)			
Stability Settings	3			
iR Compensation				
Mode	Current Interrupt			
Minimum Interrupt Time	33 μs			
Maximum Interrupt Time	715 s			
Physical Dimensions				
Weight	2 kg			
Size	24 x 6 x 27 cm (W x H x D)			
Cable	60 cm (std); 1.5 m, 3 m, 10 m			

GAMRY INSTRUMENTS
734 Louis Drive | Warminster, PA 18974 USA | +215-682-9330 | Fax: +215-682-9331 | sales@gamry.com | www.gamry.com

Appendix C

Cost analysis

Component	Cost (R)	Per sensor (R)	Reference
Perspex	300	4.20	Builders
Fibres	2229,67	1.85	Pyrograf
Hydrophobic spray	245	5	Builders
Silver	6 (per gram)	1.20	Jewellery dept.
Bleach	10	0.5	Checkers
Bicycle tyre	75	2	BMT Stellenbosch
	Total	14.75	

Table C.1: Projected cost of manufacturing a single sensor

Bibliography

[1] WHO, *Global Tuberculosis Report*. Geneva, 2018, ISBN: 9789241565646.

[2] S. Clinical *et al.*, "Tuberculosis in Patients Infected with Human Immunodeficiency Virus: Perspective on the Past Decade", *Oxford journal*, vol. 22, no. 4, pp. 683–704, 2018.

[3] A. Welte *et al.*, "Tuberculosis : well known for centuries – still difficult to diagnose", no. March, 2018.

[4] WHO, *Global Tuberculosis Report*. 2017, ISBN: 9789241565059.

[5] P. Naidoo *et al.*, "The South African Tuberculosis Care Cascade: Estimated Losses and Methodological Challenges", *Journal of Infectious Diseases*, vol. 216, no. November, S702–S713, 2017, ISSN: 15376613. DOI: 10.1093/infdis/jix335.

[6] UN, "The Sustainable Development Goals Report 2016", *United Nations*, vol. 2016, pp. 1–56, 2016, ISSN: 2518-3958. DOI: 10.18356/3405d09f-en.

[7] SANAC, "Let our actions count", 2017.

[8] World Health Organization, "High-priority target product profiles for new tuberculosis diagnostics: report of a consensus meeting", *WHO Meeting Report*, no. April, pp. 1–98, 2014. DOI: WHO/HTM/TB/2014.18.

[9] D. D. Chaplin, "Overview of the human immune response", *Journal of Allergy and Clinical Immunology*, vol. 117, no. 2 SUPPL. 2, pp. 430–435, 2006, ISSN: 00916749. DOI: 10.1016/j.jaci.2005.09.034.

[10] D. Chaplin, "Overview of the immune response", *Journal of Allergy and Clinical Immunology*, vol. 111, no. 2, S442–S459, 2003, ISSN: 00916749. DOI: 10.1067/mai.2003.125. arXiv: NIHMS150003.

[11] M. Ruhwald and P. Ravn, "Biomarkers of latent tb infection", *Expert Review of Respiratory Medicine*, vol. 3, no. 4, pp. 387–401, 2009. DOI: 10.1586/ers.09.31. eprint: https://doi.org/10.1586/ers.09.31.

[12] T. R. Frieden *et al.*, "Tuberculosis", *THE LANCET*, vol. 362, pp. 887–899, 2003.

[13] K. Suleiman, *Tuberculosis Diagnostic Tools*, L. Erica, Ed., February. New York: Treatment Action Group, 2017.

[14] *Mandell, Douglas, and Bennett's principles and practice of infectious diseases*, eng, 8th ed. 2015.

[15] R. Singhal and V. P. Myneedu, "Microscopy as a diagnostic tool in pulmonary tuberculosis", *International Journal of Mycobacteriology*, vol. 4, no. 1, pp. 1–6, 2015, ISSN: 2212-5531. DOI: 10.1016/j.ijmyco.2014.12.006.

[16] European Centre for Disease Prevention and Control, *Handbook on TB laboratory diagnostic methods in the European Union*. Stockholm, 2016, ISBN: 9789291937394.

[17] WHO, "Same-day diagnosis of tuberculosis by microscopy Policy statement", 2011.

[18] M. Fitz-Gerald, *Sputum Microscopy The handbook*. SA Pathology, 2013, ISBN: 9781742436029.

[19] F. Mirzayev *et al.*, *Xpert MTB / RIF implementation*. GPS Publishing, 2014.

[20] N. C. for Biotechnology Information, *Cid=5381226*, 2018.

[21] K. M. Kilfoil, "The evaluation of the Xpert ® MTB / RIF in the diagnosis of Mycobacterium tuberculosis complex and detection of rifampicin resistance in extrapulmonary (pleural and ascitic) fluid samples received for routine immunophenotypic analysis in a high-burden tuberculosis setting .", 2015.

[22] M. D. M. Dryden and A. R. Wheeler, "DStat : A Versatile , Open-Source Potentiostat for Electroanalysis and Integration", pp. 1–17, 2015. DOI: 10.1371/journal.pone.0140349.

[23] H. S. Whitworth *et al.*, "IGRAs – The gateway to T cell based TB diagnosis", *Methods*, vol. 61, no. 1, pp. 52–62, 2013, ISSN: 1046-2023. DOI: 10.1016/j.ymeth.2012.12.012.

[24] WHO, "Lateral Flow Urine Lipoarabinomannan assay", no. October, 2016.

[25] S. Chakravorty *et al.*, "Detection of Mycobacterium tuberculosis and Resistance to Rifampin in an Assay Suitable for Point-of-Care Testing", pp. 1–12, 2017.

[26] S. V. Kik *et al.*, "Tuberculosis diagnostics : which target product profiles should be prioritised?", *European Respiratory Journal*, pp. 537–540, 2014. DOI: 10.1183/09031936.00006414.

[27] K. R. Rogers, "Principles of Affinity-Based Biosensors", *Molecular Biotechnology*, vol. 14, no. 2, pp. 109–130, 2000, ISSN: 1073-6085. DOI: 10.1385/MB:14:2:109.

[28] S. Malhotra *et al.*, "Biosensors: Principle, Types and Applications", no. 2, pp. 3639–3644, 2017.

[29] D. Grieshaber *et al.*, "Electrochemical Biosensors - Sensor Principles and Architectures", *Sensors*, vol. 8, no. 12, pp. 1400–1458, 2008, ISSN: 1424-8220. DOI: 10.3390/s80314000. arXiv: 1011.1669.

[30] K. Mahato *et al.*, "Shifting paradigm of cancer diagnoses in clinically relevant samples based on miniaturized electrochemical nanobiosensors and microfluidic devices", *Biosensors and Bioelectronics*, vol. 100, no. July 2017, pp. 411–428, 2018, ISSN: 18734235. DOI: 10.1016/j.bios.2017.09.003.

[31] N. Prabhakar and H. Thakur, "Electrochemical biosensors: Fabrication and applications in biodiagnostics", *Nanobiosensors for Personalized and Onsite Biomedical Diagnosis*, 2016. DOI: 10.1049/PBHE001E_ch3.

[32] P. Chandra *et al.*, "Ultrasensitive detection of drug resistant cancer cells in biological matrixes using an amperometric nanobiosensor", *Biosensors and Bioelectronics*, vol. 70, pp. 418–425, 2015, ISSN: 18734235. DOI: 10.1016/j.bios.2015.03.069.

[33] K. Mahato *et al.*, "Paper based diagnostics for personalized health care: Emerging technologies and commercial aspects", *Biosensors and Bioelectronics*, vol. 96, no. April, pp. 246–259, 2017, ISSN: 18734235. DOI: 10.1016/j.bios.2017.05.001.

[34] N. J. Ronkainen *et al.*, "Electrochemical biosensors", *Chemical Society Reviews*, vol. 39, no. 5, p. 1747, 2010, ISSN: 0306-0012. DOI: 10.1039/b714449k.

[35] R. Koncki, "Recent developments in potentiometric biosensors for biomedical analysis", vol. 599, pp. 7–15, 2007. DOI: 10.1016/j.aca.2007.08.003.

[36] K. Inoue *et al.*, "A competitive immunochromatographic assay for testosterone based on electrochemical detection", *Talanta*, vol. 73, no. 5, pp. 886–892, 2007, ISSN: 00399140. DOI: 10.1016/j.talanta.2007.05.008.

[37] K. Talley and A. Emil, "On the pH-optimum of activity and stability of proteins", *Proteins*, vol. 78, no. 12, pp. 2699–2706, 2011. DOI: 10.1002/prot.22786.On.

[38] Y. Zhang *et al.*, "Fabrication of an interferon-gamma-based ITO detector for latent tuberculosis diagnosis with high stability and lower cost", *Journal of Solid State Electrochemistry*, vol. 19, no. 10, pp. 3111–3119, 2015, ISSN: 14328488. DOI: 10.1007/s10008-015-2936-2.

[39] Y. Zhang *et al.*, "Electrochemical immunosensor for interferon-γ based on disposable ITO detector and HRP-antibody-conjugated nano gold as signal tag", *Materials Science and Engineering C*, vol. 59, pp. 577–584, 2016, ISSN: 09284931. DOI: 10.1016/j.msec.2015.10.066.

[40] M. Fethi *et al.*, "Detection of ESAT-6 by a label free miniature immuno-electrochemical biosensor as a diagnostic tool for tuberculosis", vol. 74, pp. 465–470, 2017. DOI: 10.1016/j.msec.2016.12.051.

[41] S. Eissa *et al.*, "Electrochemical immunosensors for the detection of survival motor neuron (SMN) protein using different carbon nanomaterials-modified electrodes", *Biosensors and Bioelectronics*, vol. 101, no. October 2017, pp. 282–289, 2018, ISSN: 18734235. DOI: 10.1016/j.bios.2017.10.015.

[42] B. Malhotra and M. Ali, *Nanomaterials for Biosensors: Fundamentals and Applications*, ser. Micro and Nano Technologies. Elsevier Science, 2017, ISBN: 9780128135150.

[43] R. L. McCreery, "Advanced carbon electrode materials for molecular electrochemistry", *Chemical Reviews*, vol. 108, no. 7, pp. 2646–2687, 2008, ISSN: 00092665. DOI: 10.1021/cr068076m.

[44] R. Polsky *et al.*, "Diazonium-functionalized horseradish peroxidase immobilized via addressable electrodeposition: Direct electron transfer and electrochemical detection", *Langmuir*, vol. 23, no. 2, pp. 364–366, 2007, ISSN: 07437463. DOI: 10.1021/la062916a.

[45] C. Bourdillon *et al.*, "Immobilization of glucose oxidase on a carbon surface derivatized by electrochemical reduction of diazonium salts", *Journal of Electroanalytical Chemistry*, vol. 336, no. 1-2, pp. 113–123, 1992, ISSN: 00220728. DOI: 10.1016/0022-0728(92)80266-7.

[46] D. Bélanger and J. Pinson, "Electrografting: a powerful method for surface modification", *Chemical Society Reviews*, vol. 40, no. 7, p. 3995, 2011, ISSN: 0306-0012. DOI: 10.1039/c0cs00149j.

[47] J. Pinson and F. Podvorica, "Attachment of organic layers to conductive or semiconductive surfaces by reduction of diazonium salts", *Chemical Society Reviews*, vol. 34, no. 5, p. 429, 2005, ISSN: 0306-0012. DOI: 10.1039/b406228k.

[48] M. M. Chehimi, *Aryl Diazonium Salts*, M. M. Chehimi, Ed. France: Wiley-VCH, 2012, pp. 323–335, ISBN: 9783527650446. DOI: 10.1002/9783527650446.index.

[49] B. P. Corgier *et al.*, "Diazonium-protein adducts for graphite electrode microarrays modification: Direct and addressed electrochemical immobilization", *Journal of the American Chemical Society*, vol. 127, no. 51, pp. 18 328–18 332, 2005, ISSN: 00027863. DOI: 10.1021/ja056946w.

[50] C. M. A. Brett, *Electrochemistry : principles, methods, and applications*, eng, ser. Oxford science publications. Oxford: Oxford University Press, 1993, ISBN: 0198553889.

[51] P. A. Brooksby and A. J. Downard, "Electrochemical and atomic force microscopy study of carbon surface modification via diazonium reduction in aqueous and acetonitrile solutions", *Langmuir*, vol. 20, no. 12, pp. 5038–5045, 2004, ISSN: 07437463. DOI: 10.1021/la049616i.

[52] F. Anariba *et al.*, "Mono-and multilayer formation by diazonium reduction on carbon surfaces monitored with atomic force microscopy "scratching"", *Analytical Chemistry*, vol. 75, no. 15, pp. 3837–3844, 2003, ISSN: 00032700. DOI: 10.1021/ac034026v.

[53] P. J. Easterbrook *et al.*, "High Rates of Clustering of Strains Causing Tuberculosis in Harare , Zimbabwe : a Molecular Epidemiological Study High Rates of Clustering of Strains Causing Tuberculosis in Harare , Zimbabwe : a Molecular Epidemiological Study", *Journal of Clinical Microbiology*, vol. 42, no. 10, pp. 4536–4544, 2004. DOI: 10.1128/JCM.42.10.4536.

[54] I. Wergeland *et al.*, "Cytokine patterns in tuberculosis infection; IL-1ra, IL-2 and IP-10 differentiate borderline QuantiFERON-TB samples from uninfected controls", *PLoS ONE*, vol. 11, no. 9, pp. 1–12, 2016, ISSN: 19326203. DOI: 10.1371/journal.pone.0163848.

[55] N. N. Chegou *et al.*, "Beyond the IFN-γ horizon: Biomarkers for immunodiagnosis of infection with Mycobacterium tuberculosis", *European Respiratory Journal*, vol. 43, no. 5, pp. 1472–1486, 2014, ISSN: 13993003. DOI: 10.1183/09031936.00151413.

[56] L. R. F. Allen J. Bard, *Electrochemical Methods: Fundamentals and Applications*, 2nd ed. Wiley, 2000, ISBN: 0471043729,9780471043720.

[57] K. J. Rountree *et al.*, "A Practical Beginner ' s Guide to Cyclic Voltammetry", 2017. DOI: 10.1021/acs.jchemed.7b00361.

[58] Gamry Instruments, *Interface 1010*, Warminster, USA, 2018.

[59] PalmSens, *PalmSens4*, Houten, The Netherlands, 2018.

[60] Metrohm, *Metrohm Autolab*, Utrecht, The Netherlands, 2018.

[61] DropSens, *DropStat*, Asturias, Spain, 2018.

[62] Dropsens, *uStat 200 Bipotentiostat*, Asturias, Spain, 2018.

[63] Gamry, *Potentiostat fundamentals*, 2018.

[64] A. A. Rowe *et al.*, "Potentiostat for Analytical and Educational Applications", vol. 6, no. 9, 2011. DOI: 10.1371/journal.pone.0023783.

[65] P. Bezuidenhout *et al.*, "The characterisation and design improvement of a paper-based E.coli impedimetric sensor", vol. 10036, p. 100360L, 2017, ISSN: 1996756X. DOI: 10.1117/12.2245754.

[66] Texas Instruments, "LMP91000 Sensor AFE System : Configurable AFE Potentiostat for Low-Power Chemical", 2014.

[67] C.-y. Huang, "Design of a Portable Potentiostat with Dual-microprocessors for Electrochemical Biosensors", vol. 3, no. 6, pp. 159–164, 2015. DOI: 10.13189/ujeee.2015.030601.

[68] A. Ainla *et al.*, "Open-Source Potentiostat for Wireless Electrochemical Detection with Smartphones", 2018. DOI: 10.1021/acs.analchem.8b00850.

[69] DropSens, *Screen-printed electrodes*, 2018.

[70] W. Zong *et al.*, "Cyclic voltammetry : A new strategy for the evaluation of oxidative damage to bovine insulin", vol. 19, pp. 263–268, 2010. DOI: 10.1002/pro.313.

[71] P. A. Rock and P. A. Rock, "The Standard Oxidation Potential of the Ferrocyanide-Ferricyanide Electrode 25 ° and the Entropy of Ferrocyanide Ion", vol. 945, no. 1, pp. 576–580, 1965. DOI: 10.1021/j100874a042.

[72] A. Mesnage, "Diazonium salts induced anchoring process : mechanism , applications", 2011.

[73] M. Delamar *et al.*, "Covalent Modification of Carbon Surfaces by Grafting of Functionalized Aryl Radicals Produced from Electrochemical Reduction of Diazonium Salts", *Journal of american chemical society*, no. 12, pp. 5883–5884, 1992. DOI: 10.1021/ja00040a074.

[74] B. B. Dunford and H. Hasinoff, "Kinetics of the Oxidation of Ferrocyanide by Horseradish Peroxidase", *Biochemistry*, vol. 9, no. 2, pp. 4930–4939, 1970. DOI: 10.1021/bi00827a015.

[75] K. Aoki *et al.*, "Reversible square-wave voltammograms independence of electrode geometry", *Electroanalytical Chemistry*, pp. 25–39, 1986.

[76] *Rust-oleum neverwet liquid repelling treatment.*

[77] Cloud-Clone, *Recombinant interferon gamma (ifng)*, 2018.

[78] ThermoFisher, *Avidin-biotin interaction*, 2018.

[79] A. C. Maehly, "Measurement of Enzyme Purity by Spectrophotometry.", vol. 337, pp. 801–813, 1950.

[80] N. N. Chegou *et al.*, "Diagnostic performance of a seven-marker serum protein biosignature for the diagnosis of active TB disease in African primary healthcare clinic attendees with signs and symptoms suggestive of TB", *Thorax*, vol. 71, no. 9, pp. 785–794, 2016, ISSN: 14683296. DOI: 10.1136/thoraxjnl-2015-207999.

[81] X. Wu *et al.*, "Recombinant early secreted antigen target 6 protein as a skin test antigen for the specific detection of Mycobacterium tuberculosis infection", pp. 81–87, 2008. DOI: 10.1111/j.1365-2249.2008.03605.x.

[82] G. Battaglia *et al.*, "Expression of the SMN gene , the spinal muscular atrophy determining gene , in the mammalian central nervous system", vol. 6, no. 11, pp. 1961–1971, 1997.